Stockholm University

Master Thesis

Degree Project in Geology 60 hp

Exploring the source of metals in Archean orogenic gold deposits in the Abitibi Greenstone Belt, Canada

Nikolaos-Georgios Leventis

Stockholm 2017

Department of Geological Sciences
Stockholm University
SE-106 91 Stockholm

Cover page picture information: Kirkland Lake Miners' Memorial, Ontario, Canada.

Credit: Nikolaos-Georgios Leventis, July 2016

Contents

Abstract

The sources of metals and fluids in orogenic-Au deposits of Archean age is still under debate. This study tests the metamorphic model in the Archean Abitibi Greenstone Belt, Canada, an extensively mineralized area, that hosts a large number of orogenic Au-deposits and has been an exploration and mining centre for more than 150 years. The metamorphic model suggests that the metals and fluids that form orogenic gold deposits are produced from metamorphic devolatilisation reactions within the terrane hosting the deposits. This model is well accepted for Phanerozoic aged deposits but less so for Archean aged terranes. A complete set of metasedimentary rock samples were collected from the Pontiac subprovince, the Cadillac group and the Porcupine assemblage from the southern Abitibi and analysed for Au, As, Sb, Se, Te and Bi using low-detection limit methods at Stockholm University, Sweden. The metamorphic grade in the Pontiac increases southwards, with lower-grade rocks being adjacent to the Cadillac-Larder Lake Fault and the associated Au-deposits. For the Pontiac samples, the concentration in Au decreases systematically from 4.2 ppb (range 0.25 to 30 ppb) in biotite zone greenschist facies to 0.33 ±0.1 ppb in sillimanite zone amphibolite facies samples. Systematic decreases are also observed for As and Sb, but Se, Te and Bi show no systematic change with increasing metamorphic grade. The sillimanite zone rocks are significantly depleted in Au (-92%), As (-98%), Sb (-78%), C (-90%), and H_2O (-34%) than the biotite zone samples. The main pulse of water liberation occurred between garnet and staurolite zone conditions and coincides with the breakdown of chlorite at the greenschist-amphibolite facies transition. The hydrothermal fluid had an approximate composition of 89% H_2O and 11% CO_2. In situ LA-ICP-MS analyses in sulphides showed that Au is hosted in pyrite and that concentrations are above detection limits only in the biotite and garnet zone samples, indicating that the controlling mechanism for metal liberation during metamorphism is the Py-Po transition. Mass balance calculations show that >10t of Au, >32000t As, >360t Sb and >20Mt C could have been mobilised from each km^3 of Pontiac rock metamorphosed from biotite greenschist to sillimanite zone amphibolite facies conditions. Average Au concentrations are higher in the Pontiac than in the Cadillac and Porcupine samples, suggesting variable terrane-scale Au-fertility. The Pontiac subprovince dips north underneath the south-eastern Abitibi and its timing of metamorphism coincides the timing of orogenic Au-deposits formation (2680-2660 Ma). Thus, the Pontiac rocks represent a potential high fertility metasedimentary source of metals and fluids in the Archean orogenic-Au deposits of the southeastern Abitibi.

1. Introduction

Orogenic Au deposits provide the 2nd largest amount of gold globally, with world production and reserves having been estimated to 16k tons Au as of 2005 (Dubé and Gosselin, 2007). The study of orogenic Au deposits has driven geological research the last 100 years regarding Archean tectonics, metallogeny and ore exploration (Robert et al., 2005). They are found in metamorphic terranes of all ages, associated with greenschist facies metamorphic rocks and large-scale fault zones. The vast majority of gold endowment occurred in three distinct periods of time, during the Late Archean at ≈2.7 Ga, the Paleoproterozoic and the Phanerozoic era. Archean deposits are mostly hosted in metavolcanic or intrusive rocks in granite-greenstone belts, Proterozoic deposits are found in either metavolcanics or metasedimentary rocks and deposits of the Phanerozoic are dominantly hosted in metasedimentary sequences (Goldfarb et al., 2001).

The Abitibi Greenstone Belt in Canada is the largest and best preserved greenstone belt of Archean age in the world (Robert et al., 2005) and comprise the main source of Canadian gold production and reserves (81%, 4470 metric tons, (Dubé and Gosselin, 2007). It is located at the southeastern part of the world's largest craton, the Superior Province, and it mainly consists of metavolcanic rocks and igneous bodies. Metasedimentary sequences occur as well. On its southern part, it hosts a large number of ore deposits, dominantly situated proximal to the Cadillac-Larder Lake and Porcupine-Destor Fault Zones (Fig. 1.1).

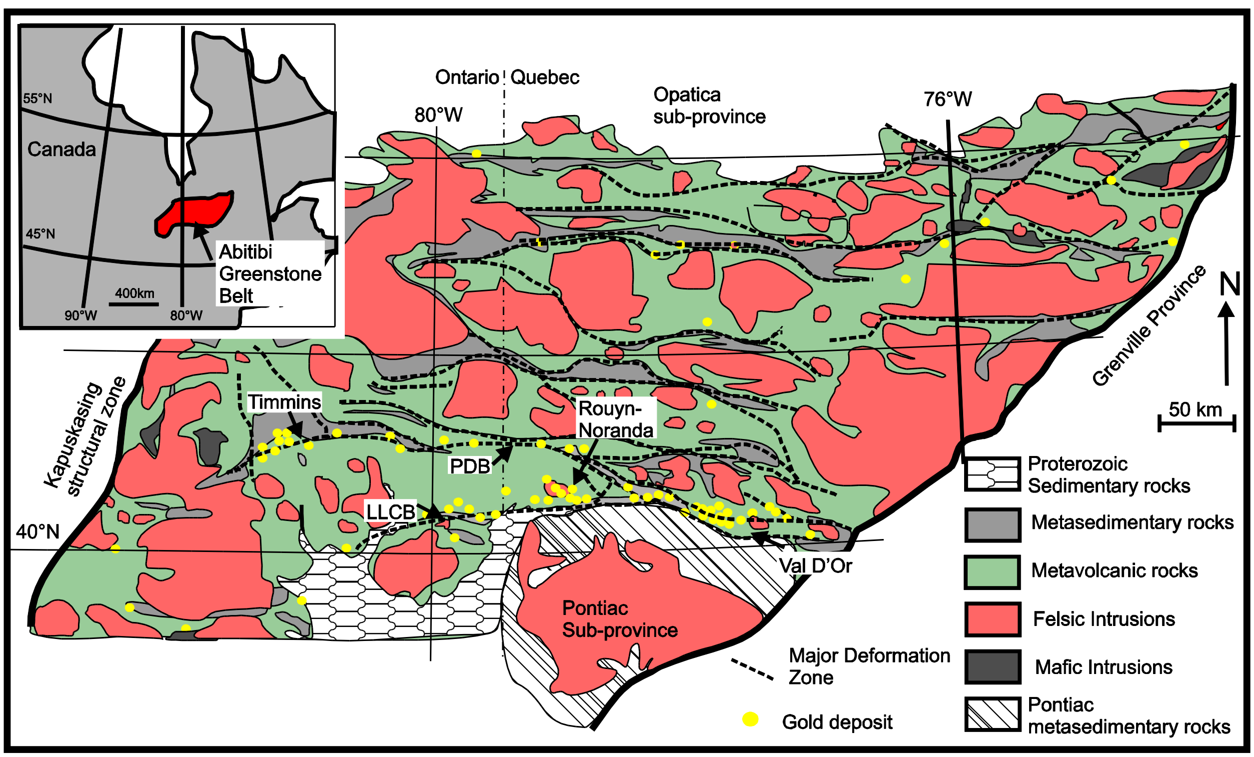

Figure 1.1. *The southeastern part of the Abitibi Greenstone Belt and its gold deposits situated along the Larder-Lake Cadillac "Break" or Fault Zone (LLCB) and the Porcupine-Destor Break (PDB). Modified after Mercier-Langevin et al. (2014).*

The proposed genetic models for the formation of orogenic Au deposits refer to magmatic, metamorphic, mantle and/or meteoric origin for the sources of metals and/or fluids (Goldfarb and Groves, 2015). Each different model and its accompanying genetic processes lead to diverse exploration techniques, so the constraint of the real mechanism of ore formation, is rather important in terms of developing exploration models for orogenic Au deposits. Despite the amount of research, there are still questions regarding the sources of metals and fluids in orogenic gold deposits (Goldfarb and Groves, 2015), especially for the Archean examples. The Phanerozoic deposits are better understood and their formation is strongly linked with the metamorphism of metasedimentary rocks (Pitcairn et al., 2006a; Pitcairn et al., 2015).

1.1. Aim of the study

This study aims to test the metamorphic model of orogenic Au deposits formation in the Archean-aged Abitibi Greenstone Belt in Canada, by investigating metasedimentary rocks as potential sources. Samples were collected from three different metasedimentary sequences, the Pontiac subprovince, the Cadillac group and the Porcupine assemblage in southern Abitibi. The principal aim of this research study is whether the metal content of these metasedimentary rocks is systematically decreasing with increasing metamorphic grade, as reported in other sequences associated with orogenic Au mineralisations (Pitcairn et al., 2006a; 2015). This hypothesis is tested through:

1) analyses for Au and related elements (As, Sb, Se, Te, Bi) with low-detection limit methods (Pitcairn et al., 2006b)
2) the investigation of the trace element content in sulphides, and
3) the determination of which minerals and/or mineral reactions control the distribution of metals and fluids in the rocks.

Thus, it will be evaluated whether these sequences might represent a potential source to the formation of the adjacent gold deposits. The study and comparison between different sedimentary sequences (Pontiac, Cadillac, Porcupine) in terms of metal potential introduces the concept of variable terrane fertility which is considered as controlling factor to ore endowment.

This study aims to shed light upon the sources of metals and fluids in orogenic Au deposits of Archean age.

2. Geological Setting

2.1. Superior Province

The Superior Province is located in Canada and is the world's largest craton of Archean age, occupying an area of 2 Mkm^2 (Calvert and Ludden, 1999; Davis, 2002; Robert et al., 2005). It has produced >8,500 t Au, which has driven both research and the mining industry the last 100 years (Robert et al., 2005). It grew through subduction-related accretion tectonics and experienced several periods of magmatism and deformation due to successive collision of oceanic arcs and micro-continental fragments ("terranes") (Calvert and Ludden, 1999; Davis, 2002; Robert et al., 2005). Its southeastern portion is dominated by rocks of the Opatica Subprovince to the north, an amphibolite facies gneissic terrane, the well-known Abitibi Greenstone Belt with its abundant ore mineralizations, and the Pontiac subprovince to the south. The rocks are progressively younger towards the Pontiac which is interpreted to indicate the southward migration of the subduction zone and the progressive accretion of domains to the south through time (Dimroth et al., 1982; Calvert and Ludden, 1999). Cessation of volcanism corresponded to increase in clastic sedimentation which included greywackes, mudstones (Porcupine and Callidac groups), conglomerates (Timiskaming group) and extensive areas of turbidites (Pontiac; Robert et al., 2005). Collisional events occurred 2720-2710 Ma in the northern part of the Superior craton and at about 2680 Ma in its southern part. The terminal stage of orogeny is bracketed from 2660 to2650 Ma (Robert et al., 2005).

The Opatica Belt consists of amphibolite-facies rocks and gneisses with ages 2800-2702 Ma. The older pluton of the domain ("Lac Rodayer") is located in the northern part and intruded between 2833 and 2820 Ma. In the central part of the belt, migmatites and late (2691-2680 Ma) granites also occur. The whole terrane experienced three phases of deformation at 2702, 2700-2690 and 2665-2657 Ma respectively. The deformation involved folding, shearing and faulting events (Robert et al., 2005). The latter refers to the formation of large-scale SE trending strike-slip shears, having also affected the northern Abitibi Belt (Calvert and Ludden, 1999).

2.2. Abitibi Greenstone Belt

The Abitibi Greenstone Belt (AGB) is the largest and the best-preserved greenstone belt of Archean age in the world. It consists of both mafic and felsic rocks with ages ranging ≈2730-2680 Ma (Jackson and Cruden, 1995). Its northern boundary with the Opatica Plutonic Belt corresponds to the Casa-Berardi tectonic zone and its southern one which separates it from the adjacent Pontiac subprovince, is the Cadillac-Larder Lake Fault zone (Feng et al., 1992; Calvert and Ludden, 1999). The Abitibi Belt is further divided into three main zones, the Northern Volcanic zone (NVZ), the Central Granite-Gneiss zone and the Southern Volcanic zone (SVZ) (Calvert and Ludden, 1999). At its southern part, it is overlain by the Huronian Supergroup, a Paleoproterozoic sequence of sedimentary rocks (Dimroth et al., 1982).

The Belt represents an ancient arc-trench system which also exhibits progressively younger rocks from north to south, supporting the idea of the southward migration of an arc-type system (Jackson and Cruden, 1995). The very last stage of orogeny involved continental collision (≈2.7-2.68 Ga) and terrane-scale thrusting, with deformation of the volcano-sedimentary sequences of the Abitibi and pluton emplacements such as the Preissac-Lacorne Batholith (Dimroth et al., 1983a; Robert et al., 2005).

2.2.1. Northern Volcanic Zone & Central Granite-Gneiss zone

The Northern Volcanic Zone formed from multiple stages of volcano-sedimentary evolution, basin development, deformation and plutonism (Chown et al., 1992). It represents an ancient volcanic arc, mainly composed of two (mafic & felsic) volcanic cycles overlain by an epiclastic sedimentary sequence. The mafics consist of basalt plains aged 2730-2725 Ma and the felsic, second phase of volcanism took place ≈2722-2712 Ma. Syn-volcanic/tectonic intrusions (diorites and tonalites) were emplaced into two age groups (2722-2714 and 2703-2690 Ma respectively) with terminal shoshonites being extruded between 2710 and 2705 Ma and late-deformation plutons intrude as late as 2479 ±69 Ma. Dextral faulting occurred at 2695-2690 Ma) and refers to late, localized extension (Chown et al., 1992). Seismic data suggest that the NVZ was obducted onto the Opatica Belt during the Opatica-Abitibi collision (Calvert and Ludden, 1999).

2.2.2. Southern Volcanic Zone (SVZ)

The Southern Volcanic Zone (SVZ) is located in the southern part of the Abitibi belt and hosts the vast majority of gold deposits of the Abitibi (Fig. 1.1). It is characterized by numerous volcanic units and has been interpreted as a back-arc basin environment which then collided with the Pontiac subprovince (Feng et al., 1992; Davis, 2002). Komatiites and other ultramafic rocks of the SVZ display slight to negligible crustal contamination which indicates the probable involvement of a mantle plume which provided material from deep asthenospheric sources (Corfu and Noble, 1992; Calvert and Ludden, 1999; Davis, 2002). Ages are significantly younger than in the NVZ and bracketed 2715-2694 Ma (Corfu et al., 1989) while the oldest rocks of the SVZ appear slightly younger than the ones of the central and northern Abitibi, a fact which supports the model of southward migration of an ancient subduction zone (Calvert and Ludden, 1999). The evolution of the zone is associated with successive volcanic cycles, basin formation and sedimentary rocks deposition, metamorphism, pluton emplacement and regional faulting (Dimroth et al., 1983b). The tectonic accretion of the SVZ is constrained 2685-2680 Ma (Davis, 2002).

Volcanic cycles

Throughout the whole Abibiti Belt, three volcanic cycles have been identified and thoroughly studied (Dimroth et al., 1982; Corfu et al., 1989). The correlations between the rocks of the cycles firstly relied upon lithostratigraphic similarities and not exact or reported ages (Dimroth et al., 1982). Later geochronological studies have shed light to the age of the rocks in the area (Corfu et al., 1989; Corfu and Noble, 1992).

Cycle 1 is represented by the Hunter Group (2713 ±2 Ma, Corfu et al., 1989) which is located near Lake Abitibi and consists of rhyolitic flows with thickness exceeding 2 km. Minor basaltic flows are also present (Dimroth et al., 1982). In Timmins, Ontario, it corresponds to the Upper Deloro Formation (2725±1 Ma) which contains volcanoclastic rocks and shows limited crustal contamination (Corfu and Noble, 1992).

Cycle 2 is further divided into three divisions, the lower ultramafic, the middle tholeiitic and the upper diverse division. The Roquemaure-Stoughton Group (tholeiitic komatiite flows, ≈7 km thickness, 2714 ±2 Ma, (Corfu and Noble, 1992) and the Malartic Group (peridotitic komatiites flows and also tholeiites, ≈6 km thickness) represent the lower ultramafic division in the central and eastern Abitibi respectively. In the western part, the Roquemaure-Stoughton Group is correlated with the lower Tisdale Formation in Ontario side (Corfu et al., 1989).

The middle, tholeiitic division of Cycle 2 comprise the Kinojevis Group (2702-2701 Ma), which displays mantle provenance and consists of tholeiitic flows with coarse plagioclase phenocrysts but also minor intercalated rhyolites (Corfu and Noble, 1992; Ayer et al., 2002). To the southeast, it displays variation in rock composition and has been further subdivided into the Jacola (pyroxenitic komatiite flows, 2703.8 ±1.3 Ma) Val D'Or (rhyodacites, 2704 ±2 Ma) and Heva (felsic volcaniclastics, 2702 ±1 Ma) formations (Dimroth et al., 1982; Mueller et al., 2012) and references therein) (Fig. 4.2). In Timmins area (to the west), it correlates with the Middle Tisdale Formation (Corfu et al., 1989).

Lastly, the "upper diverse" division comprises the Blake River Group (BRG) (2701 ±2 Ma) which is mainly composed of both mafic volcanic rocks and several, felsic volcanics as well. It correlates with the "Upper Tisdale Formation" to the west, which is dated 2703 ±1.5 Ma (Corfu et al., 1989). Recent studies proposed that Blake River rocks' represent an Archean mega-caldera complex with successive volcanic centers. In addition, the evolution of the volcanic complex has been correlated with the formation of southeastern Abitibi VMS deposits (Pearson and Daigneault, 2009).

The magmatic suites of the southern Abitibi comprise are described in the literature as TTG (tonalite-trondhjemite-granodiorite, syn-volcanic, 2700 Ma), TGGM (tonalite-granodiorite-granite-monzodiorite, syn-tectonic, 2695-2680 Ma) and SMG (sub-alkaline monzogranite, late-tectonic, 2685-2670 Ma). Their age distribution clearly shows the temporal evolution of the arc system; the emplacement of shoshonites indicates the end of activity in the area (Feng et al., 1992).

Sedimentary sequences

Sedimentary rocks occur in narrow, structurally-controlled basins that formed between 2690 to 2680 Ma and isotopic data indicate terrigenous provenance for these sediments (Feng et al., 1993). The most distinguished sequences are the Porcupine assemblage in Timmins area to the west, and the Cadillac (or Kewagama) Group to the east. These sequences were deformed and metamorphosed within the deforming arc or back-arc complex, at the same time as deposition and early deformation occurred in the Pontiac subprovince to the south (Davis, 2002). Lastly, the Timiskaming Group, a shallow marine sequence of metasandstones, is found along the PDF and CLL fault zones (Ayer et al., 2002; Robert et al., 2005).

Cadillac Group metasediments

The rocks of Cadillac Group are found near the town of Cadillac, Quebec and consist of >70% metamorphosed greywackes and argillites. Zircon studies showed that its depositional age is <2687±3 Ma (Davis, 2002) and it is interpreted that they have been deposited on submarine fans along with pelagic facies graphitic shales (Dimroth et al., 1982). The Cadillac Group is also correlated with rocks of the Kewagama Group, which is exposed to the eastern side of the Belt and on the northern side of the Cadillac-Larder Lake Fault, towards the Porcupine-Destor Fault (Lajoie and Ludden, 1984).

Porcupine assemblage

The metasedimentary rocks of the Porcupine assemblage are exposed in the western part of the Abitibi Belt and are closely associated with the Porcupine-Destor Fault zone. They consist of wackes and mustones of turbiditic origin and minor conglomerates (≈2696-2692 Ma) (Ayer et al., 2002; Robert et al., 2005). The sequence unconformably overlies Tisdale Formation and displays maximum depositional ages of 2699- 2685±6 Ma. Several zircon inheritance ages are reported suggesting provenance from volcanic rocks from the Abitibi Belt or the northernmost Opatica Plutonic Belt (Ayer et al., 2002).

Timiskaming assemblage

Rocks belonging to the Timiskaming assemblage are found in narrow zones proximal to the Porcupine-Destor and Cadillac Larder Lake Fault zones and comprise immature, coarse-grained sandstones and polymictic conglomerates of alluvial-fluvial origin (Ayer et al., 2002). Its age is bracketed ≈2685-2675 Ma and provenance suggest variable sources from volcanic rocks of the Abitibi Belt (Ayer et al., 2002).

Lacorne Block

The Lacorne Block represents a high-grade tectonic window of the Pontiac Subprovince in the SVZ of the Abitibi Belt (Feng and Kerrich, 1990; Feng et al., 1992). The block was uplifted at ≈2630 Ma, later than both metamorphism and overstacking of the subducted Pontiac rocks (Feng et al., 1992). It consists of St-Bt schists, amphibolite-facies metasedimentary rocks, plutons and pegmatites and contains old, 3 Ga detrital zircons (Feng and Kerrich, 1991; Feng et al., 1993). The rocks were intruded by syn- to late-tectonic monzodiorite-monzonite-granodiorite-syenite (abbreviated as MMGS, 2690-2670 Ma) and the syn-collisional S-type garnet-muscovite granite (GMG, 2643±12 Ma) (Feng and Kerrich, 1991). These magmatic suites are of similar affinity with the ones found in the central and southern Pontiac Subprovince (Feng et al., 1993). The sediments of the Lacorne Block contain 3042±6 Ma zircons, older than the SVZ which surrounds it, indicating a different material source, pointing out and supporting the idea of being an allochthonous terrane (Feng and Kerrich, 1991).

2.3. Pontiac Subprovince

The Pontiac subprovince is a late Archean metasedimentary granitoid-gneiss terrane situated along the southeastern margin of the AGB (Benn et al., 1994). It is limited to the north by the Cadillac-Larder Lake fault zone, a major, steep-dipping reverse shear zone >200km long (Dimroth et al., 1983a). It mainly consists of sedimentary rocks of intermediate-pressure metamorphism (Feng et al. 1992) (part of the Kenoran orogenic cycle), igneous intrusions (syn-tectonic MMGS Lac Frichette, and Decelles Batholith) and the Opasatica gneiss (Feng et al., 1992; Camiré et al., 1993; Mortensen and Card, 1993; Benn et al., 1994). The metasedimentary sequence is mainly exposed in the northern part of the subprovince and consists of flyschoid greywackes, pelites and also quartz-rich sandstones, deposited as turbidites in a fore-arc tectonic setting (Feng et al., 1992; Benn et al., 1994).

Zircon U/Pb dating bracketed the deposition of the Pontiac sediments from 2695 to 2685 Ma. Geochemical studies indicated that the source material for these rocks was mostly derived from felsic igneous rocks with a minor addition of an older (3-2.8 Ga) evolved component (Corfu and Noble, 1992; Feng et al., 1993; Mortensen and Card, 1993). Sedimentation in the Pontiac was coeval with arc volcanism and regional deformation to the north (Southern Abibiti Belt, SVZ) (Davis, 2002).

The sequence experienced its first metamorphic event at 2670±5 Ma but there are also younger ages reported, while it is not clear whether they indicate a second thermal event or later, low-T fluid infiltration which resets the isotopic systems (Feng et al., 1992). The domain collided with the Abitibi Belt to the North and syn- to late- tectonic plutons intruded the sequence (Dimroth et al., 1982).

Structural studies have indicated that schistosity becomes steeper towards the north, in the contact with the Cadillac-Larder Lake fault zone (Camiré et al., 1993) supporting the idea of a relict accretionary prism of a northward-dipping subduction zone (Calvert and Ludden, 1999). The proposed wedge-shape geometry of the Pontiac sequence being under-thrusted beneath the southern Abitibi Belt is coupled with seismic studies and evolutional models which show the characteristic prism geometry of the Pontiac metasediments extending beneath the Abitibi Belt to the north (Dimroth et al., 1982; Calvert and Ludden, 1999) (Fig 7.10). Geochemical evidence from late orogenic intrusions in the SVZ indicate the probable release and involvement of fluids from the subducted sediments towards the overriding plate (Corfu and Noble, 1992).

The metamorphic grade in the Pontiac increases southwards, with evidence for the presence of a complete Barrovian-type sequence with rocks of biotite zone greenschist to sillimanite zone amphibolite facies (Benn et al., 1994; Davis, 2002). The sillimanite zone rocks are in contact with the igneous complexes ”Lac Frechette” (MMGS series, monzonites-monzodiorites-syenites) emplaced at ≈2675 Ma and Decélles Batholith (GMG series, garnet-muscovite granite) dated 2663-2635 Ma (Feng et al., 1993) which are exposed in the middle of the sub-province (Dimroth et al., 1982; Benn et al., 1994). The mineral assemblage of the metasedimentary rocks is quartz + plagioclase + biotite ± muscovite ± chlorite ± garnet ± staurolite ± kyanite ± sillimanite (on each characteristic metamorphic zone and mostly occur in thin pelitic beds) ± K-feldspar ± ilmenite ± rutile with minor apatite, sphene, tourmaline, epidote and calcite (Camiré et al., 1993). Lastly, in the western part of the sub-province lies the Opasatica Gneiss which is strongly foliated, lineated and locally migmatized. The age of the last metamorphic event has been constrained at 2660 Ma (Benn et al., 1994).

3. Orogenic Gold Deposits

3.1. General characteristics

Orogenic gold deposits, also referred to in the literature as “shear-zone hosted”, “mesothermal” or “gold-only” deposits, are a specific type of gold deposit distributed along major compressional or transpressional crustal-scale fault zones (McCuaig and Kerrich, 1998; Goldfarb et al., 2005). They are found in deformed accretionary belts and metamorphic terranes of all ages and are frequently located between terrane boundaries (Groves et al., 1998). The deposits primarily occur in greenschist facies rocks and are hosted in variable rock types including mafic-ultramafic volcanic rocks, Fe-rich tholeiites, granitoids or clastic metasedimentary rocks and banded iron formation (BIF) (Groves et al., 1998; Robert et al., 2005; Dubé and Gosselin, 2007). However, there are also examples of orogenic mineralization hosted in sub-greenschist or even amphibolite-granulite facies rocks (Groves, 1993). Orogenic Au deposits are emplaced in compressional-transpressional tectonic settings, frequently along terrane boundaries of either collision between continental terranes or continental-oceanic crust convergence (Groves et al., 1998).

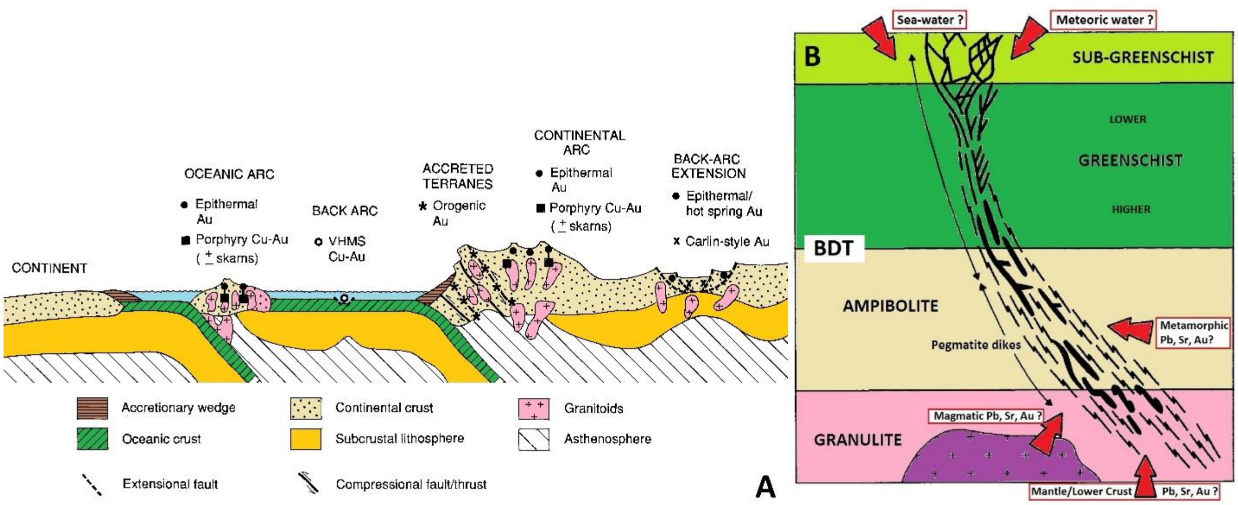

Figure 3.1. *A) The tectonic setting where various gold deposit types form (modified after* Groves et al., 1998)*. B) The “crustal continuum model”, crustal profile during orogenic-Au mineralization (modified after* Groves, 1993)*.*

The deposits are structurally controlled and occur proximal to major crustal fault zones (Fig 3.2) although the 2nd and 3rd order structures are commonly those that are most heavily mineralized (Groves, 1993; Kerrich and Cassidy, 1994; Robert et al., 2005).

There are examples of deposits hosted in amphibolite-granulite facies rocks, therefore they form in a variety of depths in the crust and in variable P-T conditions (180-700 °C and <1-5 kb) (Groves et al., 1998). The ore-hosting structures comprise steeply dipping brittle faults in low-grade greenschist facies rocks, brittle-ductile shear zones in mid-crustal depths, and ductile shear zones and isoclinal folds in high-grade rocks (Robert et al., 2005). This fact has introduced the concept of an extensive, continuous hydrothermal system throughout the crust; the “crustal continuum model” (Groves, 1993 - Fig. 3.1B). The crustal-scale fault zones display reverse and/or strike-slip motion are considered to be the pathway of hydrothermal fluids towards higher crustal levels (Groves et al., 1998; Dubé and Gosselin, 2007).

The most common mineralization style is Qz-carbonate veins but disseminated sulphides or stockwork mineralization also occur. The ore can be also found in brecciated zones at lower grade rocks, or fold hinges at higher ones (Robert et al., 2005; Dubé and Gosselin, 2007). The timing of mineralization is typically syn- to post-peak metamorphic and gold is precipitated syn-kinematically (Kerrich and Cassidy, 1994; McCuaig and Kerrich, 1998). The deposits are characteristically enriched in Au, Ag, As, W, B, Sb, Te and Mo. Gold:silver ratio ranges ≈5-10. Base metal concentrations (Cu, Zn, Pb) generally display slight, but not remarkable, enrichment (Groves et al., 1998).

Gold is transported as reduced sulphur complex, mainly in the form of $Au(HS)_2^-$ under neutral pH conditions (Seward, 1973; Stefánsson and Seward, 2004) and deposition takes place at 300 ±50 °C and 1-3 kb (Groves et al., 1998). The hydrothermal fluids are dominantly H_2O-CO_2±CH_4 fluids of low salinity (typically <5 wt%) (Kerrich and Cassidy, 1994), with anomalous concentrations of CH_4 (methane), N_2, K and sulphur (S) (Dubé and Gosselin, 2007). The deposits often display large-scale carbonate alteration (Fe-carbonatization, ankeritic) and sericitization while there is no evidence for vertical metal zoning.

Ore mineralogy consists of native gold, pyrite, ± arsenopyrite ± pyrrhotite ± chalcopyrite or disseminated sulphides at low metamorphic grades and pyrrhotite ± arsenopyrite ± loellingite ($FeAs_2$) at higher metamorphic grades (Groves, 1993). Gangue minerals involve quartz, albite, chlorite, tourmaline ± scheelite ± fuchsite. Carbonates (calcite, dolomite, ankerite ± siderite) and alkali metasomatism comprise the alteration assemblages in lower metamorphic grade rocks, while amphiboles and -in lesser extent-carbonates mostly occur in higher-grade rocks (Groves et al., 1998; McCuaig and Kerrich, 1998).

Gold endowment eras

Orogenic Au deposits were produced in three distinct periods of the geological history; during the Archean, the Paleoproterozoic and the Phanerozoic. The vast majority of Archean deposits are sited in volcanic-plutonic rocks (greenstones) while Paleoproterozoic deposits are hosted in both magmatic and metasedimentary rock sequences (Goldfarb and Groves, 2015). The deposits of Phanerozoic age are mostly hosted in clastic sedimentary rock sequences (Pitcairn et al., 2006a; Goldfarb and Groves, 2015).

The Abitibi Greenstone Belt in Canada (>5600t Au), the Eastern Goldfields in Yilgarn Craton, W. Australia (2800t Au), the Rio das Velhas in SE South America (950t Au) and the Dhawar Belt in India (≈875t Au) comprise noteworthy gold provinces of Archean age. Proterozoic deposits of high production occur in Birimian Greenstone Belt, W. Africa (1550t Au) and the Trans-Hudson orogen, Central-North Canada (>1250t Au). Phanerozoic domains comprise the Lachlan Fold Belt, SE Australia (1050t Au), Central Asia (Muruntau, Uzbekistan and others, 1550t Au), Russia (Ural Mountains) and the Juneau gold belt, E. Alaska (≈220t Au) (Goldfarb et al., 2001).

The apparent ≈2 Ga gap in orogenic gold deposits formation (2.4-0.3 Ga) is discussed to reflect lack of gold-enriched sources areas, differences in plate tectonics style and motion and their influence to related tectonic settings (extension, rifting and anorogenic magmatism), and different thermal state of the lithosphere at that time (Goldfarb et al., 2001). Probably, changes in plate motions and tectonic settings, in favor towards the formation of gold deposits, thrived during the gold endowment eras; though the exact mechanism(s) which drove gold mineralization in Archean terranes is difficult to be precisely defined (Groves, 1993; Goldfarb and Groves, 2015).

3.2. Abitibi deposits

The Abitibi Greenstone Belt is one of the most mineralized zones in the world with Au deposits having produced more than 6000 tons of Au during time, continuously being mined since the 1920s (Robert et al., 2005). It hosts a significant number of orogenic Au deposits some of which are considered as "world-class" (>100 t, ≈3.2 Moz Au), and also Zn-Cu VMS or Au-rich VMS deposits (Robert et al., 2005). Average Au grade for the orogenic gold deposits in the Abitibi is ≈8-8.5 g/t, slightly higher than the globe average (7.6 g/t) (Dubé and Gosselin, 2007). They all lie upon the Timmins-Val d'Or gold belt (5600t Au) which occupies an area of 30,000 km² (400km x 75km), comprising the largest and best-defined gold belt in the Superior craton (Robert et al., 2005). Camps with >150t Au ("world-class" type) comprise the quartz-carbonate vein hosted Hollinger-McIntyre, Kirkland Lake and Dome in Ontario, and Sigma Lamaque, Québec; the Campell-Red Lake which displays both Qz-carbonate veins and sulphidic replacements and the Cu-Mo-rich Malartic, Hemlo and Kerr Addison deposits on which the ore is found in disseminated stockwork zones (Fig. 3.2) (Robert et al., 2005).

All these Au-deposits are mainly distributed along the Cadillac-Larder Lake and Porcupine-Destor Fault zones and the orogenic examples are spatially and temporally linked with the final stages of orogeny, when terrane accretion, deformation and plutonism occurred in the southern Superior Province, between 2700 and 2630 Ma (Kerrich and Cassidy, 1994; Robert et al., 2005). Field and geochronological evidence indicate at least two gold mineralization events while discussion about the sources of metals has already started since the 80s (Robert et al., 2005).

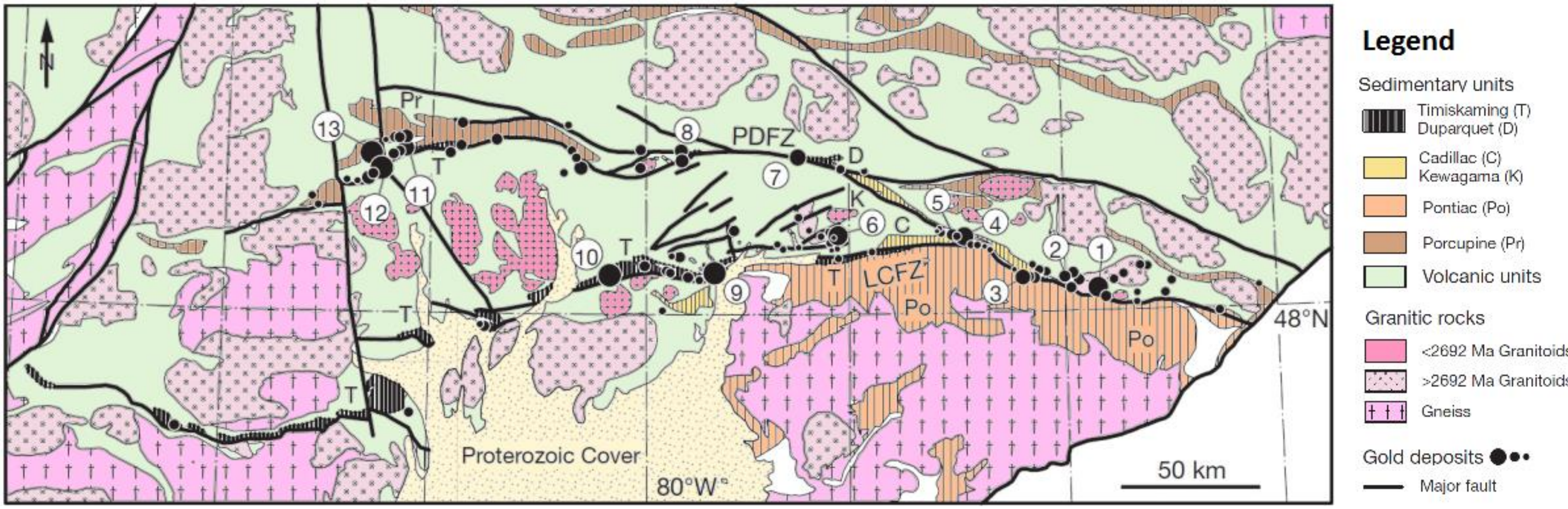

Figure 3.2. *Simplified map of the SE Abitibi showing the localities of important gold deposits. 1. Sigma-Lamaque, 2. Camflo, 3. Malartic, 4. LaRonde, 5. Doyon, 6. Horne, 7. Beattie, 8. Holloway, 9. Kerr Addison, 10. Kirkland Lake, 11. Pamour, 12. Dome, 13. Hollinger-McIntyre. Modified after Robert et al., 2005.*

3.3. Genetic models

There are several genetic models proposed for the formation of orogenic Au deposits involving magmatic, metamorphic and mantle sources (Thompson and Newberry, 2000; Pitcairn et al., 2006a; Phillips and Powell, 2010). The sources of metals and fluids in Archean deposits is still debated (Goldfarb and Groves, 2015), while the formation of Phanerozoic deposits is better understood, with the metamorphic model being generally accepted (Pitcairn et al., 2006a; Pitcairn et al., 2010; Large et al., 2012).

The metamorphic devolatilisation model has been highly supported by studies which demonstrated simultaneous leaching and mobilisation of Au and related metals by metamorphic fluids in Phanerozoic terranes (Pitcairn et al., 2006a; 2015). This hydrothermal fluid was internally produced during prograde metamorphism of the sedimentary pile and transported significant amount of Au, Ag, As, Sb, Hg, Cd, Mo and W from the Otago and Alpine Schists, New Zealand (Pitcairn et al., 2006a) and Au, As and Sb from the Dalradian of Scotland (Pitcairn et al., 2015). The amount of fluid produced in the Otago has been attributed to the breakdown of chlorite which indirectly drives the pyrite-pyrrhotite transition; the controlling reaction for metal liberation during metamorphism (Pitcairn et al., 2010).

It is now discussed whether potential metal and/or fluid sources come from high fertility sedimentary rocks of limited volume (Large et al., 2012), whole sedimentary sequences (Pitcairn et al., 2006a; Pitcairn et al., 2015) or metamorphosed volcanic rocks (Phillips and Powell, 2010). The metamorphic model suggests that metals are released during the metamorphic transition from pyrite to pyrrhotite; which commonly accompanies the production of metamorphic fluid due to chlorite breakdown at the greenschist to amphibolite facies transition (Phillips and Powell, 2010). The aforementioned mechanisms comprise the controlling factors for metal and fluid production respectively, related to the formation of orogenic Au deposits. Metamorphic devolatilization will though not proceed to the formation of a gold province if the source rocks lack Au, carbonates, or sulphide minerals (Phillips and Powell, 2010).

Some gold deposits often occur near igneous bodies or just show magmatic isotope sources, so the magmatic model refers to the involvement of fluids and/or metals provided by deep magmatic suites to the adjacent orogenic, shear-zone system (Fig. 3.1B). Evidence involve fluid inclusion and Pb-isotope studies (Sillitoe and Thompson, 1998). The contribution of a fertile upper lithospheric mantle towards higher crustal rocks has also been described as a potential source of metals (Hronsky et al., 2012). In addition, the interaction with mantle plumes has also been hypothesized because of the strong association the deposits have with komatiites. The hypothesis comprises the drifting of a continental terrane over a mantle plume, or simultaneous presence of a plume in a convergent setting (Wyman et al., 2002; Dubé and Gosselin, 2007). Another scenario involves the convection of surface water (meteoric or seawater); this mainly accounts for orogenic deposits sited shallow in the crust, in lower sub-greenschist facies rocks. The involvement of these type of fluids most likely takes place in the later stages of mineralization (Groves, 1993).

Several studies have pointed out geochemical differences between the proposed models. Absolute distinction between magmatic/metamorphic/mantle origin for the ore fluids is difficult since hydrothermal fluids can also show mixed sources and immiscibility (Robert and Kelly, 1987; Beaudoin and

Chiaradia, 2016). The combination of different techniques along with geochemical data can provide strong evidence for or against each proposed model. The metamorphic model has a major advantage over alternative models because gold can be leached from the rock and dissolve in the fluid at the same time as the fluid forms during prograde metamorphism (potential both metal and fluid source) (Phillips and Powell, 2010; Tomkins, 2010).

4. Sampling

Fieldwork was conducted in Canada in summer 2016 with the aim to collect a representative suite of metasedimentary rocks from the Abitibi and Pontiac subprovince. A set of 121 metasedimentary rock samples was collected from the Pontiac subprovince, the Cadillac group and the Porcupine assemblage within the SVZ of the Abitibi Belt. Rocks from the Pontiac were collected in N-S transects from lowest (biotite zone) to highest (sillimanite zone) metamorphic grade (Fig. 4.1) following the main roads south of Rouyn-Noranda and Val D'Or, Quebec. The majority of the samples were collected from road-cuttings, which offered the freshest bedrock exposures. A set of samples of increasing metamorphic grade was also collected from the Cadillac Group, north of the town of Cadillac in Québec and also from the Porcupine assemblage east of Timmins, Ontario. Rock samples showing evidence of surface weathering or abundant veining were avoided.

4.1. Pontiac samples

A complete Barrovian-type sequence occcurs south of Rouyn-Noranda, Québec (Fig. 4.1) (Benn et al., 1994). Sampling was conducted in transects which have almost been striking N-S, straight along the metamorphic zones via the domestic roads (from W to E) 101, 391 and Route des Pioneers respectively. South of Val D'Or, sampling on a straight line has been difficult due to lack of exposure (Fig. 4.2); though samples collected, were taken from all metamorphic zones present in the area.

Sampling in the Pontiac; in total, 22 samples were collected from the biotite zone; 11 from the transects south of Rouyn-Noranda and 11 more, from the low-grade sequence south of Val d'Or, Québec. Fourteen (14) samples were collected from the garnet zone. A total of 22 samples were collected from the staurolite zone; 12 samples from the transects south of Rouyn-Noranda and 10 more, from the high-grade sequence south of Val d'Or, Québec. Lastly, 14 kyanite zone and 13 sillimanite zone samples completed the set (Appendix 1.1).

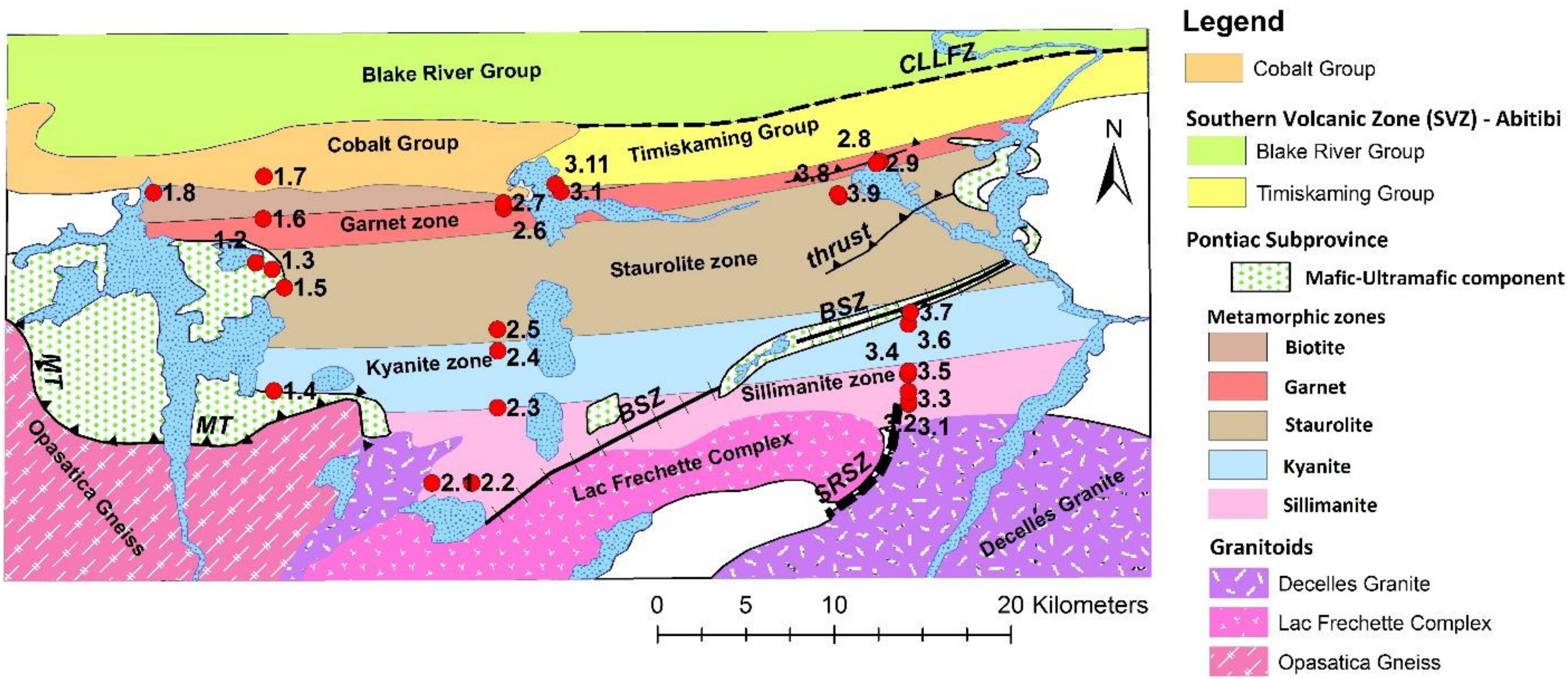

Figure 4.1. *Simplified geological map of the study area in the northern Pontiac subprovince. Red dots indicate sample localities (Appendix 1.1). Modified after Benn et al. (1994). Abbreviations: CLLFZ – Cadillac-Larder Lake fault zone, MT – Montbeillard thrust, BSZ – Bellecombe shear zone, SRSZ – Saint-Roch shear zone.*

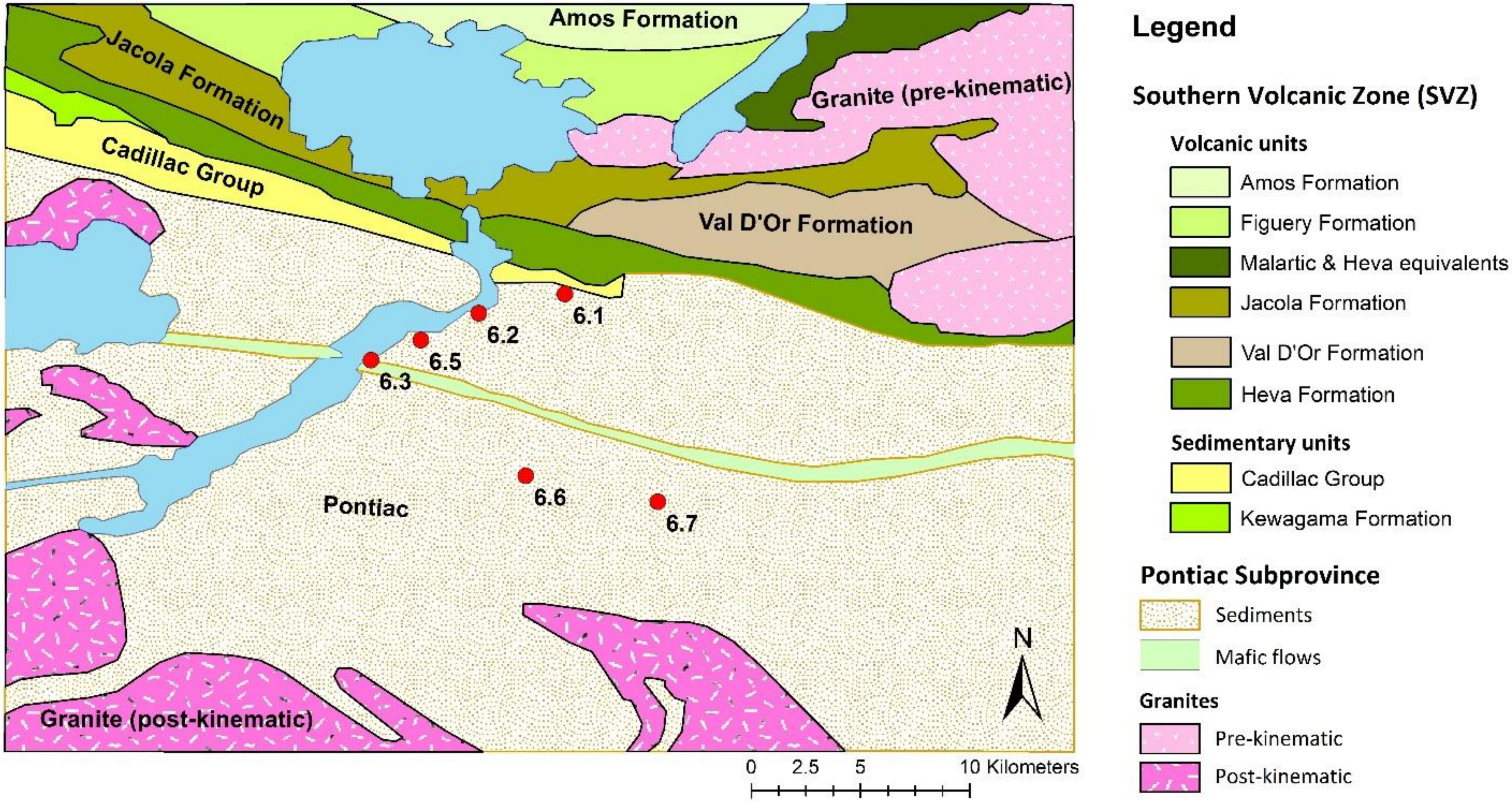

Figure 4.2. *Geological map of the study area south of Val d'Or, Québec. Red dots indicate sample localities (Appendix 1.1). Modified after Dimroth et al. (1982).*

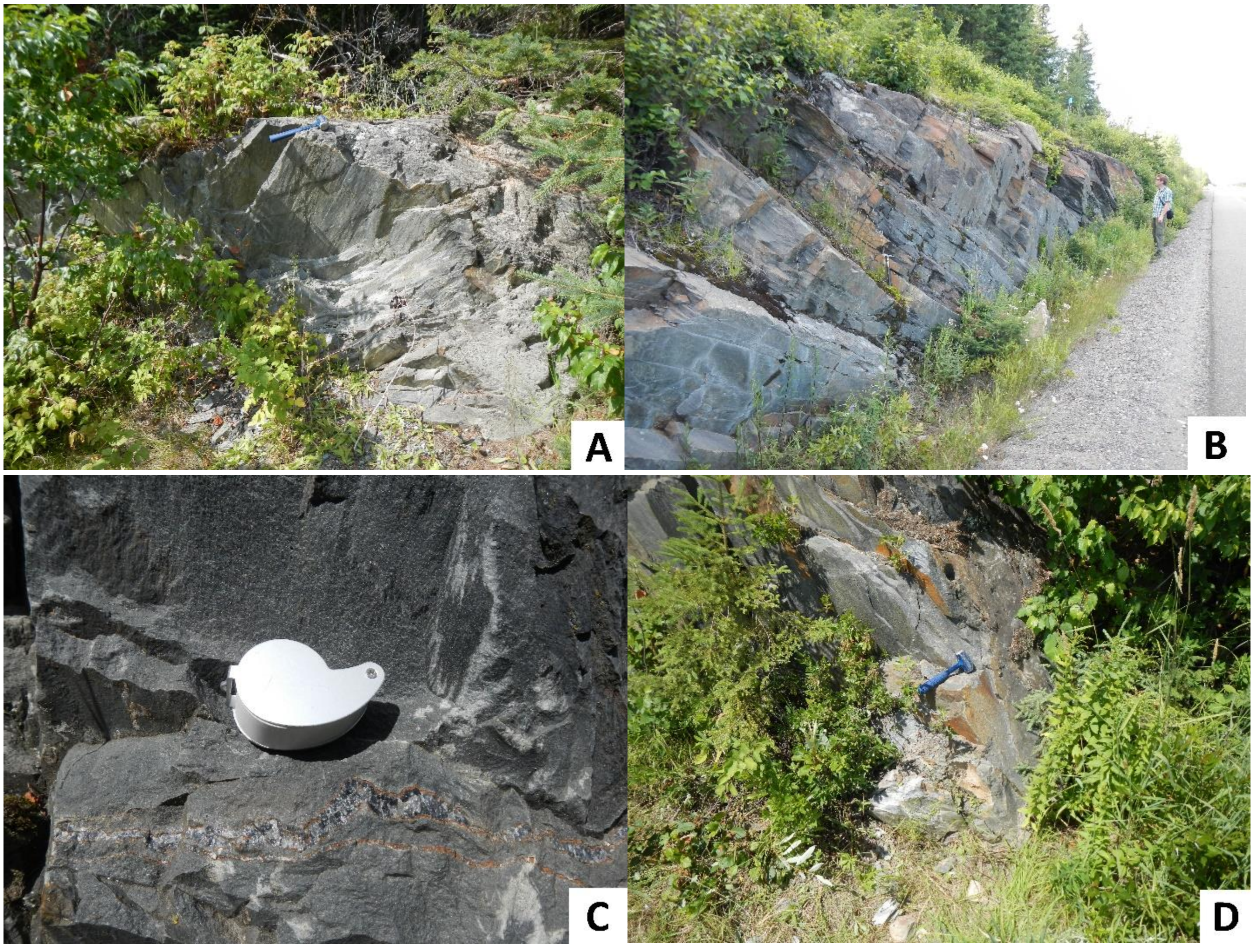

Figure 4.3. *Selected field photographs from the sampling of the Pontiac sediments. A) Exposure at stop 3.10 inside the biotite zone. B) Road-cutting exposure at sampling stop 1.6 inside the garnet zone. C) Ankerite vein alteration on site 2.8 in the garnet zone. D) Bedrock exposure on site 3.7 in the kyanite zone.*

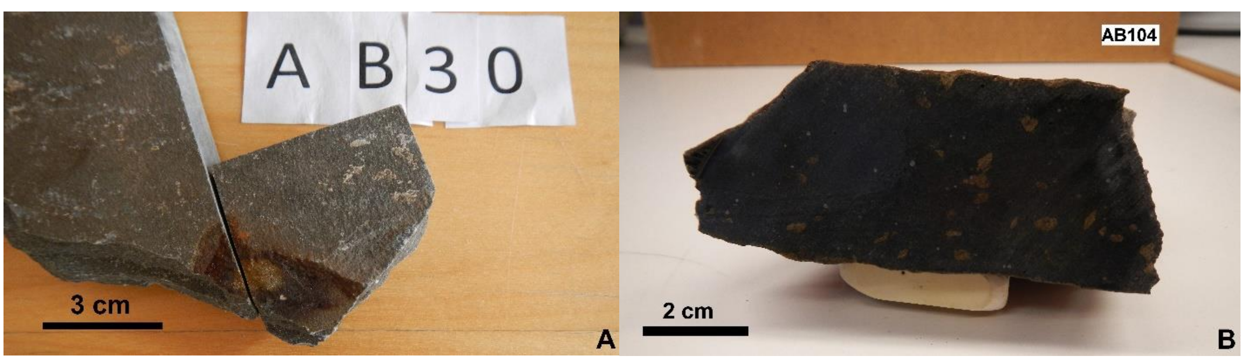

Figure 4.4. *Hand-samples from the Pontiac subprovince with: A) oxidized pyrite aggregates and B) subhedral-euhedral staurolite crystals.*

4.2. Cadillac Group samples

A total of 20 samples were collected from the Cadillac Group north of Cadillac town, Québec comprising chlorite- and biotite- zone samples (Fig. 4.5). The set includes nine (9) samples from the Chlorite zone and 11 samples from the Biotite zone. Sampling stops and samples collected, available on Appendix 1.2.

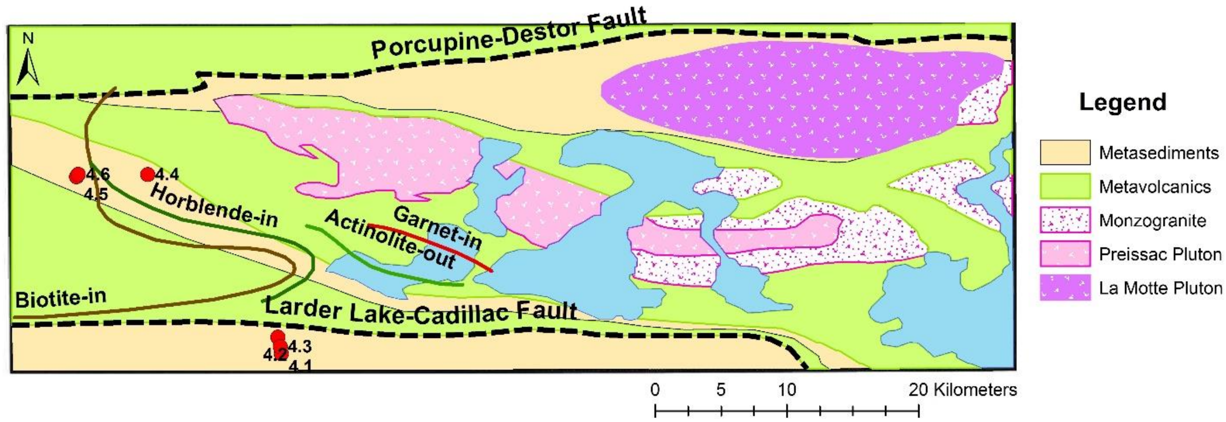

Figure 4.5. *Geological map of the Cadillac area including isograds and sampling stops. The metamorphic grade increases towards the plutons. Modified after Powell et al., 1995.*

Figure 4.6. *Chlorite zone samples of the Cadillac Group.*

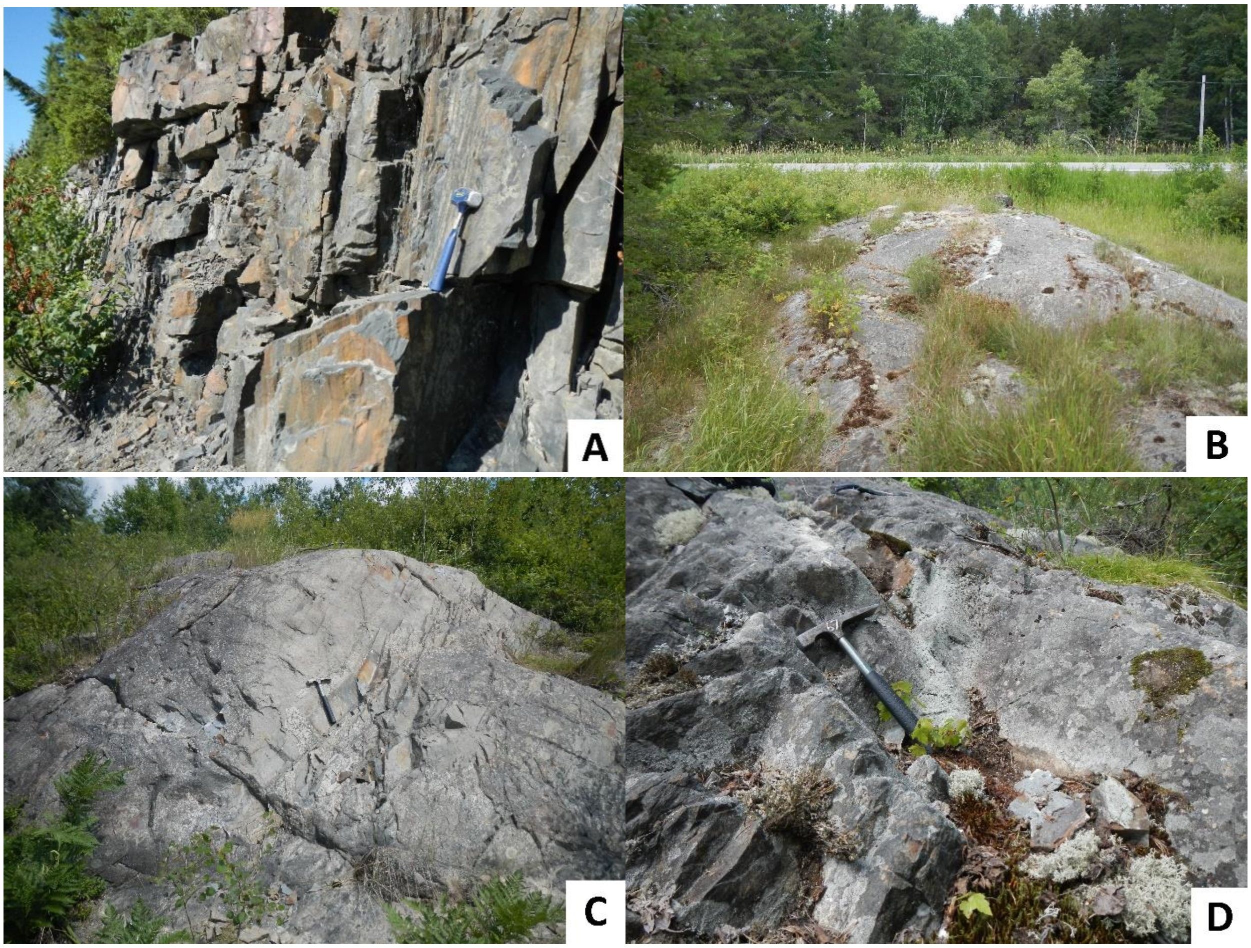

Figure 4.7. *Selected field photographs from the Cadillac Group sediments. A) Exposure at stop 4.1 inside the biotite zone. B) Road-cutting exposure at sampling stop 4.4 in the biotite zone. C) & D) Chlorite zone rocks exposed at 4.5 and 4.6 stops respectively.*

4.3. Porcupine assemblage

A set of 9 samples (AB 113-120) of the Porcupine assemblage were collected from a locality north of Porcupine town, east of Timmins, Ontario (48°29.65988' N, 81°12.78076' W). The unconformity with the underlying Timiskaming meta-conglomerate is exposed (Fig. 4.8B).

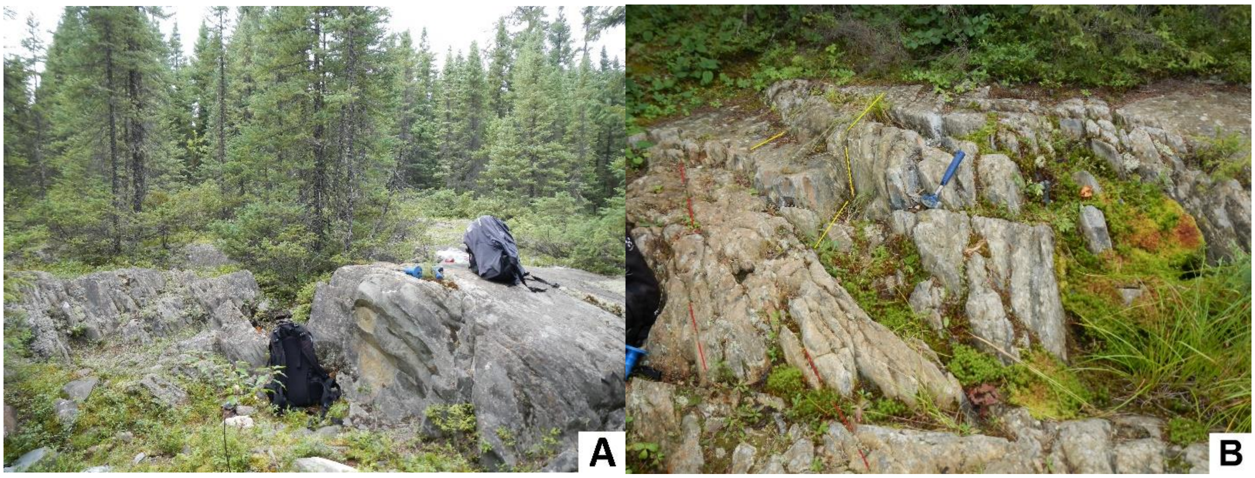

Figure 4.8. *A) Sampling locality. B) The unconformity between Porcupine and Timiskaming sedimentary sequences with their foliations shown with yellow and red lines respectively.*

Figure 4.9. *Fine grained meta-greywackes of the Porcupine assemblage, some bearing sulphide aggregates.*

5. Methods

5.1. Rock preparation

The samples were cut at the Rock Preparation Laboratory of Stockholm University. Both weathered layers/surfaces and ink marks were removed from all samples. For geochemical analyses, a fresh piece was collected for crushing and milling. All thin-section chips were cut perpendicular to the foliation. Crushing and milling of the rock samples was conducted at the facilities of Naturhistoriska Riksmuseet (Natural History Museum, Stockholm). All samples were powdered using the hardened steel tema. Careful cleaning of both the crusher and the miller was performed after each sample.

5.2. Geochemical analyses

5.2.1. Major and trace elements

Major and trace elements were measured in Activation Laboratories Ltd., Canada using the analytical packages 4Litho, 4B1 and 4F-C,S. For major oxides and trace elements, the method involved mixing of the samples with a flux of lithium metaborate and lithium tetra-borate and then fuse in an induction furnace (4Litho). Values were then defined by either Thermo Jarrell-Ash ENVIRO II ICP or Varian Vista 735 ICP. The instrument was calibrated every 10 samples with certified USGS and CANMET reference materials. Especially for Cu, Zn, Pb, Ni, S, Ag and Cd values, the samples were digested with four acids (hydrofluoric, nitric, perchloric and hydrochloric) and measured with a Varian Vista 735 ICP (4B1). Precision was attained through certified reference materials GXR-4, DNC-1a, SBC-1, SdAR-M2 (USGS). Lastly, for carbon and sulphur, 2g of sample were combusted in an induction furnace. Carbon is released and binds with oxygen to form CO_2. Sulphur is reduced and forms SO_2. The concentration of either compounds are detected as a reduction in the individual detectors. Values were defined with and analytical instrument Eltra CS-800 or CS-2000.

Detailed information: http://www.actlabs.com/list.aspx?menu=64&app=226&cat1=549&tp=12&lk=no

5.2.2. Au, As, Sb, Se, Te, Bi

Gold analyses were carried out at Stockholm University following an ultra-low (2ppt) detection limit method (Pitcairn et al., 2006b). Analyses were performed using a Thermo XSeries 2 ICP-MS after multiple digestion of the samples with hydrofluoric, nitric and Aqua Regia acids, followed by chromatographic separation of Au from matrix elements using DIBK (Diisobutyl Ketone). Values for As, Sb, Se, Te and Bi were defined using a PSA10.055 Millennium Excalibur hydride generation atomic fluorescence spectrometer (HG-AFS). Analytical precision and quality control was attained through multiple analyses of NRCAN reference materials TDB-1, WMS-1 and CH-4. The 3σ method detection limit is 0.033 ppb for Au, 0.043 ppb for As and 0.079 ppb for Sb. Reference material results are reported below (Table 5.1).

Table 5.1. *Reported measurements for reference materials.*

		Au	As	Sb	Se	Te	Bi
	Blank (ppb)	0,0086 ± 0.0084	0,02 ± 0,019	0,046 ± 0,026	0,014 ± 0,012	0,06 ± 0,05	0,14 ± 0,07
	MDL (ppb)	0,025	0,058	0,08	0,038	0,14	0,14
Reference Materials		**Au (ppb)**	**As (ppm)**	**Sb (ppm)**	**Se (ppm)**	**Te (ppm)**	**Bi (ppm)**
TBD1 (NRCAN)	**Certified Value**	**6,3**[1]	**2,2 ± 0,5**[1]	**0,72 ± 0,4**[1]	***0,35***		***0,06***
	Average	6,65	2,08	0,59	0,37		0,1
	SD	1,05	0,34	0,23	0,1		-
	% recovery	99,1	94,5	82,6	104,5		158
	%RSD	15,8	16,3	38,1	26,2		-
	n	*29*	*27*	*27*	*21*		*1*
WMS-1 (NRCAN)	**Certified Value**	**246**[2]	**19,1 ± 0,7**[1]	**7,34 ± 1**[3]	***93***[3]	***4,2***[3]	***1***[3]
	Average	244	21,03	7,07	67,7	2,1	0,95
	SD	97	0,34	1,64	12,4	0,63	-
	% recovery	100,4	110,1	96,3	72,8	50	94,8
	%RSD	39,9	26,4	23,2	18,3	30,2	-
	n	*23*	*23*	*22*	*10*	*10*	*1*
CH-4 (NRCAN)	**Certified Value**	**713**[2]	**8,8 ± 0,6**	**0,77 ± 0,4**	**2,1 ± 0,2**	**-**	***0,6***
	Average	718,7	7,64	0,85	1,9	0,39	0,51
	SD	210	0,68	0,51	0,2	0,23	-
	% recovery	96,9	86,9	110,8	90	-	85
	%RSD	29,3	8,8	60,1	11	58	-
	n	*25*	*25*	*19*	*7*	*7*	*1*

- *All certified values are certified by NRCAN except for where the following updated references are used: **(1)** (Bédard and Barnes, 2002), **(2)** (Constantin, 2009) and **(3)** (Dare et al., 2011).*
- *NRCAN – Natural Resources Canada*
- *MDL = method detection limit which is: 3 x standard deviation of the blank*
- *Certified values – those in italic are suggested rather than certified values*
- *% recovery - % difference between our analyses and certified values*
- *% RSD = % difference of standard deviation to average value (SD/average*100)*
- *Further info on values for reference materials can be found at http://georem.mpch-mainz.gwdg.de*

5.3. Optical Microscopy – S.E.M.

Thin sections of 55 representative samples were made at Vancouver Petrographics, Ltd. They were then studied using a Nikon Optiphot2-Pol petrographic microscope (both under transmitted and reflected light) equipped with Leica EC3 digital colour microscope camera at Stockholm University, Sweden.

In addition, SEM-EDS analyses were carried out at Stockholm University with a PhilipsXL30 FEG scanning electron microscope (ESEM), operating at 20 kV equipped with the OXFORD energy dispersive analytical X-ray spectrometer.

5.4. In-situ LA-ICP-MS

A representative set of 9 (nine) samples (Table 5.2) was selected for in situ LA-ICP-MS analyses in sulphides and silicates. The analyses were performed at the Department of Earth Sciences, University of Gothenburg using an Agilent 8800QQQ triple Quadrupole ICP-MS coupled to a New Wave NWR 213 laser ablation system. A spot-size of 25µm was initially selected but ablations were also carried out with 15µm for smaller grains. The energy output and the repetition rate have been 2 $J \cdot cm^{-2}$ and 5Hz respectively. Helium flow rate was set to 800 $ml \cdot min^{-1}$. Time for background counts was set to 25s; ablations were performed for 20s and 20s were spent as dwell time. The following isotopes were measured: ^{27}Al, ^{29}Si, ^{34}S, ^{57}Fe, ^{59}Co, ^{60}Ni, ^{63}Cu, ^{66}Zn, ^{75}As, ^{77}Se, ^{95}Mo, ^{107}Ag, ^{121}Sb, ^{125}Te, ^{182}W, ^{197}Au, ^{202}Hg, ^{208}Pb and ^{209}Bi. Isotope ^{57}Fe was set as the internal standard.

The calibration of the instrument was performed with reference glass material NIST-SRM-610 (Jochum et al., 2011). Fractionation effects due to matrix differences between the glass standard and the sulphide minerals being analyzed, were controlled using sulphide reference materials MASS-1 (polymetal sulphide, pressed powder pellet - Wilson et al., 2002) and Po-725 (synthetic pyrrhotite - Sylvester et al., 2005) in order to check the accuracy and precision. GSD-1G (synthetic basalt glass in epoxy mount - Guillong et al., 2005) was selected as an extra glass standard. All reference materials were analyzed after every 10 (ten) sulphide analyses.

Data processing and reduction were carried out using "Glitter" software (Fig. 5.1B) with ^{57}Fe used as internal standard. The Fe concentration of each mineral (either sulphide or silicate) was obtained through SEM-EDS analysis and although SEM data is qualitative, it was considered to be more accurate using this data than for example stoichiometric Fe concentrations. The internal standard is used to correlate between the calibration standard and the analyzed sulphide grains and to convert counts per seconds (CPS) in the LA-ICP-MS and concentrations for each element. The measured values for the other reference materials are used to evaluate the accuracy and precision of the analyses. Reference values from the GeoRem (Jochum et al., 2005) were also taken into consideration. They are all reported on Table 5.3.

Table 5.2. *The thin sections under LA-ICP-MS study.*

			Sections	
Unit	**Metamorphic zone**	**Sample ID**	**Rouyn-Noranda**	**Val d'Or**
Pontiac	Biotite	AB97	-	X
		AB65	X	-
	Garnet	AB28	X	-
		AB31	X	-
	Staurolite	AB56	X	-
		AB111	-	X
	Kyanite	AB43	X	-
	Sillimanite	AB20	X	-
Porcupine	-	AB115	-	

__Table 5.3.__ Reference material measurements and certified values.

Standard ID		Values		Reference
		Measured	Certified	
NIST-SRM-610	**As**	288.59 ±12.39	330 ±19	Jochum et al., 2011
			272 - 496	Juchum et al., 2005
	Au	22.66 ±0.8	22.5 ±0.6	Jochum et al., 2011
			15.6 - 26.9	Juchum et al., 2005
MASS-1	**As**	65.54 ±3.68	65 - 128 (65)	Juchum et al., 2005
			65	Wilson et al., 2002
	Au	58.41 ±8.65	47	Wilson et al., 2002
			32 - 60 (47)	Juchum et al., 2005
Po-725	**Au**	48.92 ±8.51	34.58 ±1.73 (Po41)	Sylvester et al., 2005
			45.8 - 45.85 (Po727)	Juchum et al., 2005
GSD-1G	**Sb**	41.35 ±1.11	36-53 (39-42)	Juchum et al., 2005
			39 ±20	Guillong et al., 2005
	As	32.91 ±1.36	25 ±15	Guillong et al., 2005
			18.5-35 (23-30)	Juchum et al., 2005
	Au	4.14 ±1.03	5.2 ±3	Guillong et al 2005
			4.4	Juchum et al., 2005

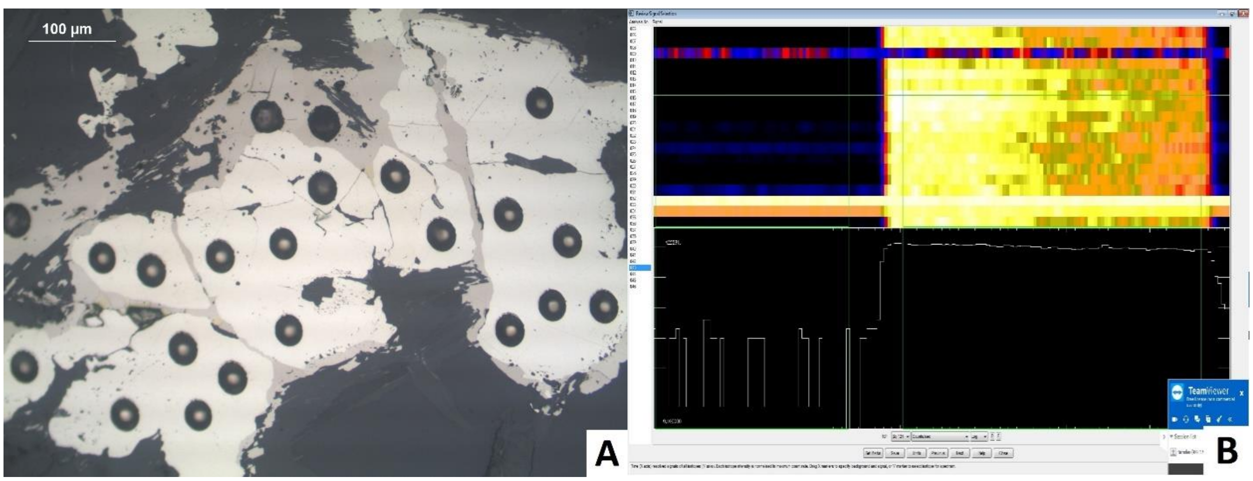

***Figure 5.1.** A) Laser ablation pits in pyrites (white) and pyrrhotites (pink). B) Print-screen image of Glitter software while processing the background and ablation signals.*

6. Results

6.1. Optical Microscopy – SEM

6.1.1. Pontiac Subprovince

Biotite zone

The rocks from the biotite zone comprise foliated schists and they also display early-deformation textures. In places, a few samples display kink bands or crenulation cleavage. These rocks consist of quartz +plagioclase +biotite ±muscovite ±chlorite ±muscovite ±epidote ±calcite ±garnet. Quartz occurs as subhedral crystals with ≈0.15mm average size. Larger, angular grains (>0.40mm) display undulose extinction. Plagioclase crystals are subhedral, have an average size of 0.20mm and display thin twinning. Biotites comprise platy subhedral-euhedral crystals and are commonly aligned to the foliation planes.

Sulphide minerals comprise pyrrhotite, chalcopyrite, pentlandite, pyrite ±sphalerite ±galena ±cobaltite. Pyrites occur as patches, frequently being replaced by pyrrhotite which is the dominant sulphide throughout the matrix. The largest patches reach 0.4-0.5mm. This replacement texture is characteristic (Fig. 6.2 A-B-C). Chalcopyrite is either found as isolated grains or in direct contact with pyrrhotite. Pentlandite occurs as lamellae within pyrrhotite. Sphalerite is less common and occurs either in contact with chalcopyrite or as isolated crystals in the matrix. Galena is frequent and occur as inclusions or in cracks inside pyrrhotite, while cobaltites are scarce and occur as tiny, isolated grains (Fig. 6.2D).

The samples from this zone display limited alteration. Sericitization has not been identified on every sample and where it occurs, it is limited and only found in plagioclase crystals. Calcites with rhombohedral colorful cleavage occur in elongated areas/cavities aligned to the foliation but they are generally uncommon.

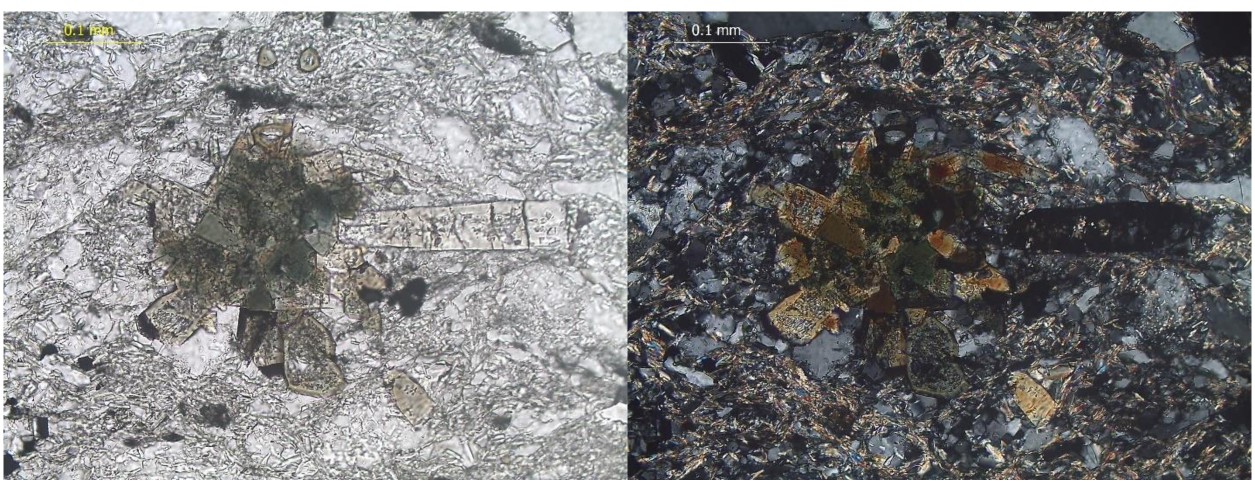

Figure 6.1. *Tourmaline crystals under PPL and XPL (sample AB63, Biotite zone).*

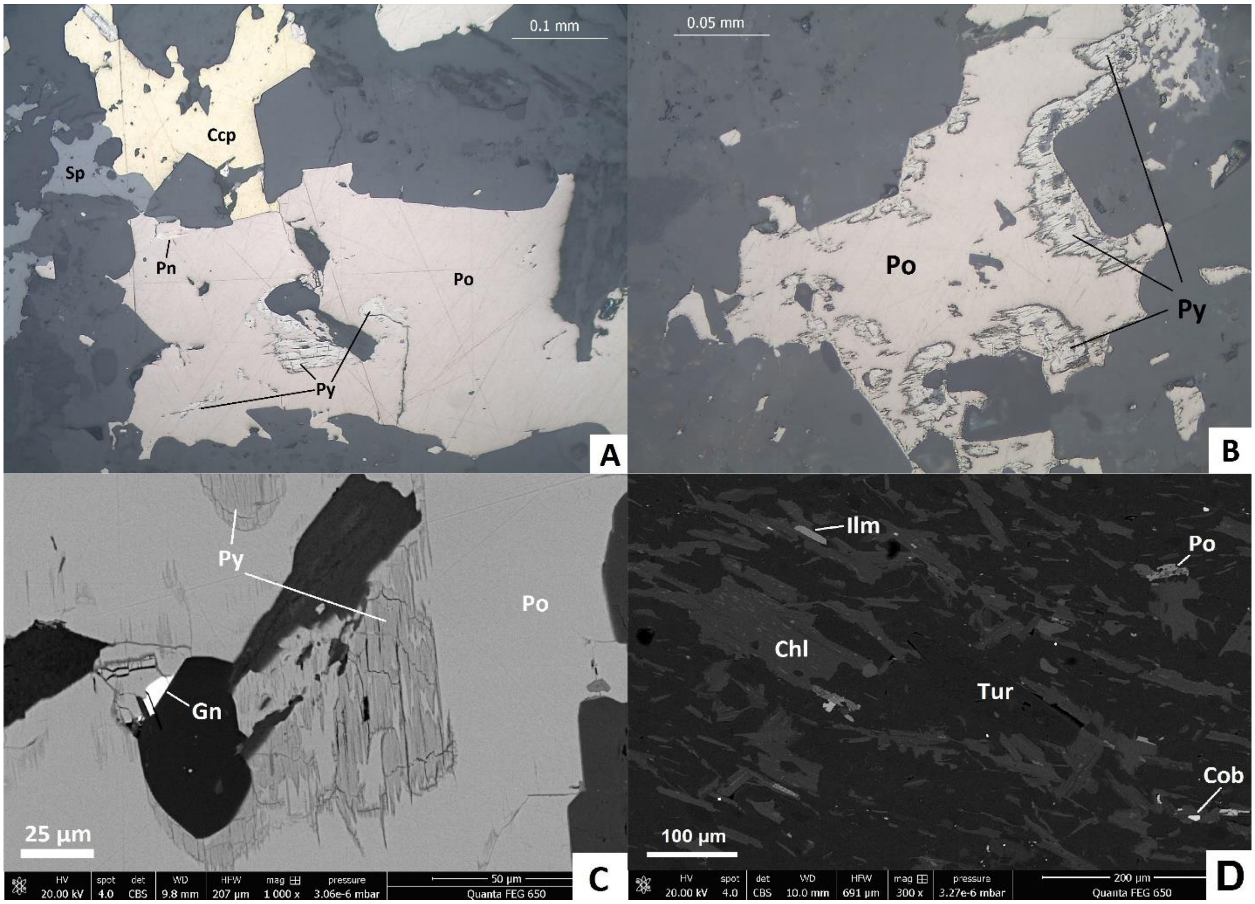

Figure 6.2. *Reflected light microscope pictures: A) Pyrrhotite replacing pyrite. Chalcopyrite in contact with sphalerite. B) Pyrrhotite replacing pyrite. SEM backscatter images: C) Pyrite's replacement texture. D) Small cobaltite grain in Qz-Pl-Bt-Chl*

Garnet zone

The vast majority of rock samples taken from the garnet zone are strongly foliated, frequently displaying crenulation cleavage and/or kink bands (Fig. 6.3B). The rocks consist of quartz ±garnet ±biotite ±chlorite ±plagioclase ±white mica ±epidote ±tourmaline. Quartz occurs as subrounded-subhedral, recrystallized grains with ≈0.10-0.15mm average size. There are also larger, boudinaged porphyroclastic grains (≈0.35mm of size) which display undulose extinction. Plagioclase is not frequently present but it comprises syn-deformational porphyroblasts. Garnets are present and have an average size of ≈1mm in diameter (Fig. 6.3A). Biotite occurs as subhedral-euhedral crystals oriented in parallel to the foliation. Thin veins are isoclinally folded.

Sulphides comprise pyrrhotite, chalcopyrite, pentlandite, ±pyrite ±sphalerite ±cobaltite. Pyrrhotite is the dominant sulphide throughout the matrix. Pyrite occurs as aggregates and it is often being replaced by pyrrhotite (Fig. 6.4C). Chalcopyrite is found as isolated grains or in contact with pyrrhotite. Pentlandite occurs as thin lamellae inside pyrrhotite and sphalerite is either found in contact with chalcopyrite or ilmenite. Cobaltites are frequently found as small grains enclosed to pyrrhotite patches (Fig. 6.4D). All opaques are aligned to the foliation and follow the crenulation cleavage geometry. Recrystallized -possibly sedimenetary- pyrites occur as aggregate patches (Fig. 6.4A).

Sericites are limited and are only found in plagioclase crystals. Carbonates are rare and chloritization is limited to micas and only present in some of the rock samples under study. In general, the rocks from the garnet zone display no pervasive alteration.

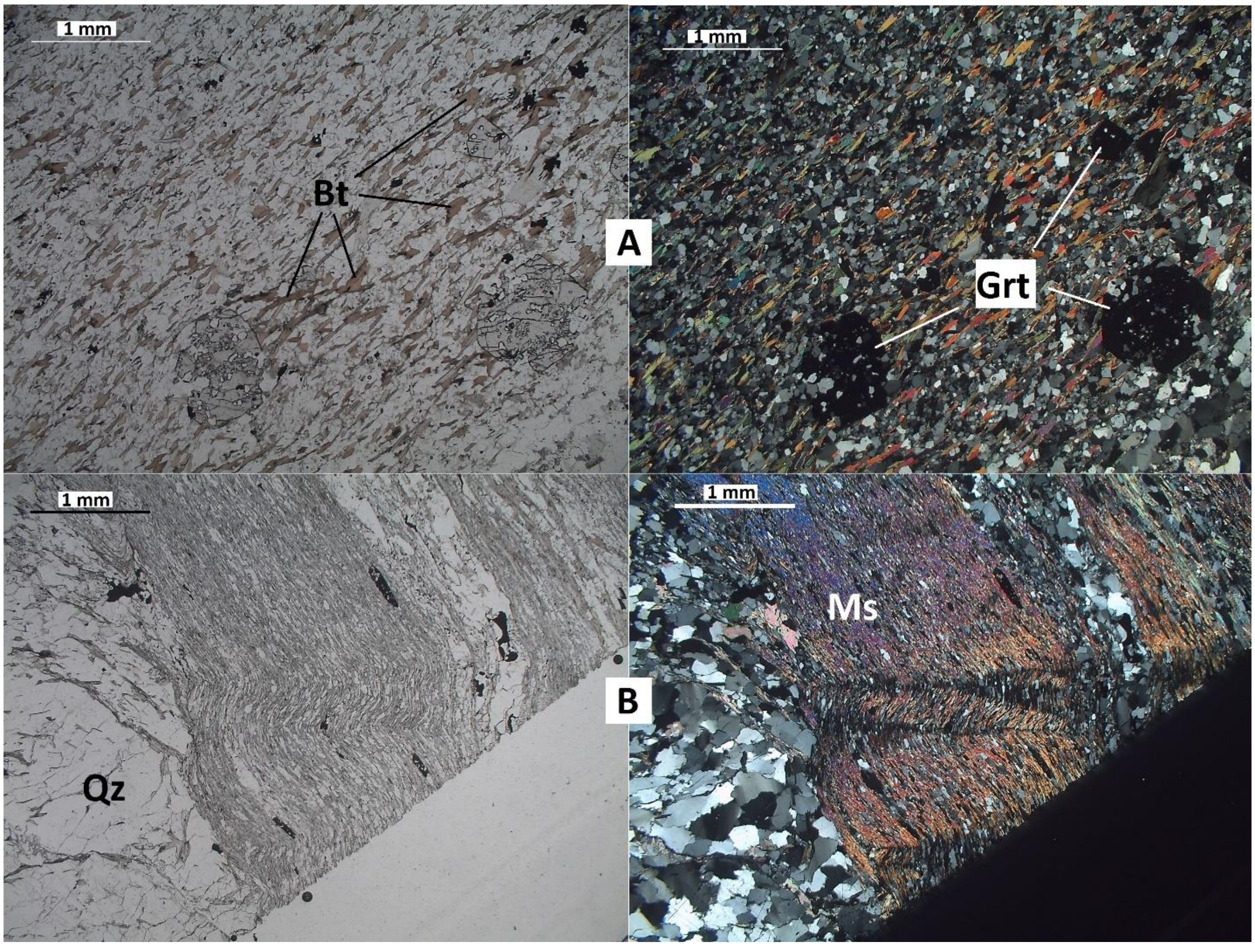

Figure 6.3. *A) Garnet-bearing schist with Qz-Bt±Pl matrix. B) Distinct kink bands on sample AB28. Opaques are aligned to the foliation.*

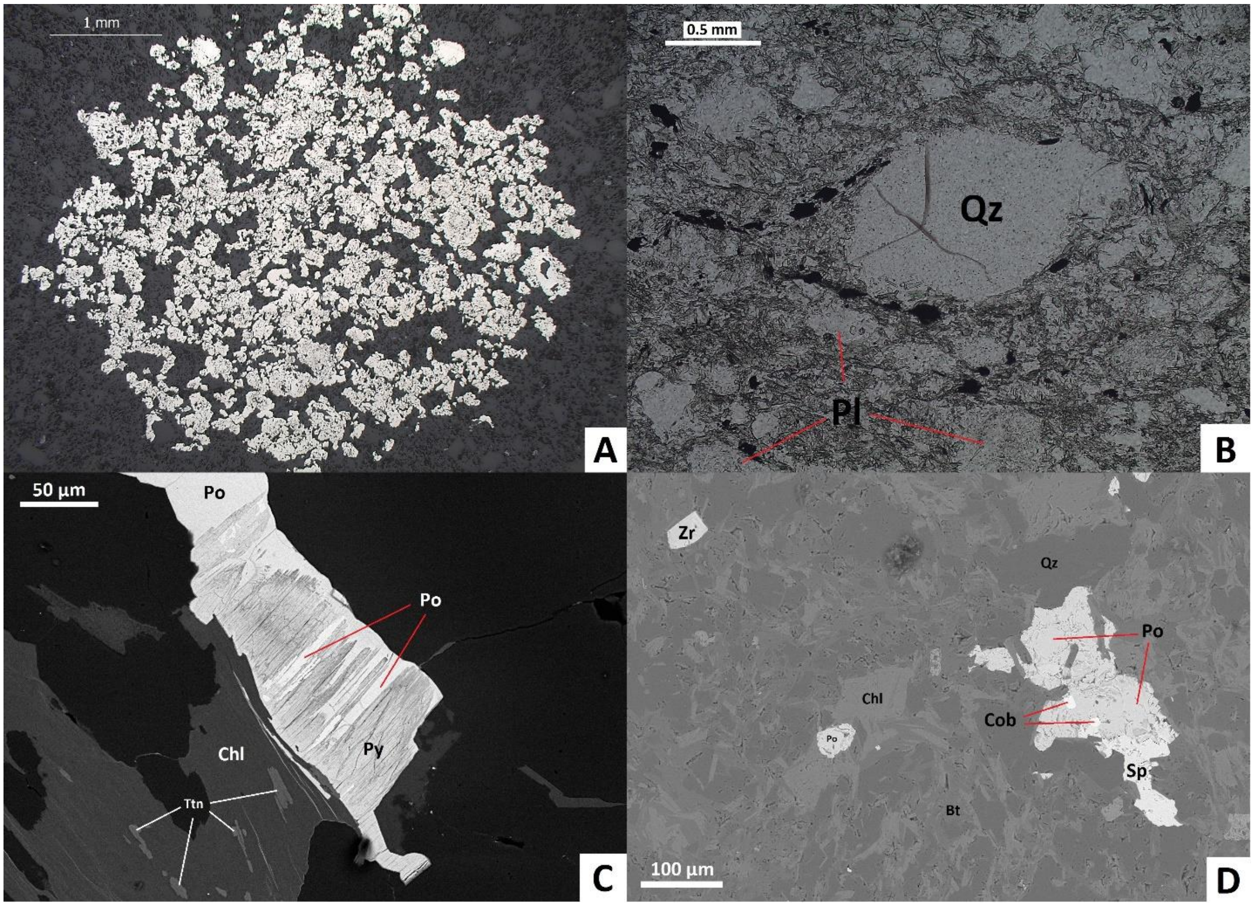

Figure 6.4. *Microscope pictures: A) Reflected light picture of recrystallized, former sedimentary aggregates of pyrite (sample AB31). B) Opaques aligned to the tails of a quartz σ-clast (AB33). SEM backscatter images: C) Pyrrhotite replacing early pyrite grain (sample AB28). D) Pyrrhotite patch with inclusions of cobaltite, being in contact with sphalerite (sample AB31).*

Staurolite zone

Staurolite zone samples comprise moderately-strongly foliated schists with almost slaty cleavage. The rocks are composed of quartz +plagioclase +biotite ±staurolite ±muscovite (or white mica) ±chlorite ±epidote ±calcite. Quartz is found as either small, rounded, or subhedral-angular crystals. They vary in size (≈0.2-0.6mm) among the studied samples. Plagioclase porphyroblasts are found as >1mm rounded crystals; the ones on matrix comprise subhedral syn-deformational crystals with ≈0.4mm average size. Biotite crystals occur as subhedral-euhedral porphyroblasts, often aligned to the foliation and displaying lepidoblastic texture. Chlorite is either present in the strain shadows of grown plagioclase crystals, or in matrix as patches, with some evidence for growing after micas. Staurolite porphyroblasts are found as either twinned or single euhedral-subhedral crystals (Fig. 6.6). Single staurolite crystals have an average size of 2-3mm, while twinned crystals might reach 5-6mm on the long axis (Fig. 6.5).

Pyrite, pyrrhotite, chalcopyrite, pentlandite ±sphalerite comprise the sulphide minerals present in staurolite zone rocks. Pyrite is rare and is commonly replaced by pyrrhotite. Pyrrhotite is the most common sulphide throughout the matrix with pentlandite frequently present as lamellae or patches inside it (Fig. 6.7 C-D). Chalcopyrite occurs as isolated grains or in contact with pyrrhotite and/or pyrite (Fig. 6.7C). Sphalerite is uncommon and found either in contact with chalcopyrite or as isolated patches. Ilmenite always lies in contact with rutile.

The samples vary in terms of degree of alteration. There are samples with a few sericites grown over plagioclase crystals, while others display progressed sericitization. Chlorites in micas are limited, but there are samples where chlorites display the same cleavage as biotite. Carbonates were only identified in elongated cavities/boudins which lie in parallel to the foliation. Veins are generally quite thin, consisting of calcite and probably ultra-fine grained argillic material.

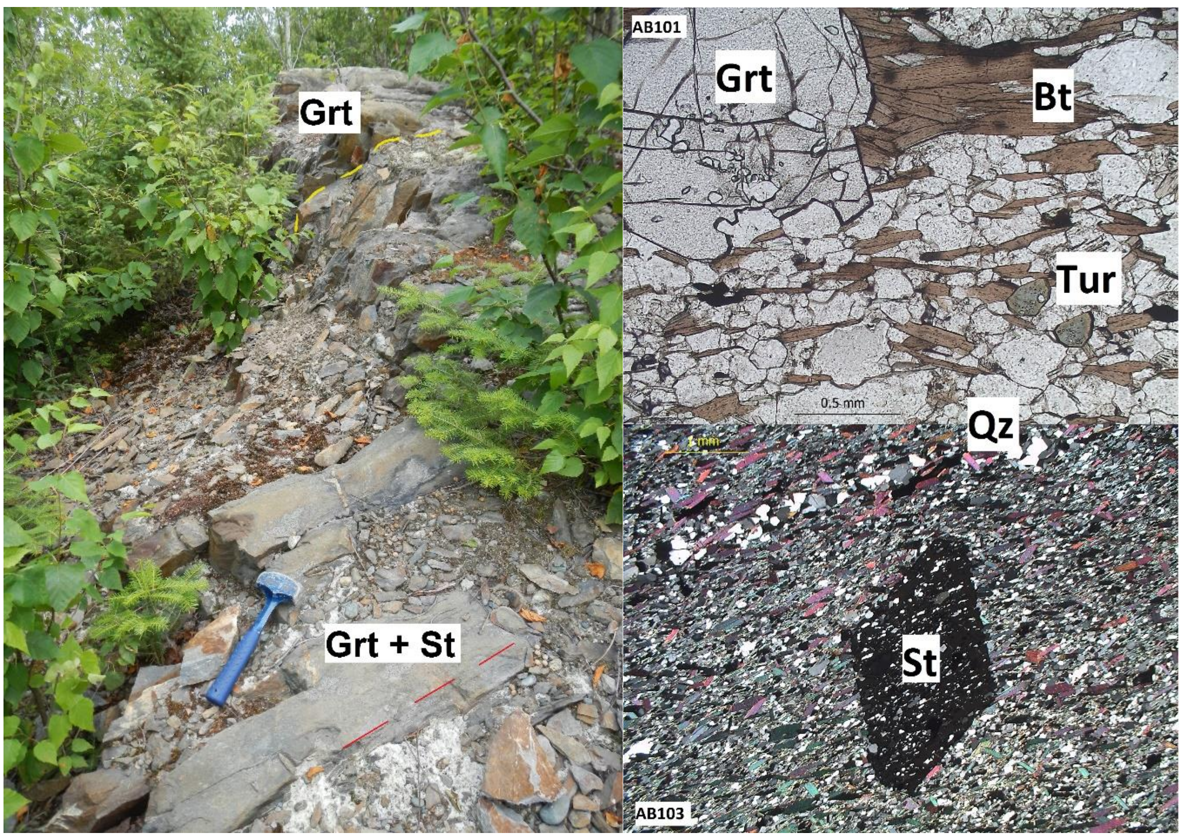

Figure 6.5. *Euhedral staurolites in grt-bearing schists. Tourmaline is abundant.*

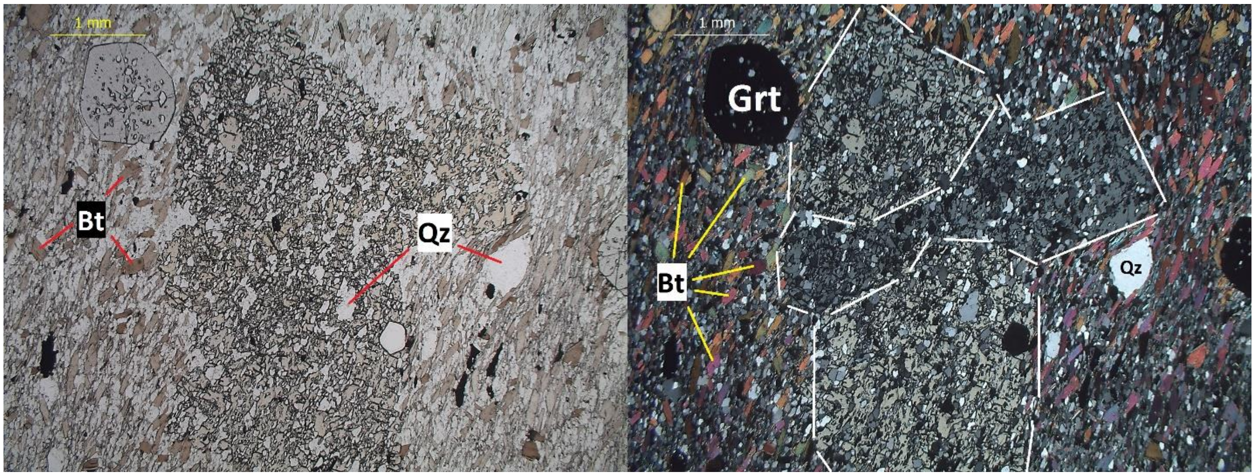

Figure 6.6. *Twinned, almost euhedral staurolite crystals in Qz-Pl-Bt-Grt matrix (sample AB103).*

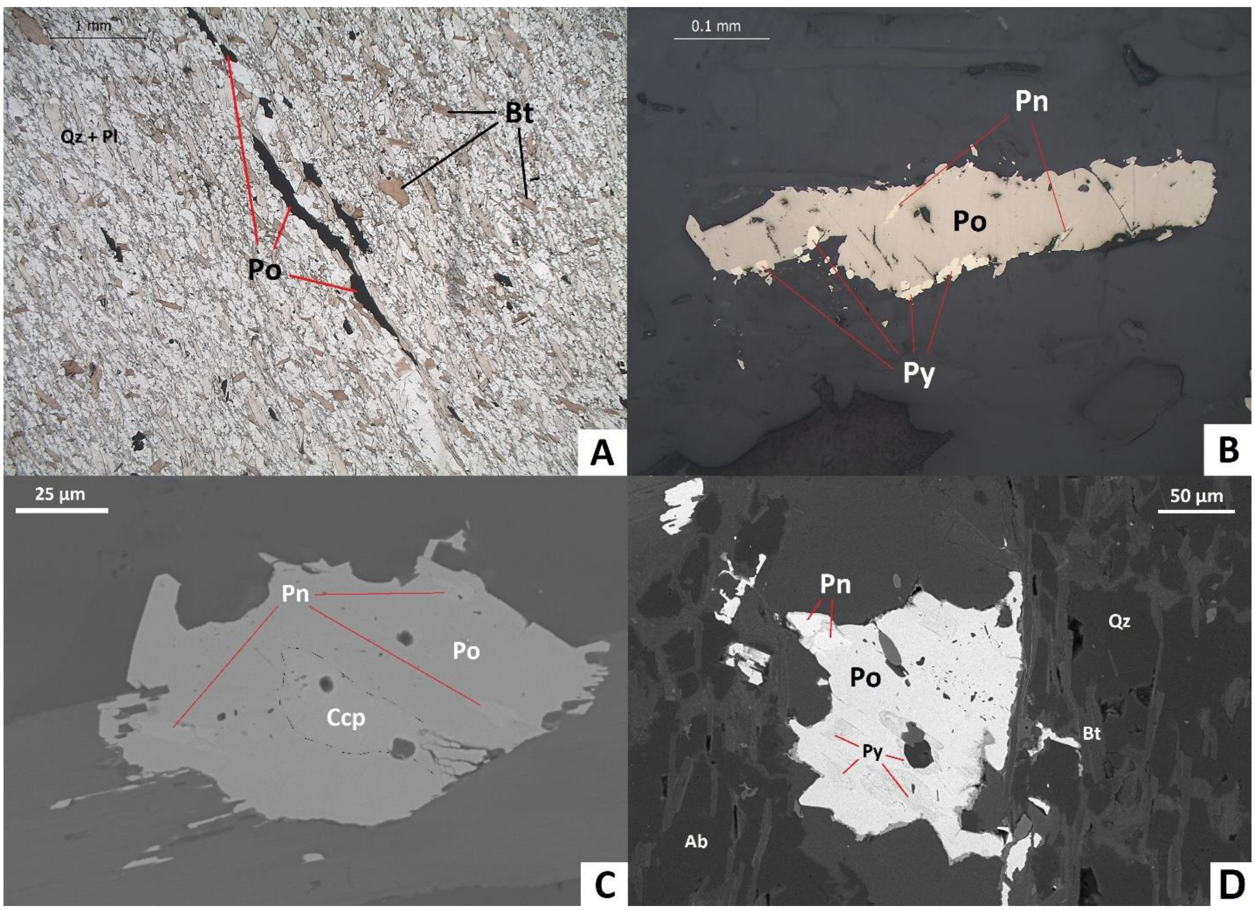

Figure 6.7. *Microscope pictures: A) Pyrrhotites aligned to the foliation with Qz-Pl-Bt matrix. B) Pyrrhotite patch with small pyrites on its rim and pentlandite lamellae. SEM backscatter images: C) Chalcopyrite enclosed in pyrrhotite. D) Relict pyrites replaced by pyrrhotite.*

Kyanite zone

Rock samples from the kyanite zone are well foliated with foliation surfaces defined by lepidoblastic mica layers. These layers display wide crenulation cleavages in places. The rocks consist of quartz +plagioclase +biotite ±kyanite ±muscovite and white mica ±chlorite ±garnet ±tourmaline. Quartz occurs as fine-grained sub-rounded crystals with ≈0.10-0.15mm average size. Plagioclase crystals are mostly subhedral porphyroblasts, have an average size of 0.50mm and thin twinning lamellae in places. Biotite crystals occur as subhedral-euhedral porphyroblasts commonly aligned to the foliation.

Sulphide minerals comprise pyrite, pyrrhotite, chalcopyrite, pentlandite ±sphalerite ±galena. Pyrite is found either in contact with pyrrhotite or as single grains with ≈0.2mm average size. Pyrrhotite is common and frequently found throughout the matrix. It also occurs in direct contact with pyrite (Fig. 6.9A) or replacing pyrite displaying distinct replacement textures (Fig. 6.9C). Chalcopyrite occurs as isolated grains or in contact with pyrrhotite. Pentlandite occurs as patches and lamellae within pyrrhotite, and sphalerite occurs spatially associated with pyrite either in contact or as intergrowths (Fig 6.9B). Galena occurs as rare small grains (Fig. 6.9D).

The samples from the kyanite zone display no pervasive alteration. Sericitization is very limited and only found in plagioclase crystals. Chloritization of biotite occurs but is rare. No carbonate was identified in these samples.

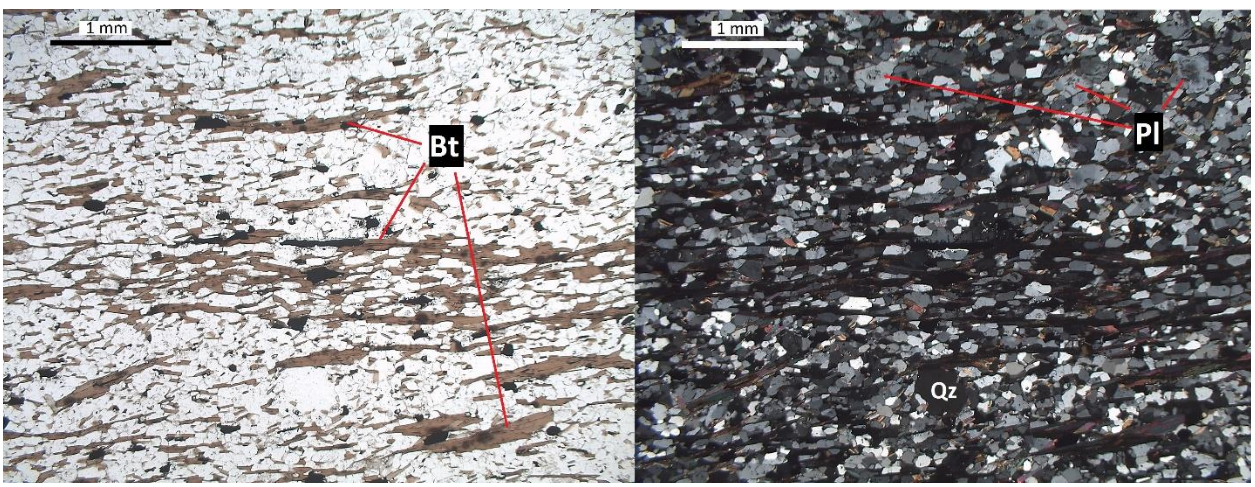

Figure 6.8. *Lepidoblastic biotite along with quartz grains and lesser plagioclase. Weak crenulations observed in places (sample AB43).*

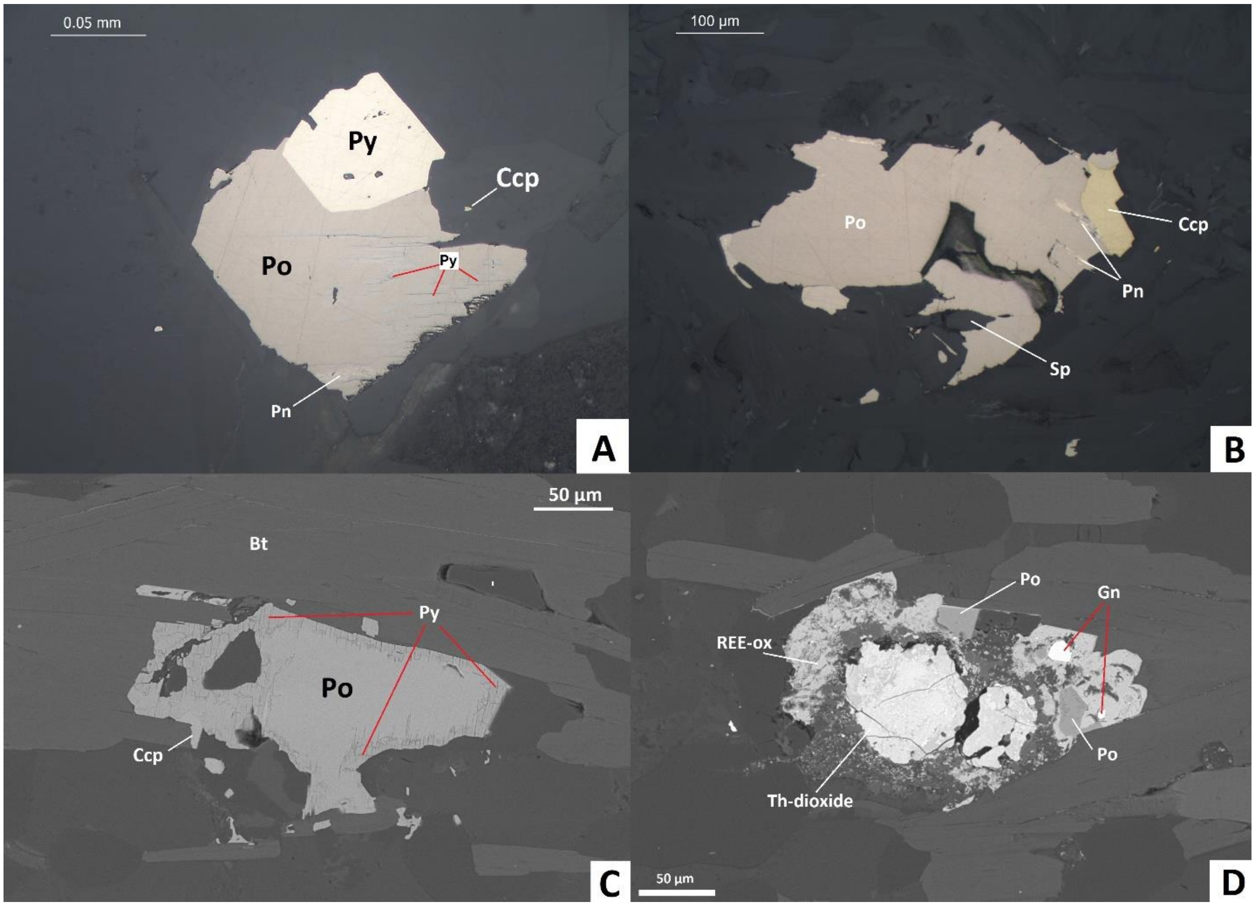

Figure 6.9. *Reflected light microscope pictures: A) Pyrrhotite, both having replaced and in contact with subhedral-euhedral, pyrite. B) Pyrrhotite in contact with chalcopyrite and sphalerite. SEM backscatter images: C) Pyrrhotite after pyrite, showing characteristic replacement textures. D) Galena in contact with REE-oxides along with pyrrhotite and thorianite.*

Sillimanite zone

Sillimanite zone samples display well-defined foliation surfaces, porphyroblastic texture and have aligned lepidoblastic mica layers. The rocks are composed of quartz +plagioclase +biotite ±garnet ±kyanite ±muscovite and white mica ±chlorite. Quartz is abundant, displays granoblastic texture and occurs as small rounded-subrounded crystals with ≈0.10-0.15 mm average size. Grains of larger size display deformation lamellae. Plagioclase mostly occurs as subhedral porphyroblasts varying in size (0.20-0.40mm). Few crystals display moderate twinning. Biotites occur as subhedral-euhedral platy crystals displaying lepidoblastic texture.

Ore minerals comprise pyrite, pyrrhotite, chalcopyrite, pentlandite, pyrite ±sphalerite ±galena. Pyrite is found as single isolated grains or in aggregates reaching 0.5mm of size (Fig. 6.11B). Wherever it is found with pyrrhotite, the characteristic replacement texture is observed. Pyrrhotite occurs as isolated grains on matrix, often replacing pyrite. Chalcopyrite is found either as small isolated grains on matrix, in contact with pyrrhotite or enclosed to it (Fig. 6.11A). Pentlandite appears intergrown in pyrrhotite while sphalerite is found less often. It occurs either in contact with chalcopyrite or as isolated crystal on matrix. Galena is rare and only found as tiny grains.

The samples display moderate alteration. Sericite is abundant in plagioclase crystals but not present in any other mineral phase. Chloritization is uncommon, though there are samples on which biotite shows grey interefence colours. Carbonates were not identified.

Figure 6.10. *Overview microphotograph of sample AB15 of the sillimanite zone. Kyanites floating in Qz-Bt-Pl matrix (PPL & XPL images).*

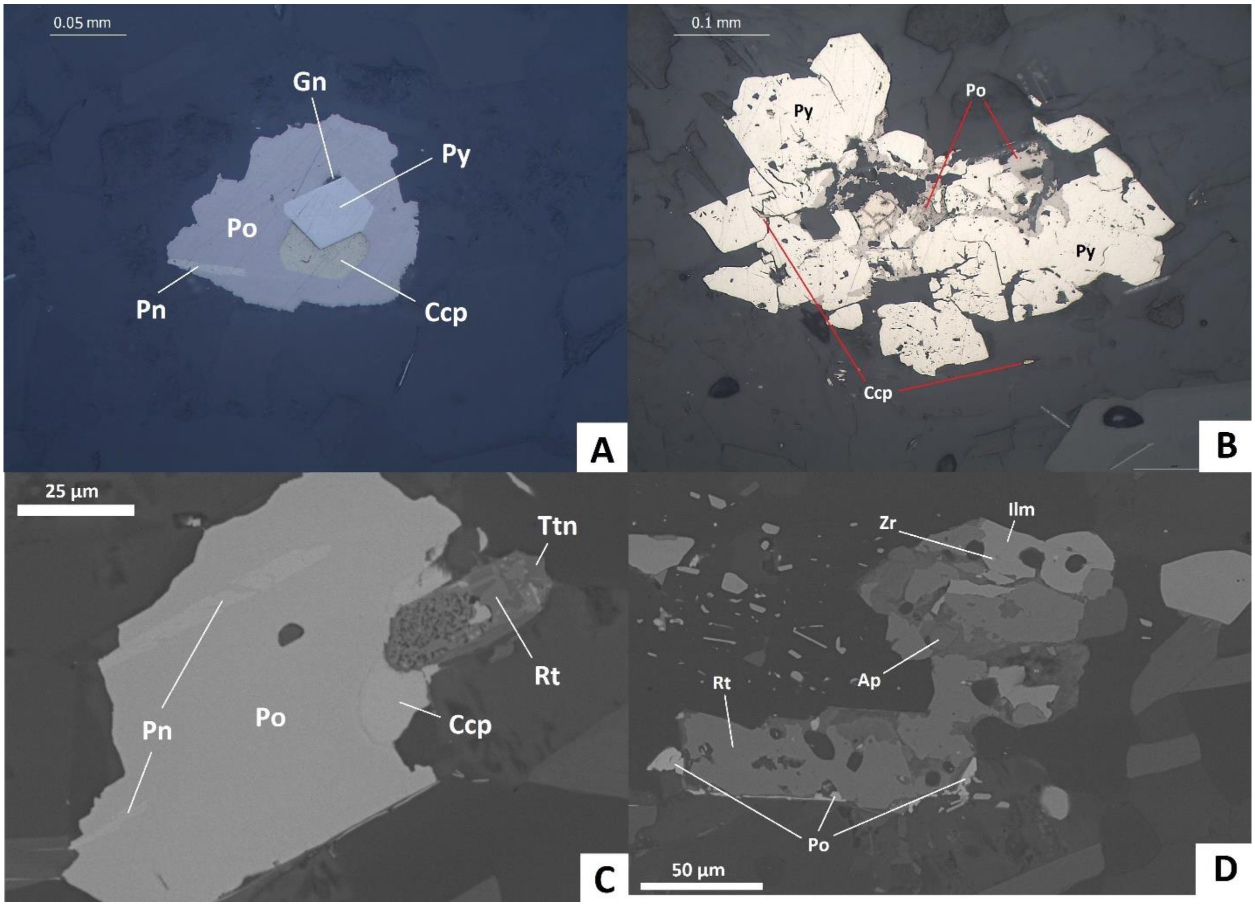

Figure 6.11. *Reflected light microscope pictures: A) Isolated pyrrhotite grain on matrix with enclosed pyrite, chalcopyrite, galena, and intergrown pentlandite. B) Pyrite grains being replaced by pyrrhotite. SEM backscatter images: C) Pyrrhotite and chalcopyrite in contact with rutile and titanite. D) Poly-phase patch consisting of pyrrhotite, rutile, ilmenite, apatite and zircon.*

6.1.2. Cadillac Group

Chlorite zone

Cadillac chlorite zone samples mostly comprise weakly foliated greywackes. Some samples display typical greywacke texture with angular fragments of quartz and plagioclase. Slightly foliated samples display early deformation textures. Thin veins are filled with fine-grained mica. The rocks are composed of quartz +plagioclase ±chlorite ±micas ±epidote. Quartz ranges in size (0.15-0.5mm) but is mostly found as ≈0.2mm subhedral crystals. Plagioclase crystals occurs as larger subhedral-anhedral crystals and they have an average size of 0.20mm. They display moderate twinning.

Sulphide minerals comprise pyrrhotite, chalcopyrite, pentlandite ±sphalerite. Pyrrhotite is abundant throughout the matrix and chalcopyrite is either found as isolated grains or in contact with pyrrhotite (Fig. 6.13 A-B). Pentlandite occurs as intergrown lamellae in pyrrhotite. Sphalerite is found either in contact with chalcopyrite or rutile-ilmenite (Ti-oxides).

The majority of the samples display limited alteration. Chlorites occur as patches upon the matrix rather than typical tabular crystals. Sericite is only found on plagioclase crystals. Carbonates were not identified in these samples.

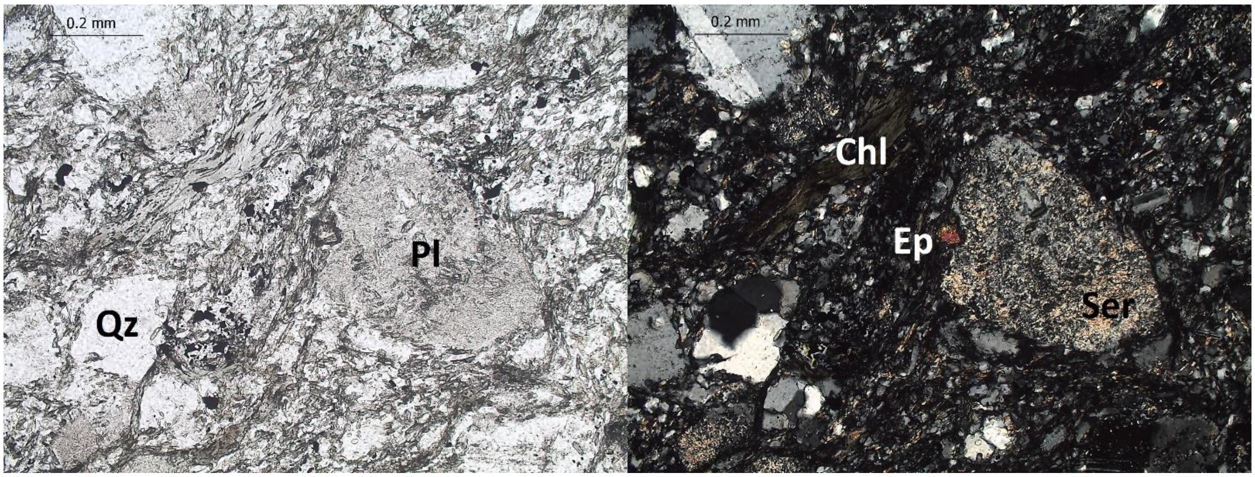

Figure 6.12. *Transmitted light pictures on PPL and XPL from sample AB81 of the Chlorite zone.*

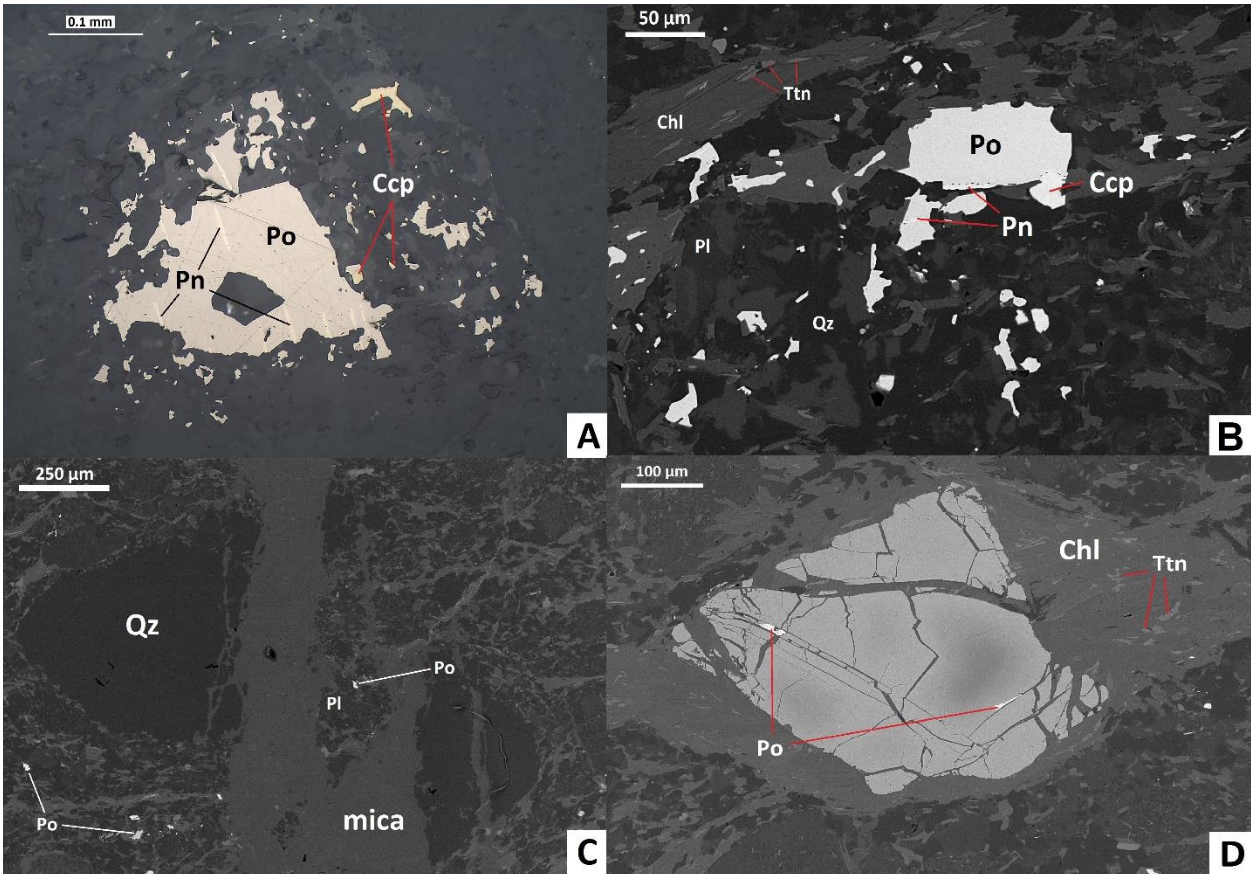

Figure 6.13. *A) Reflected light picture showing a patch of pyrrhotite with pentlandite and also chalcopyrite. SEM backscatter images: B) Pyrrhotite in contact with chalcopyrite and intergrown pentlandite. Titanites enclosed in chlorites in Qz-Pl-dominant matrix. C) Late vein filled with mica, having cut a large quartz grain. D) Fe-Cr-Al spinel surrounded by chlorite, with pyrrhotite coating its fractures.*

Biotite zone

The rocks from the biotite zone of the Cadillac Group comprise moderately foliated schists consisting of quartz +plagioclase +biotite ±muscovite ±chlorite. Quartz is found as subhedral crystals with ≈0.15mm average size while larger, angular-subangular grains (≈0.30mm) probably represent recrystallized porphyroclasts. Plagioclase crystals are subhedral-anhedral, display thin twinning and have an average size of 0.20mm. There are also larger crystals which reach 0.5mm of size (Fig. 6.14). Biotites are subhedral-anhedral and mostly occur as patches aligned to the foliation. Tourmaline is present, but not abundant (Fig. 6.15A)

Sulphide minerals comprise pyrrhotite, chalcopyrite, pentlandite, pyrite ±sphalerite. Pyrrhotite occurs as either isolated grains throughout the matrix, or as patches replacing pyrites (Fig. 6.15B). Pyrites comprise aggregates of larger size and are often rimmed or extensively replaced by goethite (Fig. 6.15 C-D). Chalcopyrite is found as isolated grains, enclosed in pyrite (Fig. 6.15B) or in contact with both pyrrhotite and pyrite. Pentlandite occurs as intergrowths in pyrrhotite while sphalerite is found in contact with either chalcopyrite or Ti-oxides.

The samples display limited alteration. A few sericites are found on plagioclase crystals, while carbonates are rare; calcite has filled a few elongated cavities/areas.

Figure 6.14. *Microscope pictures on PPL and XPL from sample AB69 of the Biotite zone.*

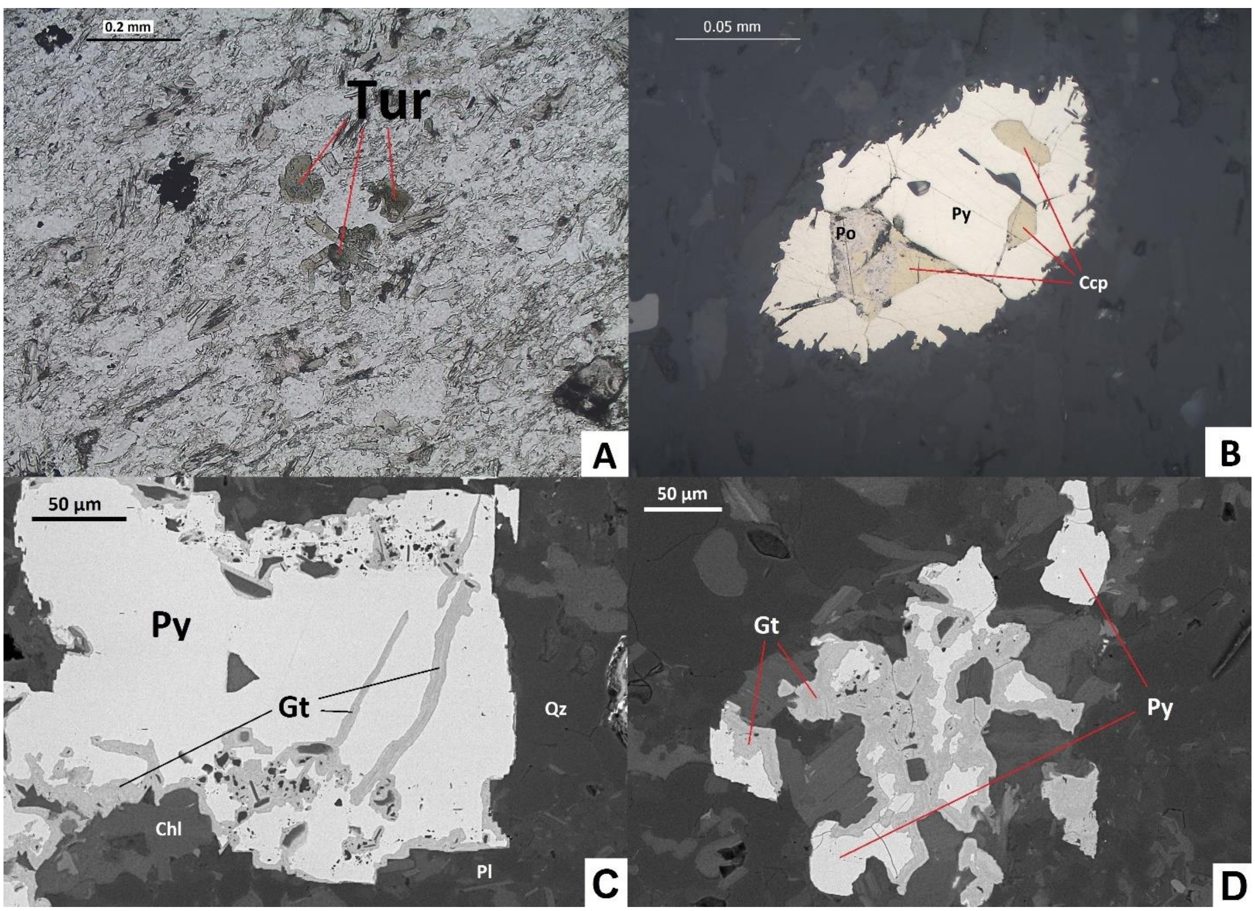

Figure 6.15. *Reflected light pictures: A) Tourmaline crystals in Qz-Pl-Bt matrix. B) Pyrite patch with enclosed chalcopyrites. Pyrrhotite developed in cracks and in mixture with chalcopyrite. SEM backscatter images: C) Pyrites weathered to goethite. D) Goethite developed both at the rims and in cracks of pyrite crystals.*

6.1.3. Porcupine assemblage

The rock samples from the Porcupine comprise fine grained and weakly foliated schists. They are composed of quartz +plagioclase +micas ±epidote. Quartz occurs as subhedral-subangular crystals with ≈0.20mm average size. Larger grains (≈0.4mm) occur as well. Plagioclase is small, subhedral and its twinning are often visible (Fig. 6.16). Epidotes have an average size of 0.2mm and are found throughout the matrix.

Pyrite, pyrrhotite, chalcopyrite, pentlandite and cobaltite are the sulphides present in these rocks. Pyrrhotite is abundant throughout the matrix and occurs as patches of 1mm maximum size. Pyrite is only found as recrystallized aggregates with porous texture (Fig. 6.17 B-C). Chalcopyrite occurs as isolated grains or in contact with pyrrhotite. Pentlandite is found intergrown in pyrrhotite (Fig. 6.17A). Cobaltite comprise small grains enclosed to pyrrhotite (Fig. 6.17D).

The samples display very limited alteration with few sericites formed on plagioclase crystals. No indication of carbonates or chloritization observed.

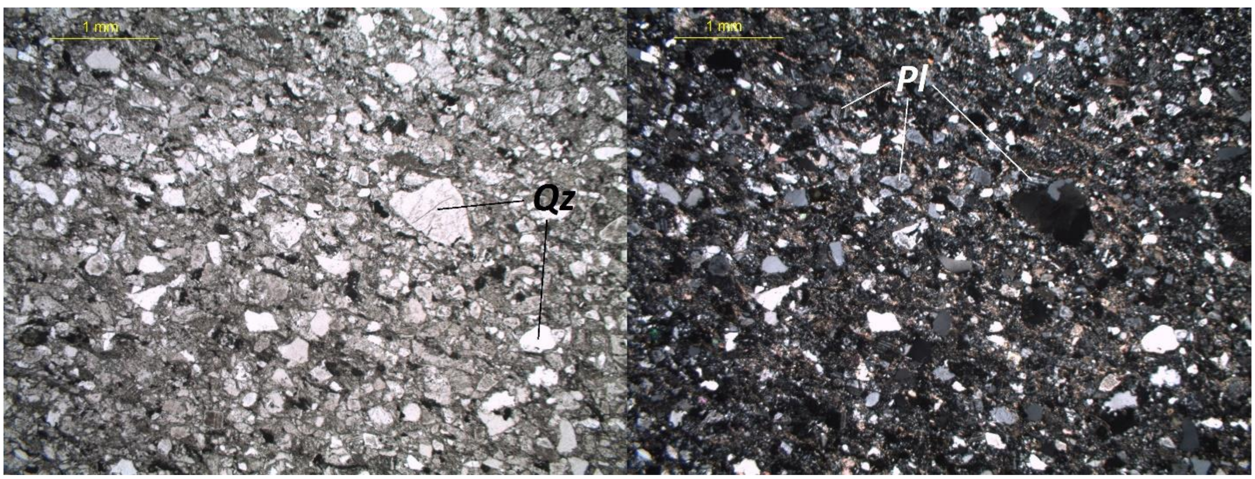

Figure 6.16. *Transmitted light microscope pictures on PPL and XPL from sample AB115 from the Porcupine assemblage.*

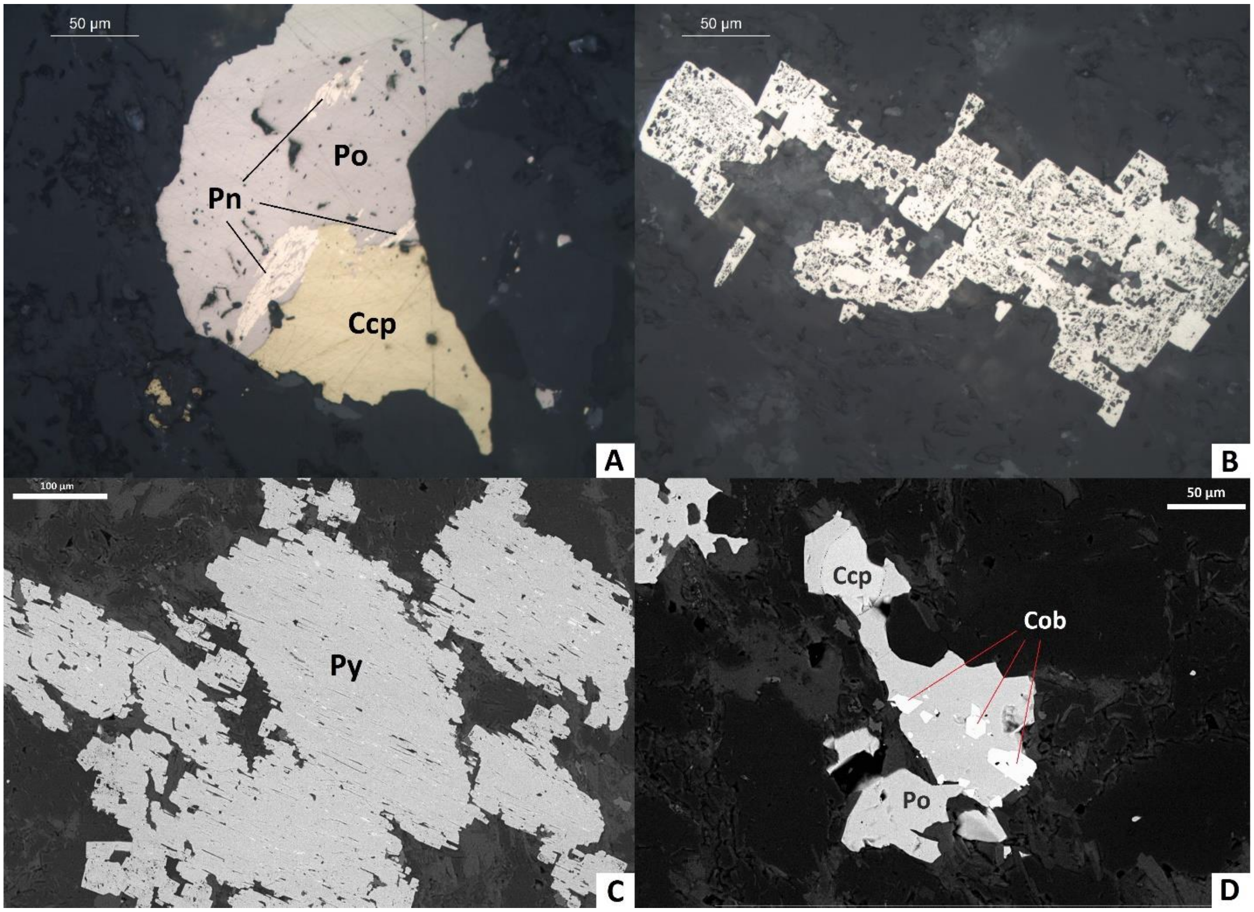

Figure 6.17. *Reflected light pictures: A) Pyrrhotite and pentlandite in contact with chalcopyrite (sample AB115). B) Euhedral, porous aggregates of pyrite (sample AB117). SEM backscatter images: C) Recrystallized pyrites (sample AB115). D) Pyrrhotite in contact with chalcopyrite, having cobaltite grains enclosed.*

6.2. Geochemistry

6.2.1. Bulk rock chemistry

The concentrations in major oxides for the samples from the Pontiac subprovince, the Cadillac group and the Porcupine assemblage were statistically analysed and are summarized below (Table 6.1). The complete major and trace elements concentrations are available on Appendix (4.1).

Table 6.1: *Values for the major oxides of the samples of the Pontiac subprovince (n=65), the Cadillac Group (n=17) and the Porcupine assemblage (n=6).*

	Pontiac Subprovince				Cadillac Group				Porcupine assemblage			
	Average	SD	**Min**	**Max**	**Average**	**SD**	**Min**	**Max**	**Average**	**SD**	**Min**	**Max**
SiO_2	62.52	4.18	53.74	69.09	62.05	3.78	54.01	66.77	63.40	4.48	56.76	68.68
Al_2O_3	16.52	1.97	13.10	21.37	15.65	1.41	13.08	18.85	15.16	2.36	13.38	18.32
Fe_2O_3	6.32	1.02	4.12	8.57	7.94	3.70	4.72	16.06	6.74	1.63	5.38	9.69
MnO	0.07	0.02	0.04	0.15	0.07	0.01	0.06	0.09	0.11	0.04	0.08	0.18
MgO	3.15	0.73	2.07	5.31	3.24	0.56	2.32	4.40	3.37	0.80	2.68	4.51
CaO	2.46	0.99	0.52	6.03	2.48	0.77	1.62	3.89	1.80	1.03	0.73	2.80
Na_2O	3.16	0.68	1.75	4.66	3.15	0.80	1.96	5.06	2.80	0.69	1.73	3.55
K_2O	2.65	0.86	0.94	4.69	1.94	0.76	0.60	3.12	2.11	0.85	1.45	3.25
TiO_2	0.61	0.10	0.44	0.82	0.60	0.08	0.44	0.72	0.61	0.10	0.53	0.74
P_2O_5	0.17	0.06	0.12	0.47	0.17	0.03	0.13	0.22	0.16	0.04	0.12	0.22
LOI	2.02	1.04	0.75	4.71	2.29	0.58	1.32	3.15	3.42	0.46	2.66	4.10

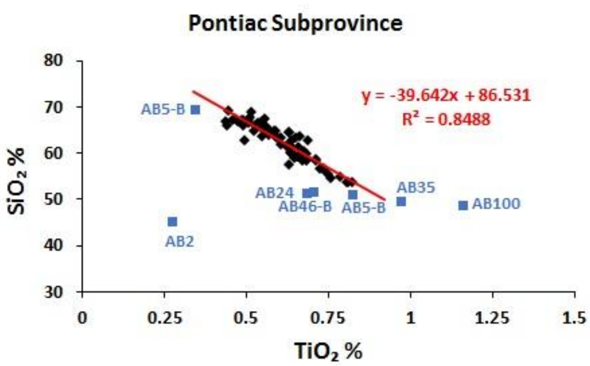

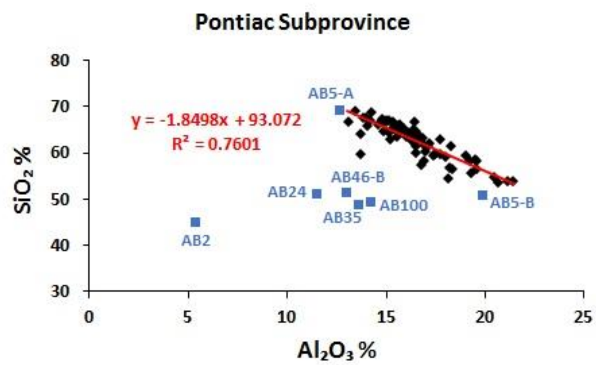

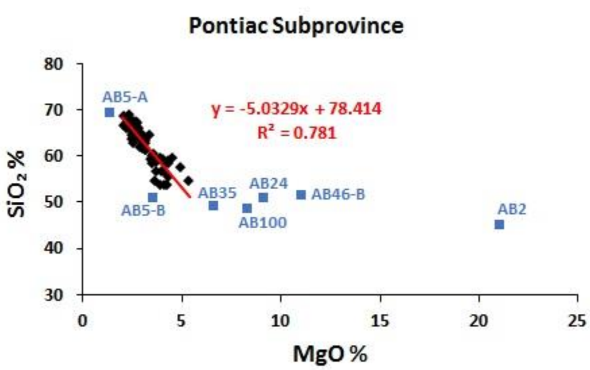

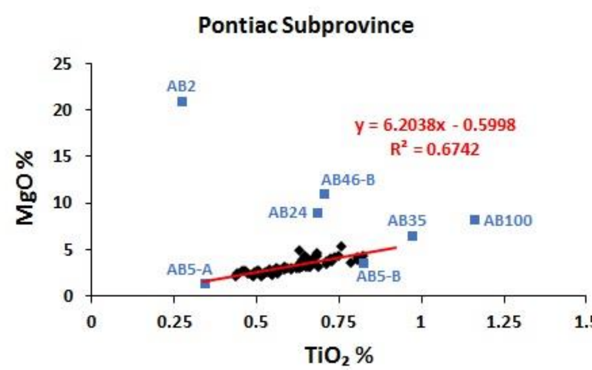

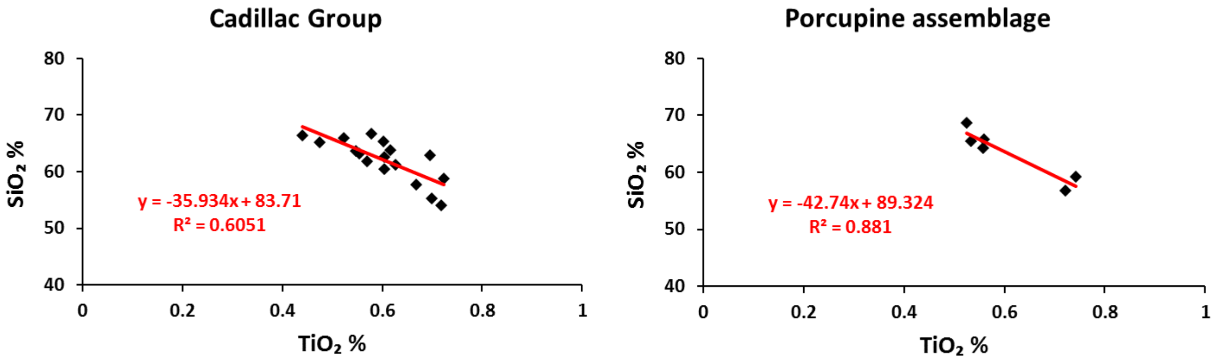

Figure 6.18. *Plots for selected major oxides of the samples under study. Blue boxes refer to samples excluded from the set.*

Especially for the rocks from the Pontiac subprovince, their concentrations in selected major oxides and elements were plotted vs increasing metamorphic temperature (Fig. 6.20). The average values of associated oxides and elements were used for separate plots (Fig. 6.19). Therefore, it is summarized the behavior of selected oxides, immobile elements and base metals from the Pontiac rocks during metamorphism.

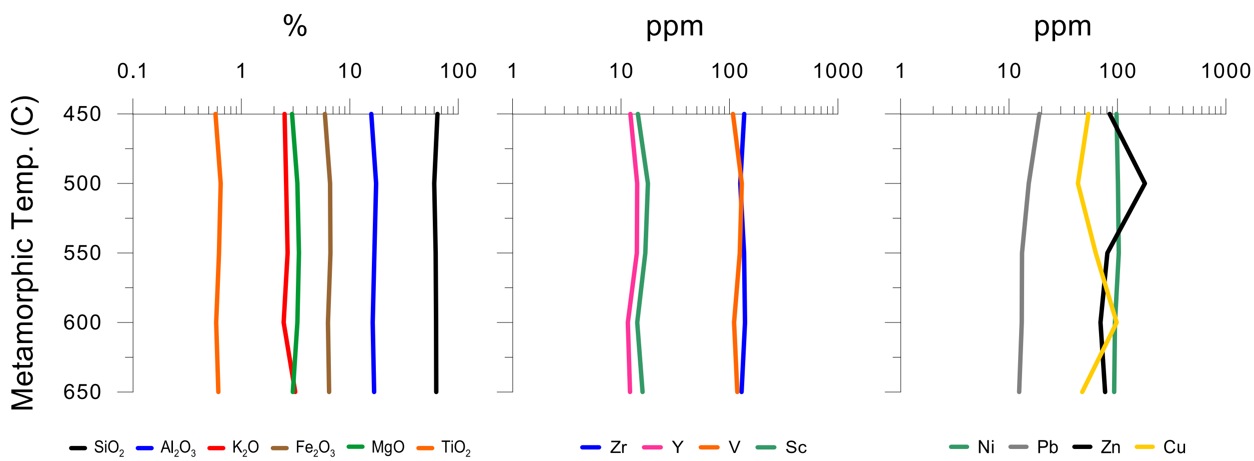

Figure 6.19. *Average concentrations vs metamorphic temperature for selected elements/oxides of the samples from the Pontiac subprovince.*

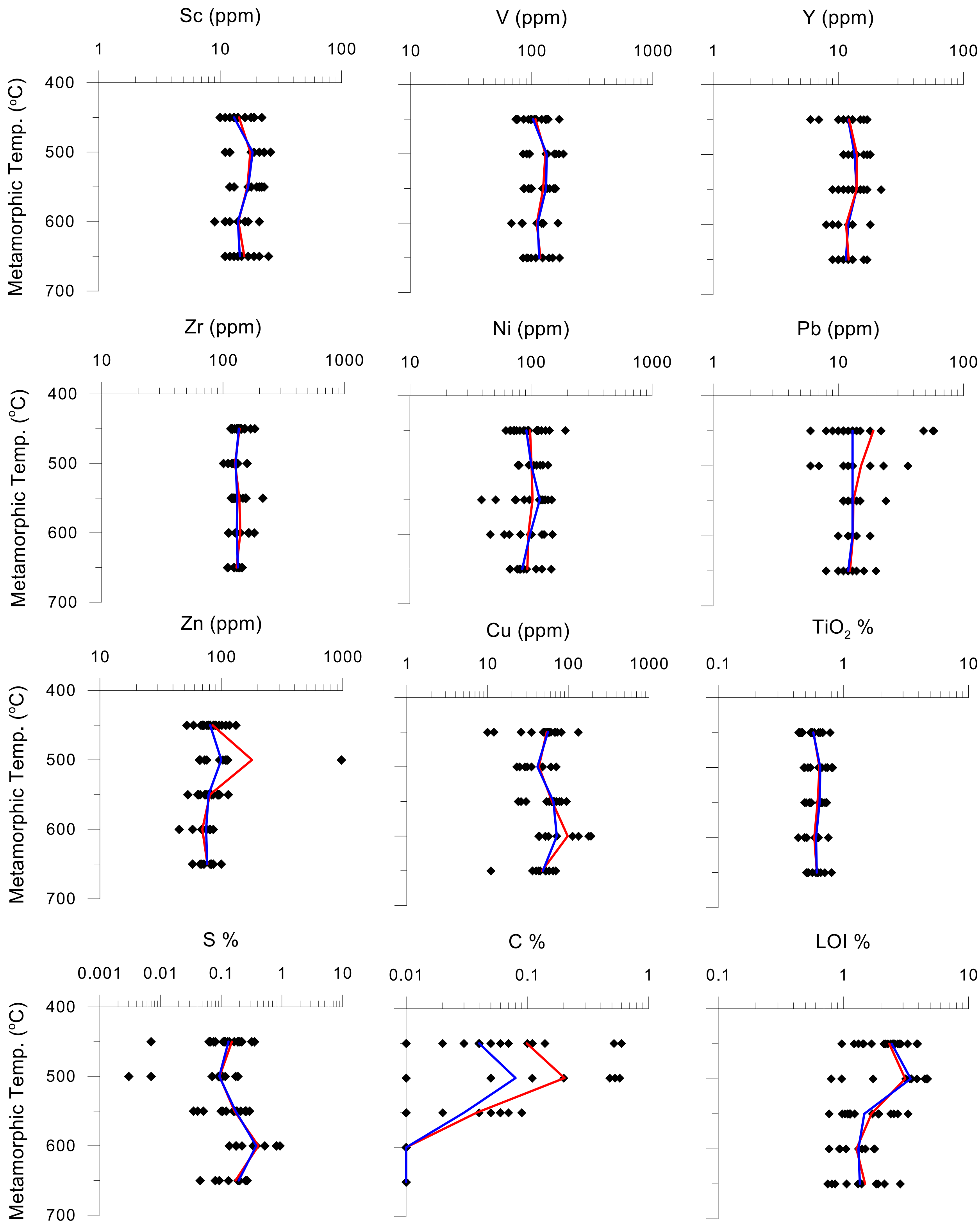

Figure 6.20. *Selected elements' concentrations vs metamorphic temperature graphs for the Pontiac samples. Red and blue lines represent average and median values respectively.*

6.2.2. Au, As, Sb, Se, Te, Bi

The concentrations of Au and related metals (As, Sb, Se, Te, Bi) for the rocks from the Pontiac subprovince, the Cadillac Group and the Porcupine assemblage were statistically analysed and are reported below, on Tables 6.2, 6.3, 6.4 respectively. The complete results are available on Appendix (4.2). Plots of the values against increasing metamorphic grade were made for the complete set of rock samples out of each studied sequence (Fig 6.21). Especially for the Pontiac samples, their Au- and As-content in the biotite and garnet zone was plotted against increasing distance from the Cadillac-Larder Lake fault (Fig. 6.22). Then, the average values of each metal out of each metamorphic zone, along with the ones for base metals and also S, C and LOI, were used to plot average lines against increasing metamorphic temperature (Fig. 6.23). This, provides a better overview for the elemental mobility among the zones and potentially, any indicative associations between the elements.

Table 6.2: *Results for Au, As, Sb, Se, Te, Bi for the rocks from the Pontiac subprovince.*

Metamorphic	Au (ppb)				As (ppm)				Sb (ppb)			
Zone	**Average**	**Median**	**Min**	**Max**	**Average**	**Median**	**Min**	**Max**	**Average**	**Median**	**Min**	**Max**
Biotite	4.17	1.41	0.24	29.98	12.39	12.69	0.16	39.29	303.3	205.1	13.66	1006
Garnet	1.58	0.80	0.44	5.92	9.20	5.38	0.12	26.25	164.3	144.2	20.58	387.5
Staurolite	0.63	0.48	0.15	1.52	0.51	0.25	0.10	4.20	104.2	62.26	11.05	279.0
Kyanite	0.48	0.41	0.11	1.36	0.21	0.17	0.11	0.39	76.64	26.59	16.03	264.8
Sillimanite	0.34	0.30	0.23	0.50	0.23	0.22	0.12	0.37	66.9	21.1	8.37	250.5

Metamorphic	Se (ppb)				Te (ppb)				Bi (ppb)			
Zone	**Average**	**Median**	**Min**	**Max**	**Average**	**Median**	**Min**	**Max**	**Average**	**Median**	**Min**	**Max**
Biotite	106.6	109.8	10.51	177.1	33.69	30.82	11.69	65.56	181.3	174.9	63.55	377.7
Garnet	76.64	78.02	5.61	149.5	31.53	28.69	17.87	53.76	118.1	108.7	68.54	195.6
Staurolite	129.5	121.3	17.88	233.5	34.33	34.07	15.65	51.45	183.9	174.3	57.49	432.3
Kyanite	239.3	142.7	69.41	627.7	32.75	27.50	16.73	54.46	97.73	93.37	64.44	176.7
Sillimanite	107.8	107.9	51.32	152.3	28.6	27.34	19.79	44.52	135.7	112.1	51.19	277.2

Table 6.3: *Results for Au, As, Sb, Se, Te, Bi for the rocks from the Cadillac Group.*

	Au (ppb)		As (ppm)		Sb (ppb)		Se (ppb)		Te (ppb)		Bi (ppb)	
Metamoprhic zone	**Chlorite**	**Biotite**	**Chlorite**	**Biotite**	**Chlorite**	**Biotite**	**Chlorite**	**Biotite**	**Chlorite**	**Biotite**	**Chlorite**	**Biotite**
Average	0.46	1.86	0.64	16.54	119.1	308.1	79.18	123.7	32.68	40.01	117.3	104.2
Median	0.51	0.85	0.57	0.81	109.6	119.1	66.33	137.8	38.37	41.63	123.0	69.19
Min	0.21	0.16	0.46	0.51	65.61	75.90	50.42	49.70	15.90	20.50	60.40	28.80
Max	0.68	9.08	1.13	87.26	191.6	1082	147.8	247.6	45.39	59.62	162.3	223.1

Table 6.4: *Results for Au, As, Sb, Se, Te, Bi for the rocks from the Porcupine Assemblage.*

	Average	Median	Min	Max
Au (ppb)	0.96	0.85	0.69	1.52
As (ppm)	19.67	18.99	14.82	25.99
Sb (ppb)	436.5	429.1	258.2	646.7

ppb	Average	Median	Min	Max
Se	86.57	79.77	17.95	147.2
Te	45.75	44.7	35.23	60.69
Bi	148.1	149.8	95.34	211.3

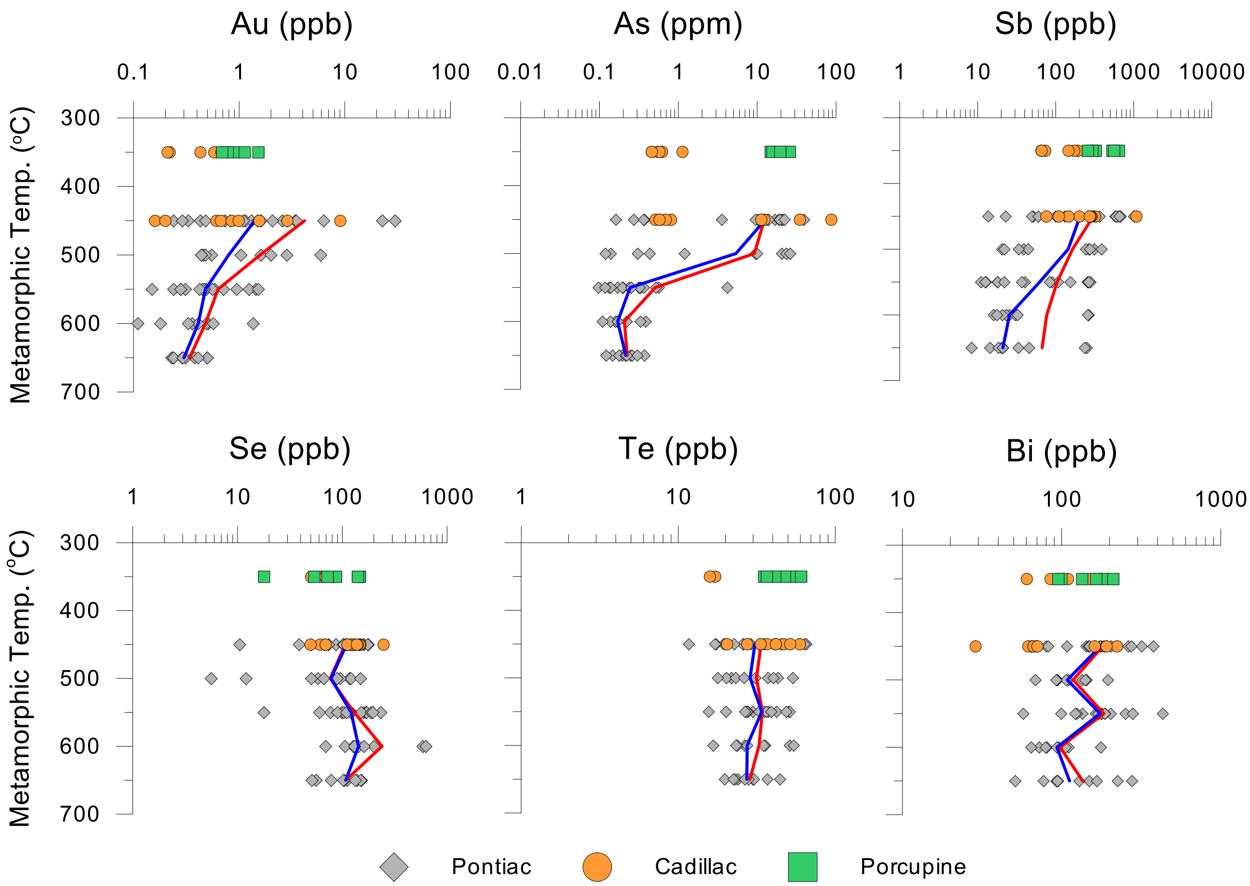

Figure 6.21. *Concentration of Au, As, Sb, Se, Te and Bi for the rock samples under study. Red and blue lines represent average and median values respectively.*

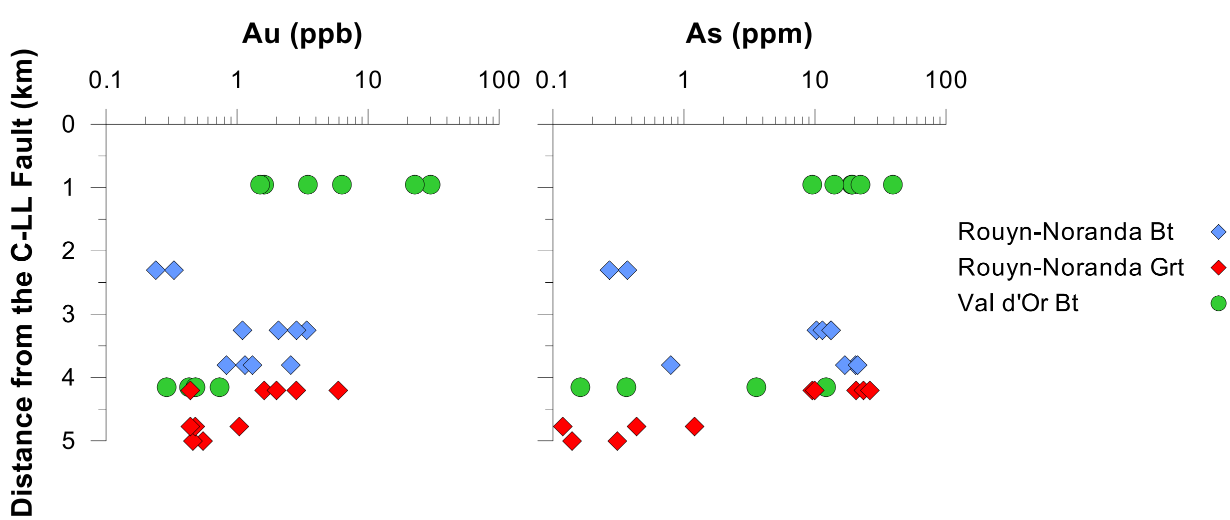

Figure 6.22. *Au & As distribution within biotite and garnet zones in the Pontiac, in respect to the distance from the Cadillac-Larder Lake fault.*

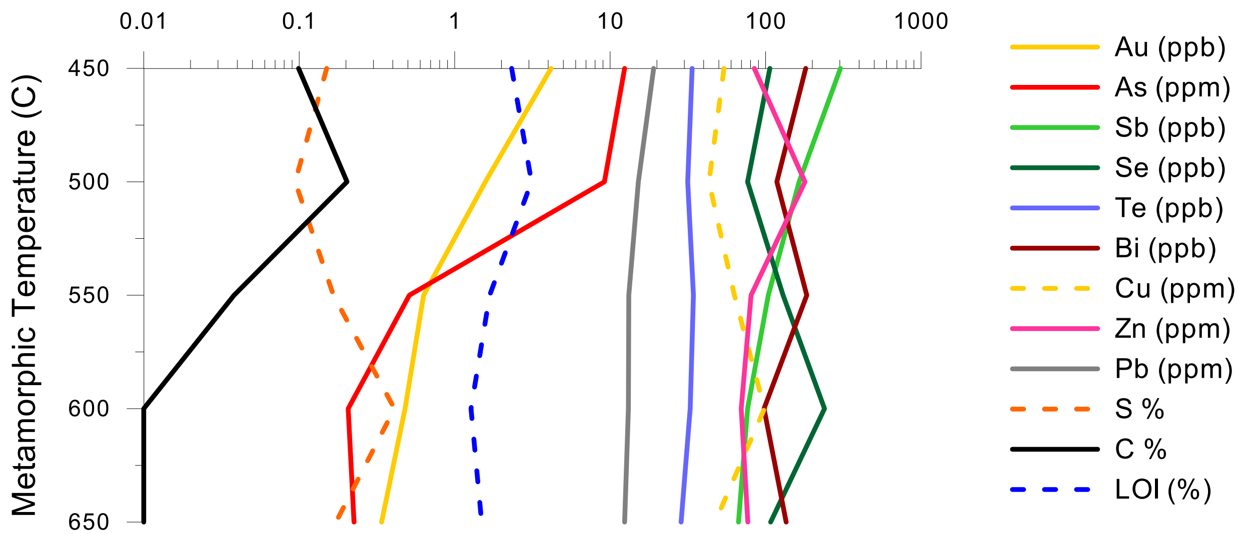

Figure 6.23. *Average concentrations of Au and related high-grade metals, base metals and S, C, and LOI vs metamorphic temperature in the Pontiac rocks.*

6.2.3. In situ LA-ICP-MS

Results for pyrites and pyrrhotites per metamorphic zone for the samples from the Pontiac subprovince are summarized below (Table 6.5, 6.6). Detailed results for detection limits, standards and complete samples are reported on Appendix 3.

Table 6.5. *Results for pyrites from the Pontiac subprovince.*

PYRITE		^{197}Au	^{75}As	^{121}Sb	^{77}Se	^{125}Te	^{209}Bi
	DL	**0.027**	**0.53**	**0.20**	**1.47**	**0.39**	**0.057**
	Average	0.15	39.3	22.1	6.45	0.47	2.60
Biotite	**SD**	0.79	32.9	27.8	3.62	0.35	8.49
(AB97)	**max**	5.84	144	121	14.9	2.35	47.1
n=53	**min**	0.027	0.88	0.20	1.47	0.39	0.057
	Average	0.031	1001	1.06	13.0	0.46	2.91
Garnet	**SD**	0.011	984	1.34	12.8	0.15	3.28
(AB31)	**max**	0.061	3306	3.70	45.2	0.80	9.39
n=9	**min**	0.027	53.8	0.20	3.85	0.39	0.057
	Average	-	-	-	-	-	-
Staurolite	**SD**	-	-	-	-	-	-
	max	-	-	-	-	-	-
	min	-	-	-	-	-	-
	Average	BDL	2.48	BDL	24.7	1.96	0.97
Kyanite	**SD**	-	2.97	-	9.23	1.89	2.11
n=10	**max**	-	9.60	-	39.4	6.57	6.65
	min	-	0.53	-	11.6	0.39	0.057
	Average	BDL	6.42	3.96	7.68	0.70	1.91
Sillimanite	**SD**	-	9.50	4.50	4.27	0.69	3.53
n=5	**max**	-	22.5	11.7	14.1	1.93	8.22
	min	-	0.53	0.28	3.11	0.39	0.14

Table 6.6. *Results for pyrrhotites from the Pontiac subprovince.*

PYRRHOTITE		^{197}Au	^{75}As	^{121}Sb	^{77}Se	^{125}Te	^{209}Bi
	DL	**0.027**	**0.526**	**0.20**	**1.47**	**0.390**	**0.057**
	Average	BDL	0.527	0.23	10.2	BDL	1.06
Biotite	**SD**	-	0.006	0.08	1.48	-	1.19
(AB65)	**max**	-	0.55	0.49	12.6	-	3.67
n=13	**min**	-	0.526	0.20	7.66	-	0.15
	Average	BDL	BDL	BDL	18.1	0.39	1.40
Garnet	**SD**	-	-	-	1.38	0.01	4.57
(AB28)	**max**	-	-	-	20.7	0.42	17.9
n=15	**min**	-	-	-	16.0	0.390	0.057
	Average	BDL	0.537	BDL	20.6	0.75	1.12
Staurolite	**SD**	-	0.06	-	1.61	1.8	1.91
(AB111)	**max**	-	0.83	-	23.9	9.3	7.90
n=26	**min**	-	0.526	-	17.4	0.390	0.057
	Average	BDL	BDL	BDL	24.2	0.391	0.26
Kyanite	**SD**	-	-	-	3.06	0.004	0.30
n=16	**max**	-	-	-	27.8	0.407	1.26
	min	-	-	-	15.3	0.390	0.057
	Average	BDL	BDL	BDL	18.4	1.42	6.76
Sillimanite	**SD**	-	-	-	2.04	3.63	18.0
n=13	**max**	-	-	-	23.3	13.5	66.5
	min	-	-	-	15.2	0.390	0.196

7. Discussion

7.1. Protolith composition

The samples show no evidence of significant, systematic SiO_2, Al_2O_3, Fe_2O_3 and K_2O mobility during metamorphism (Fig. 6.19) and therefore their protolith composition has been constrained through a discrimination diagram which is based on the SiO_2:Al_2O_3 vs Fe_2O_3:K_2O ratios (Herron, 1988) (Fig. 7.1). The vast majority of the samples from the Pontiac subprovince fall inside the field of "shale", while a few others are plotted as either "Fe-shales" or "wackes". Cadillac Group samples are also plotted inside the "shale" field but there are also samples which classify as "Fe-shales". The outlying sample in the Fe-shale field is AB70; its very low K_2O content has affected the denominator of the ratio. Then, apart from a couple of samples which are classified as "shales", the rocks from the Porcupine assemblage stand between the borders of "shale"-"wacke"-"Fe-shale"-"Fe-sand" (Fig. 7.1).

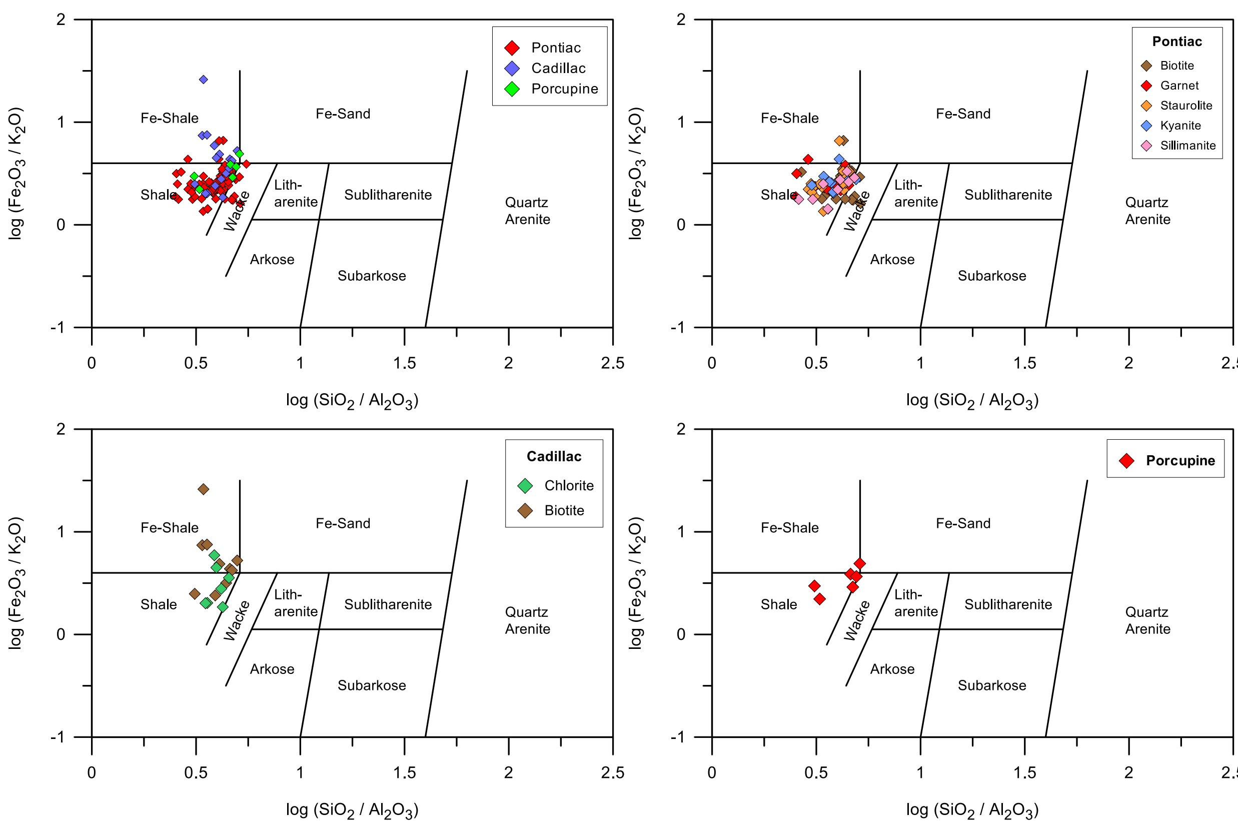

Figure 7.1. *Protolith compositions for the rock samples of each metasedimentary sequence. Diagrams after Herron, 1988)*

Major and trace element patterns normalized to both chondrite (Boynton, 1984) for the REEs of the Pontiac samples and North American Shale Composite (N.A.S.C.) (Gromet et al., 1984) for their major element oxides are shown in figure 7.2 A-B respectively. These plots allow the comparison of the geochemical signature between samples from each different group.

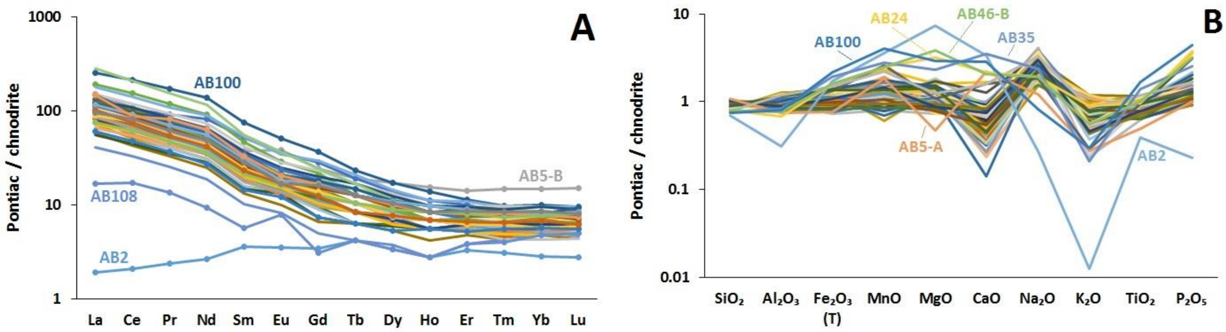

Figure 7.2. *Normalized patterns of the Pontiac subprovince samples using A) chondrite and B) NASC values.*

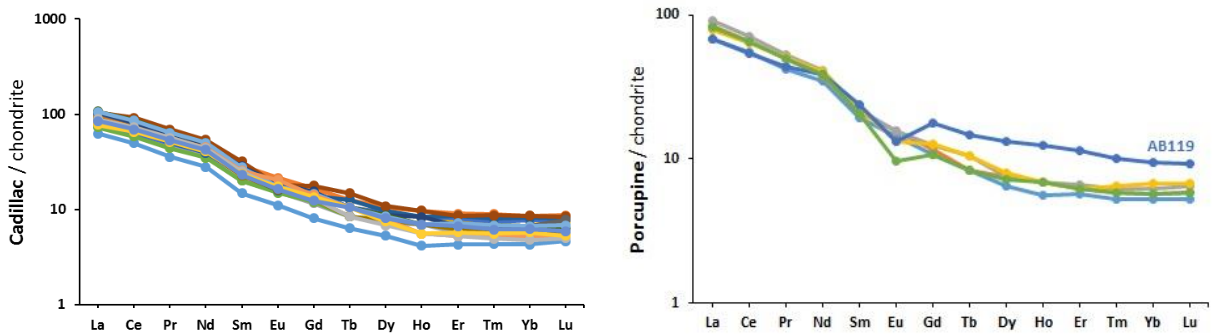

Figure 7.3. *Normalized patterns for the Cadillac Group and the Porcupine assemblage samples using chondrite values of Boynton, 1984.*

Based on the geochemical pattern and also the mineralogy observed, the following samples have been excluded from the metasedimentary sample suite as they show the characteristic of metaigneous rocks; AB2, AB5-A, AB5-B, AB24, AB35, AB46-B and AB100. The exact reasons are explained below:

- The AB2 pattern is distinctly different to the rest of the samples for both the chondrite and the NASC normalizations (Fig. 7.2A). It shows low SiO_2 and extremely low K_2O contents (45.2 % and 0.05 % respectively). K_2O content for the rest of the samples is 2.65±0.86 %. MgO is rather high (21.02%) in comparison to the rest (3.15 ±0.73 %). It also has very high Cr and Ni values. It is composed of plagioclase and chlorite. It displays progressed sericitization.
- Plagioclase and chlorite are dominant in samples AB5A and 5B respectively. The presence of amphiboles was also identified. In addition, these two samples showed extremely high bismuth contents (2780.87 ppb and 1084.24 ppb respectively) while the rest of the samples had an average Bi concentration of 152.29 ±84.5 ppb.
- AB24 is plotted outside the array of samples in the oxide diagrams (Fig. 7.2B) and then contains 9.05% MgO and 7.9% CaO while the rest of the samples have 3.15 ±0.73% and 2.46 ±0.99% respectively. It shows lower Al_2O_3 content (11.43%) and high P_2O_5 (0.49%) in comparison to the

rest (16.52 ±1.97% and 0.17 ±0.06% respectively). Lastly, its Cr content (660 ppm) is more than doubled to the rest (259.23 ±35.76 ppm).

- AB35 is composed of amphibole and plagioclase with lesser chlorite and epidote. It shows high (12.69 %) CaO content while the rest of the samples have 2.44 ±0.85 % CaO. Bismuth content is also elevated in comparison to the rest (567.12 ppb).
- AB46-B mostly consists of chlorite and plagioclase. It shows high, 10.98% MgO content (the rest display 3.2 ±0.83% MgO) and Cr is elevated. It is always plotted away of the samples' array (Fig. 7.2B).
- AB100 is composed of chlorite and plagioclase with lesser amphibole and epidote. It shows low SiO_2 (48.85%) content. Fe_2O_3 is high (12.21%) and Bi is also higher than the rest of the samples (6.64 ±1.93 % Fe_2O_3, 428.66 ppb Bi).

All samples except for AB 5A & 5B (i.e. AB2, AB35, AB46-B, AB100) have much higher MgO values (21.02, 9.05, 6.54, 10.98, 8.26 % respectively) than the rest, which show MgO contents of 3.2 ±0.83 %. Sample AB108 shows lower REE contents in respect to the chondrite and distinctly positive Eu anomaly because it is composed of syn-deformational plagioclase porphyroblasts and Eu must be incorporated to it.

The Th/U ratio for the rocks of the Pontiac subprovince are 3.46 ±0.77. Cadillac Group and Porcupine samples showed U/Th ratio values of 3.64 ±0.44 and 3.58 ±0.21 respectively. All these values are in close agreement with previous studies which reported U/Th ratios of 3.6 ±0.5 and linked these values with the absence of K-rich igneous rocks and the possible presence of mafic-ultramafic rocks in the material source areas (Camiré et al., 1993).

Cadillac Group and Porcupine samples showed no remarkable differences in between them in terms of geochemical content. Only sample AB119 of the Porcupine assemblage shows relatively lower LREE and higher HREE values in respect to the others (Fig. 7.3).

7.2. Protolith metal content

The key to any investigation into mass change during metamorphism is the robust definition of the composition of the protoliths. In this study, there are no unmetamorphosed Pontiac rocks in the area; thus the metal content needs to be defined by the samples closest to the protoliths' characteristics. The biotite zone is the lowest metamorphic grade exposed and the rocks from this zone preserve some sedimentary characteristics and show no pervasive alteration or metasomatism. AB96 and AB97 (Fig. 6.21) have slightly higher Au concentrations than the rest of the twenty (20) biotite zone samples in total. These two samples were carefully investigated in terms of alteration and sulphide mineralogy in order to evaluate whether the high Au-values are a primary feature coming from the sedimentary protolith or are from diffuse Au mineralization during metamorphism. All sulphides including the pyrites occur aligned to the foliation, which is folded in places. This indicates they were formed prior to metamorphism or, at least, early in the deformation history. There is no evidence for large-scale chloritization, sericitisation or carbonation in the rocks which is common with orogenic Au mineralization. Therefore, the metal concentrations in these samples are considered as representative of the protolith rocks (Table 7.1).

Table 7.1: *The metal content of the Pontiac subprovince biotite zone rocks which are used as protolith values.*

Element	Average	SD	Max	Min	Element	Average	SD	Max	Min
Au (ppb)	4.17	7.82	29.98	0.24	Se (ppb)	106.61	43.47	177.05	10.51
As (ppm)	12.39	9.97	39.29	0.16	Te (ppb)	33.69	15.53	65.56	11.69
Sb (ppb)	303.28	287.25	1005.74	13.66	Bi (ppb)	181.25	78.44	377.68	63.55

The chlorite zone Cadillac and the Porcupine samples have lower Au content than the Pontiac samples. Thus, there are of lower Au fertility in respect to the Pontiac rocks. The same Porcupine samples though, show high As content. This is probably because they contain recrystallized pyrite aggregates (Fig. 6.17 B-C), which are low in Au, but high in As, as evidenced through LA-ICP-MS analyses (Appendix 3.1.2). For As, the same fact is not clear; the samples also show bimodal distribution. For both Cadillac and Porcupine samples, the trend in Sb seems to continue while decreasing metamorphic temperature (Fig. 6.21). Then, it is noteworthy to mention, that for Se, Te and Bi, all Cadillac and Porcupine samples are plotted inside the range of values of that of the Pontiac samples. No significant differences/mobilities were identified for these metals.

Even though some similarities/differences can be identified between the different sequences, the results for the Porcupine samples for example (which come from a single locality and metamorphic zone) can only be of limited discussion. The same applies to the samples from the Cadillac were only two metamorphic zones were sampled because the exposure of higher metamorphic grade rock is poor. In conclusion, more samples are needed from both sequences in order to establish a complete argument for potential metal mobility as it is done with the Pontiac subprovince rocks.

Moreover, the values for Au, As, Sb, Se, Te, Bi for the rocks from the Pontiac subprovince were statistically studied through box-and-whisker plots (Fig. 7.4). Studying these graphs, it is evident that the samples with high metal content strongly affect the development of the average lines and thus, the average value itself.

For the Au graph, samples AB96 and AB97 are plotted outside the positive whisker as outliers but for a number of reasons explained before, they were not excluded from the sample set. It is interesting to see that the range in As values for the staurolite, kyanite and sillimanite zone samples is quite tight in respect to the ones of biotite and garnet zone. It indicates the mobilisation of the majority of As between garnet and staurolite metamorphic conditions. Then, Sb shows a smooth decrease in both the average values and the IQRs; though there is an abrupt change in median values between garnet and staurolite zone as well. Selenium shows minor IQ range fluctuations, though the average value of kyanite zone strongly depends upon the high-Se samples AB43 and AB44 which are rich in pyrite in respect to the others. Except for minor changes in median values, no remarkable facts were identified in the Te-content of the rocks. On the other hand, fluctuations in both average-median values and IQRs occur for the Bi of the rocks (Fig. 7.4).

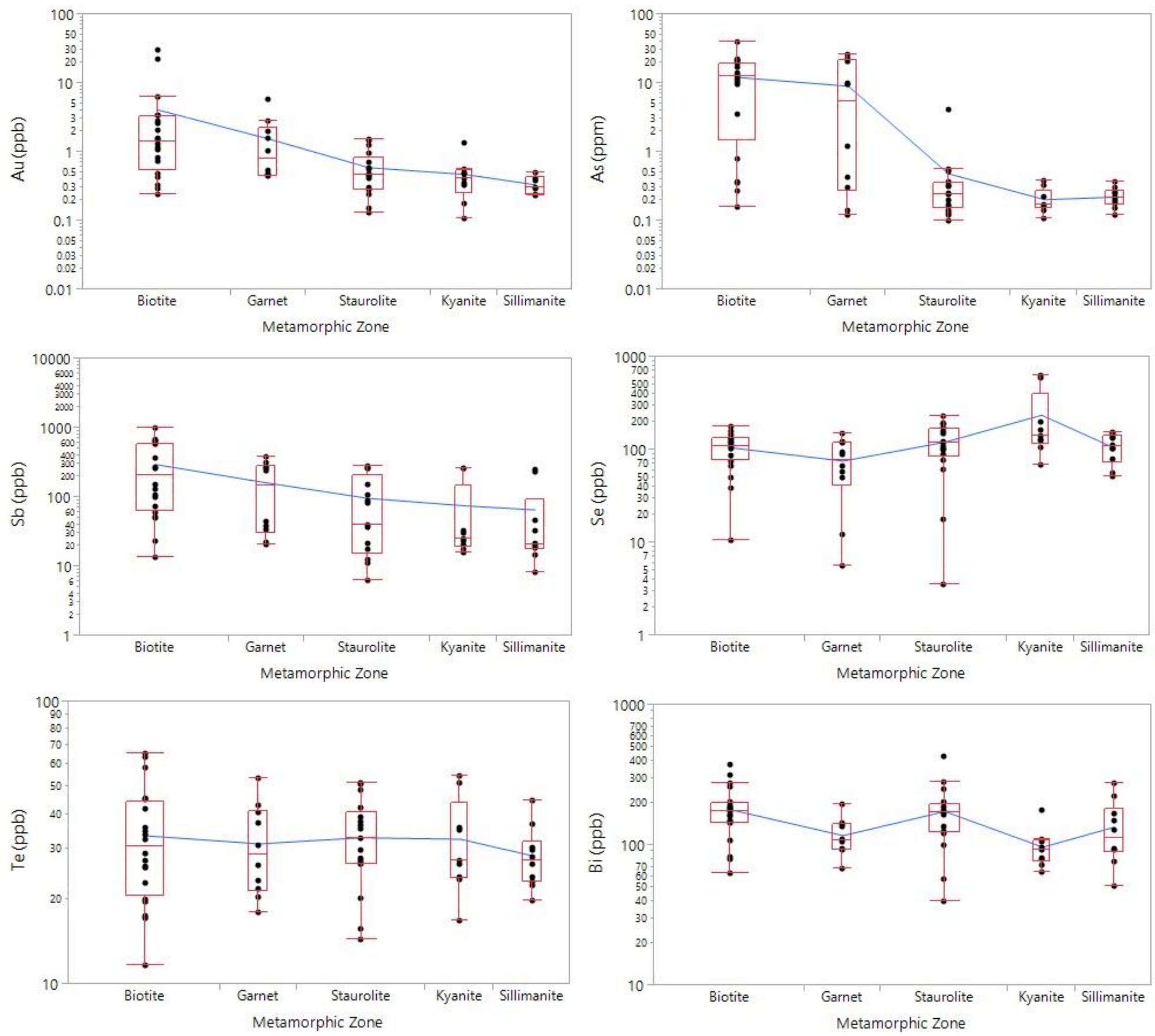

Figure 7.4. *Box-and-whisker plots for the Pontiac subprovince samples. The blue lines connect the average values of each metamorphic zone.*

7.2.1. Variation of metal content with protolith composition

Titanium (Ti) is widely used in geochemical diagrams for rock classification and elemental mobility studies because of its immobile behavior. The negative correlation between TiO_2 and SiO_2 contents corresponds to the variation in protolith rock composition. Pelites and shales have lower SiO_2 and higher TiO_2 contents than sandstones. Then the main difference between pelites and shales is the CaO content which is much higher in the latter (Bucher and Grapes, 2011).

The concentration of Au, As, Sb, Se, Te, Bi of all the rocks from the Pontiac subprovince were plotted against TiO_2 (Fig. 7.5) in order to evaluate whether there is any systematic variation in the concentrations of these elements with the protolith rock composition as defined by the TiO_2 content.

Using the biotite zone samples only, which represent the protolith samples, regression lines are plotted to show the variation of the different metal concentrations with TiO_2 content (Fig. 7.5). Except for Sb and Te, the R^2 values for the regressions are below 0.2 indicating that for these metals there is no significant variation with TiO_2. It is noteworthy that the two high-Au content samples strongly control the slope of the regression line in the TiO_2-Au graph; excluding these samples, the slope turns negative, as is the case with Sb. This would indicate that the samples closer to sandstone composition should be more fertile in Au and Sb. The graphs indicate that for Au, As, Se, and Bi there is no strong correlation between the metal content and the TiO_2.

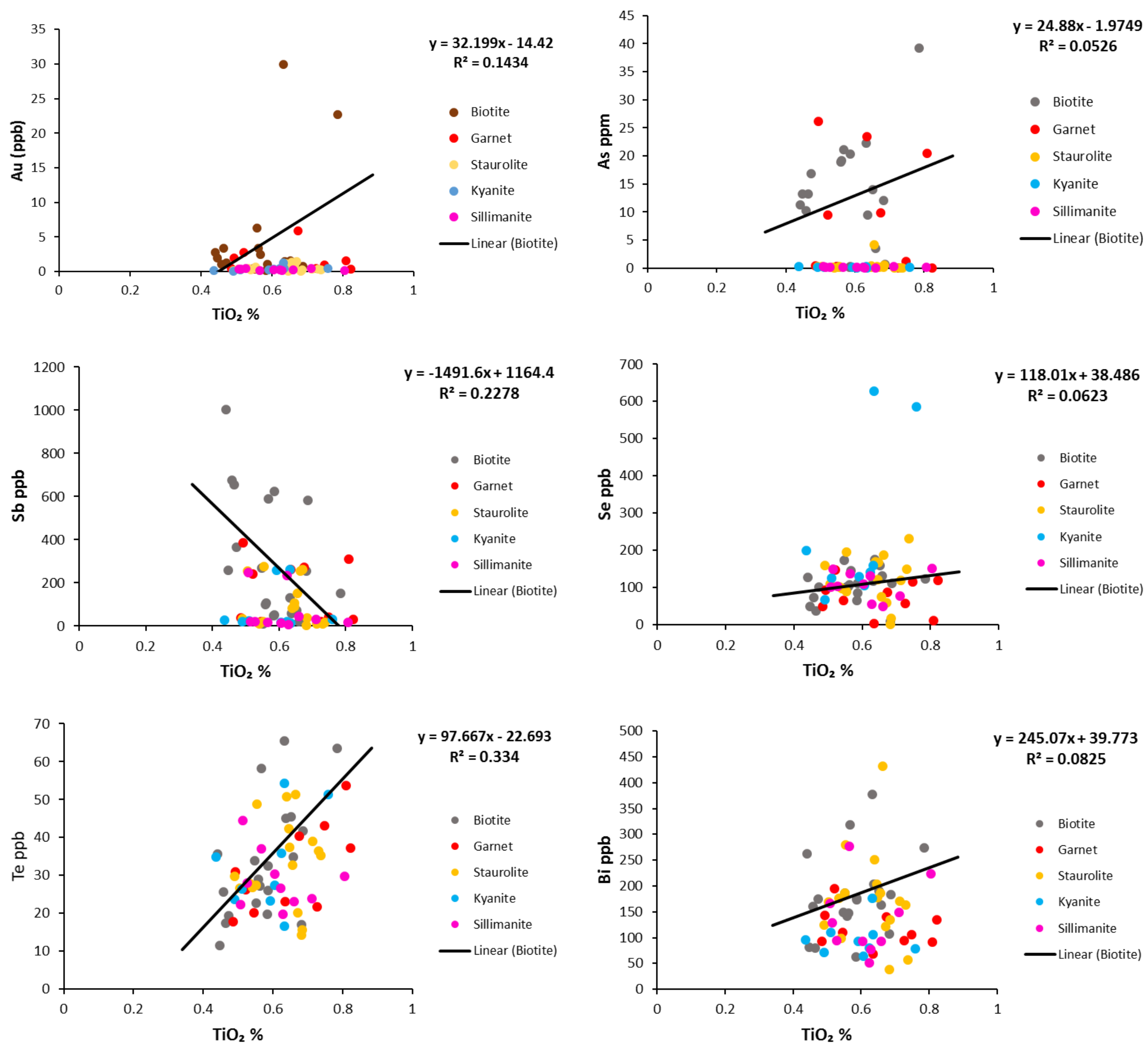

Figure 7.5. Plots for Au, As, Sb, Se, Te and Bi vs TiO_2 of the rocks from the Pontiac subprovince. Regression lines are plotted for biotite zone samples.

7.3. Metamorphic conditions

The Pontiac subprovince is a sequence of metasedimentary rocks which was regionally metamorphosed at ≈2670 Ma during the collision of the Pontiac terrane with the southern Abitibi Belt (Feng et al., 1992). The Barrovian-like sequence extends from biotite zone greenschist facies in the north to sillimanite zone amphibolite facies metamorphic rocks in the south (Benn et al., 1994, Camiré and Burg, 1993). The metamorphic isograds lie in parallel with the Cadillac-Larder Lake Fault indicating a southward increase in metamorphic grade (Fig. 4.1). The lower metamorphic grade rocks from the Pontiac subprovince display some sedimentary characteristics such as clear compositional layering with moderate foliation development, while the higher-grade samples contain almost granoblastic, fine-grained quartz and distinct metamorphic foliation with platy micas defining the foliation surfaces. Angular quartz grains only occur in lower-grade rocks. Except for sillimanite, all other index minerals of each metamorphic zone (biotite-garnet-staurolite-kyanite) were identified in the sequence. Garnet is abundant in the garnet and sillimanite zone rocks. It was also found inside the biotite zone. Staurolite crystals were euhedral indicating stable P-T conditions and equilibrium with their surrounding minerals.

The index minerals observed in this study follow the classic Barrovian sequence; biotite, garnet, staurolite, and kyanite, indicating an intermediate PT geothermal gradient that is associated with regional metamorphism. Sillimanite was not identified in the samples collected in this study but has been reported in previous work (Benn et al., 1994). The presence of andalusite has not been identified in the thin sections in this study, and has not been reported elsewhere. The temperature of metamorphism attributed for each metamorphic zone is an estimate of the average conditions based on the current understanding of Barrovian metamorphism of pelitic rocks (Baxter et al., 2002) and is considered to be accurate to ±50°. For this reason, all geochemical plots referring to the metamorphic zones were selected to be constructed with increasing metamorphic temperature from 450°C for the biotite zone samples, to 650°C for the sillimanite zone samples.

Regarding the samples from the chlorite and biotite zones of the Cadillac Group, they were set to be plotted against 350°C and 450°C respectively, based upon previous studies (Powell et al., 1995) and this study's mineralogical investigation. The Porcupine assemblage samples were plotted with 350°C as their peak metamorphic temperature.

7.4. Mass changes during metamorphism

7.4.1. Mobility of Au and related elements

As reported above, the concentration of Au and related metals (As, Sb, Se, Te, Bi) in the samples has been calculated with high precision, low-detection limit methods (Pitcairn et al., 2006b). Reference materials results showed close agreement with certified values (Table 5.1). The mobility of these metals along with a number of elements & oxides, was examined after constructing graphs with the element's average concentration vs increasing metamorphic temperature (Fig. 6.19, 6.20, 6.21).

The concentrations in Au, As and Sb systematically decrease from the biotite zone greenschist facies to sillimanite zone amphibolite facies rocks (Table 6.2). The average Au content in the biotite zone (4.17ppb, range 0.24-29.98ppb) drops almost 92% to 0.34 ±0.1 ppb in the sillimanite zone rocks. The As content of the Pontiac rocks is three (3) orders of magnitude higher than Au. Biotite samples have an average As content of 12.39ppm (range 0.16-39.29) while sillimanite zone samples show 0.23ppm (range 0.12-0.37ppm); this corresponds to even higher mass change than Au, with >98% of As mobilised during metamorphism. Average Sb values show a smoother change from the biotite zone with an average value of 303.28ppb (range 13.66-1005.74ppb), down to 66.90ppb (range 8.37-250.52ppb) in the sillimanite zone samples. This indicates a 78% Sb mass loss. It is important to mention that the average As trend differs than the ones for Au and Sb, showing a very abrupt change between the garnet and staurolite zone samples. The mass change for Se, Te and Bi shows different trends with mass variation being affected by a small number of high concentration samples or varying considerably between metamorphic zones. The fluctuation of the average values of Se, is attributed to the high content of samples AB43 and AB44 from the kyanite zone. The range of Te values with increasing metamorphic temperature shows fair consistency indicating no significant mobility of this metal from the rocks. The fluctuation of both the average and median values for Bi indicates possible Bi loss during metamorphism but the lack of systematic mass change makes this interpretation debatable.

It is clearly shown in the graphs (Fig. 6.19, 6.20, 6.21) that there is no remarkable mobility in any of the elements under study except for Au, As, Sb. Selenium, Cu and S show similar trends which indicates their association in distribution inside the rocks. The drift of average Zn content in the garnet zone (500°C) is attributed to sample AB26.

The distinct decreases in Au, As, and Sb are discussed to be a function of increasing metamorphic grade; as they have also been demonstrated in other metasedimentary sequences (Pitcairn et al., 2006a; 2015). An alternative hypothesis is that the higher metal contents in the lower metamorphic grade rocks indicate diffuse infiltration of metal-rich fluids from the adjacent Cadillac-Larder Lake Fault zone which is known that it acted as the flow pathway of hydrothermal fluids which formed the orogenic Au deposits in the area (Robert et al. 2005). In order to further investigate that fact, the metal concentrations in the biotite zone samples which are attributed the same metamorphic temperature, are plotted against distance from the LLCFZ (Fig. 6.22). The Val d'Or section shows a clear trend of increasing metal content closer to the fault, which is though strongly controlled by the two (2) Au-rich samples AB96 and AB97 which were previously evaluated as showing no evidence of mineralization. The Rouyn-Noranda samples show negative trend with distance from the CLLFZ. Mass change within the biotite zone is not particularly clear, and when including the garnet zone samples appears to be in line with changes due to the metamorphic gradient.

The distinct depletion in carbon (Fig. 6.20, 6.23) with increasing metamorphic grade, indicates that the fluid which transported Au, As and Sb was C-rich. The plot of LOI values with increasing metamorphic temperature is also interesting because it shows a significant negative change between garnet and staurolite zone facies (Fig. 6.20, 6.23). This is exactly when vast fluid production occurred during metamorphism of the Pontiac rocks and large amount of volatiles were liberated from the host rock. The values obtained through LOI (loss on ignition) account for both H_2O and CO_2 measurements, thus it is easy to calculate the water amount (LOI – Total-C = H_2O) and then its volume produced during metamorphism. It is noted that the distinct shifts in values for both C and H_2O, coincide the time where chlorite breaks down. The masses of H_2O and C mobilised, indicate that the fluid produced, would have been around 89% H_2O and 11% CO_2.

To summarize, the data shows that significant metal mobility occurred during metamorphism of the Pontiac subprovince. The high-grade rocks are remarkably depleted in Au, As, Sb, while limited, minor, Bi mobility also occurred. Except for S, all trends for Au, As, Sb, H_2O & C positively correlate between them with increasing metamorphic temperature (Fig. 6.23). This indicates that the aforementioned metals were extensively mobilised, especially during the greenschist-amphibolite facies transition, and were transported through a C-rich, S-poor fluid, in excess of water. The mobility of these metals and the distribution of their content within each metamorphic zone, their averages and median values can be comprehended more easily by looking at the box-and-whiskers graphs (Fig. 7.4).

7.5. Mineral hosts and mineral reactions

The majority of sulphide minerals in the Pontiac rocks were found aligned to the foliation, which indicates that they are most likely of diagenetic origin forming as the rocks were deposited on the seafloor. The minerals have clearly undergone textural and compositional changes during metamorphism. Pyrrhotite is dominant throughout the matrix of the rocks of each metamorphic zone and occurs either as patches of larger size or small isolated grains. Pyrites are commonly present but to a lesser extent and occur as larger grains that commonly preserve some euhedral grain boundaries and are locally porous. The majority of pyrite displays textures indicating replacement by pyrrhotite (Fig. 6.2 A-B-C, 6.4C, 6.7D, 6.9C). These textures are similar to those observed in other metasedimentary sequences such as the Phanerozoic Dalradian metasedimentary belt (Pitcairn et al., 2015) and the Otago Schists in New Zealand (Pitcairn et al., 2006a). Chalcopyrite is generally found as small grains throughout the sequence while galena becomes less abundant and its size is decreasing with increasing metamorphic grade. Cobaltites were only identified in samples from the biotite and garnet zone, either as inclusions in pyrrhotite or as isolated grains (Fig. 6.2D, 6.4D).

The abundance of pyrrhotite increases with increasing metamorphic grade while pyrite becomes less abundant (Fig. 7.6). Figure 7.6 was constructed from the total number of Py and Po grains analysed during SEM-EDS investigation of a set of samples from each metamorphic zone. It is possible that the graph is biased, because firstly, not every single grain of either Py or Po was analysed and secondly, only a small number of samples from each metamorphic zone were investigated with the SEM. Therefore, the percentages show a rough estimate which is though in agreement with the concept of pyrite breakdown due to increasing metamorphic conditions (Tomkins, 2010). The values assigned for staurolite zone (550°C) are off-trend because the samples under study have probably not been the most representative ones out of the sequence. Lastly, it is roughly estimated though that the Po-Py ratio is 2:1 in the biotite zone and increases to 4:1 in the sillimanite zone.

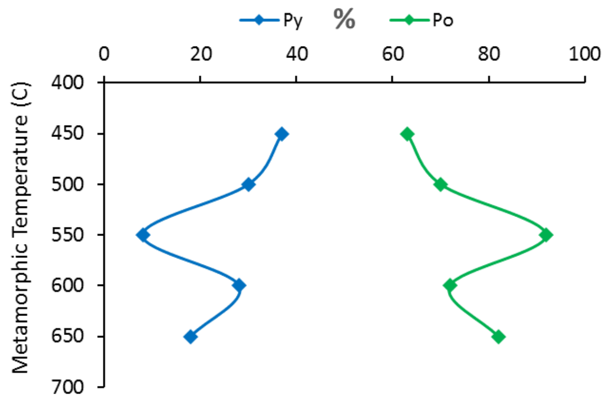

Figure 7.6. The proportion of pyrite and pyrrhotite in the rocks from the Pontiac Subprovince.

In situ LA-ICP-MS analyses in sulphides showed that pyrite is the main Au host in low-metamorphic grade samples. Multiple analyses in pyrites from the biotite zone displayed 0.15ppm Au, 39.3ppm As, and 22.1ppm Sb on average. Garnet zone pyrites, showed average Au concentrations slightly above detection limit values. The elevated average As content (1001ppm) in pyrite from the garnet zone sample is attributed to the presence and analyses of pyrite aggregates (Fig. 6.4A). After staurolite zone conditions, Au is below detection limit values in pyrite. Pyrrhotite is Au-free throughout the sequence. The results show that the Py-Po transition is the controlling mechanism for metal liberation from the rock. Rough estimations for the Py-Po proportion (Fig. 7.6) in the rocks of each metamorphic zone show that roughly 40% of pyrite is present in the biotite zone samples. This indicates that the lower (chlorite zone) metamorphic grade rocks which are expected to have higher Py content, should therefore have higher bulk rock Au-values. This would result in higher mass balance values.

During prograde metamorphism, dehydration reactions take place and hydrous minerals (zeolites, micas, chlorite, amphibole) transform to less hydrous or anhydrous minerals releasing H_2O to a fluid phase (Bucher and Grapes, 2011). The breakdown of chlorite, which terminally takes place at the greenschist-amphibolite facies transition, comprises the most important process driving sulphur and metal extraction (Phillips and Powell, 2010). Sulphur is liberated during metamorphism also, especially during the transition from pyrite to pyrrhotite with excess of water (equation 2, Pitcairn et al., 2010; Tomkins, 2010). The fluids generated, are H_2O-CO_2-rich and do not favor base metals transportation since the latter are being transported as chloride complexes. Thus, during metamorphic devolatilization, Au and related metals, can be more effectively leached than base metals (Cu, Zn, Pb, Ni) (Pitcairn et al., 2006a).

Chlorite in particular, liberates water during prograde metamorphism (while also becoming more Mg-rich) (Bucher and Grapes, 2011), but the vast water volume is produced during the transition from greenschist to amphibolite facies metamorphism (Phillips and Powell, 2010). For the case of Pontiac rocks, equation (1) can indicate the controlling mechanism of fluid production since staurolites were common in staurolite zone (early-amphibolite facies) rocks (Fig. 6.5, 6.6). There is also a vast number of equations which fit the concept of both chlorite and pyrite breakdown but the main mineral phase equations which are considered of high importance, are the following:

1. Grt + **Chl** + Ms = St + Bt + Qz + H_2O — Bucher and Grapes, 2011
2. 2 FeS_2 (pyrite) + 2 H_2O = 2 FeS (pyrrhotite) + 2 H_2S + O_2 — Pitcairn et al., 2010
3. C_2H_6 (ethane) + 2H_2O = CO_2 + CH_4 + 3H_2 — Gaboury, 2013

In addition, a number of equations are reported, in which degradation reactions for ethane (C_2H_6) and consumption of water take place during metamorphism of carbonaceous sedimentary rocks (Gaboury, 2013). The observed C mobility in the Pontiac rocks is possibly attributed to high initial ethane content in the rocks; metamorphism then favored the production and mobility of CO_2 according to equation (3).

7.6. Implications for formation of orogenic Au deposits in the Abitibi

7.6.1. Mass balance

Mass balance calculations aim to constrain the total metal mobility between protolith and high-metamorphic grade rocks. These calculations most likely contain significant errors due for example to the use of average concentrations, and the results should be considered to be semi-quantitative. They are useful however to get a general idea of the extent of mass loss and mobility (Patten et al., 2016).

The mass change can either be calculated using average metal concentrations or using the trend of metal content plotted against TiO_2 content, which would indicate a variation of metal content with the protolith rock composition. As the trends vs TiO_2 in this study do not show particularly strong R^2 values (all less than 0.35) (Fig. 7.5), the average values for the protolith samples are instead used (Table 6.2).

The mass change in % was calculated using the following formula:

*Mass change % = (Cs – Cp) * 100/Cp*

where *Cs* is the concentration of any element of the sample and *Cp* is the estimated concentration of the same element in the protolith rock.

As evidenced through the study of the average and median values, As displays ≈96% of change after staurolite zone (550°C) (Table 7.2, Fig. 7.7) while Sb shows a smoother decrease in % of mass change (Fig. 7.7). The mass loss percentage accounted for Au, shows an almost constant increase until the staurolite zone where-after it is dramatically increased. Average Se % is affected by the high-Se kyanite zone samples while Te shows no remarkable change. Bismuth reaches 50% of loss in the kyanite zone samples, though the pattern fluctuates significantly. The plots of Se, Te and Bi show no systematic change as Au, As and Sb. This is the reason why there are not included in the metal mobility calculations (Table 7.3). Moreover, ≈43% of water has been liberated by kyanite zone conditions, while carbon reaches -90% at the same metamorphic grade (Table 7.2, Fig. 7.8).

Assuming a density of 2.7 $cm \cdot gr^{-3}$ for the Pontiac rocks which is consistent for crustal rocks (Bucher and Grapes, 2011), the results show that a Pontiac biotite zone rock of 1 km^3 in volume, if metamorphosed to amphibolite facies sillimanite zone conditions would release ≈10t Au, ≈32800t As, ≈630t Sb, ≈20Mt H_2O and 2.4Mt C (Table 7.3). Table 7.3 also shows the masses of metals mobilised from 125 km^3 (10km·10km·1.25km) which is considered as a sufficient volume of rock at deposit-scale and has been previously used as an estimate of a source area size for the Macraes orogenic gold deposit in New Zealand (Pitcairn et al., 2006a).

The last calculations were performed for a source area of 30000 km^3 which is an estimate of the total volume of the Pontiac subprovince which extends under the southern Abitibi. This is based on the fact that the Pontiac extends more than 100km east-west, extending 40-50km north and being >5km deep based on the seismic studies (Fig. 7.10) (Calvert and Ludden, 1999). The results show that >300k Au could have been mobilised from that source area, while the whole Abitibi production (both orogenic Au and VMS) has been 4700t by 2005 (Dubé and Gosselin, 2007). Even though there are assumptions and errors, the mass balance calculations suggest that a very large mass of metals were mobilised from the Pontiac metasedimentary rocks, sufficient to provide significantly more Au than has been mined from the Abitibi. It is now questioned whether the fertility of each terrane is the controlling factor to vast ore deposition or more sufficient trapping mechanisms which do not allow the vast metal mobility to

Table 7.2. *Average mass changes (%) for the rocks from the Pontiac Subprovince.*

Met. Zone	Au	As	Sb	H_2O	C
Biotite	0	0	0	0	0
Garnet	-62	-26	-46	31	105
Staurolite	-85	-96	-66	-26	-61
Kyanite	-88	-98	-75	-43	-90
Sillimanite	-92	-98	-78	-34	-90

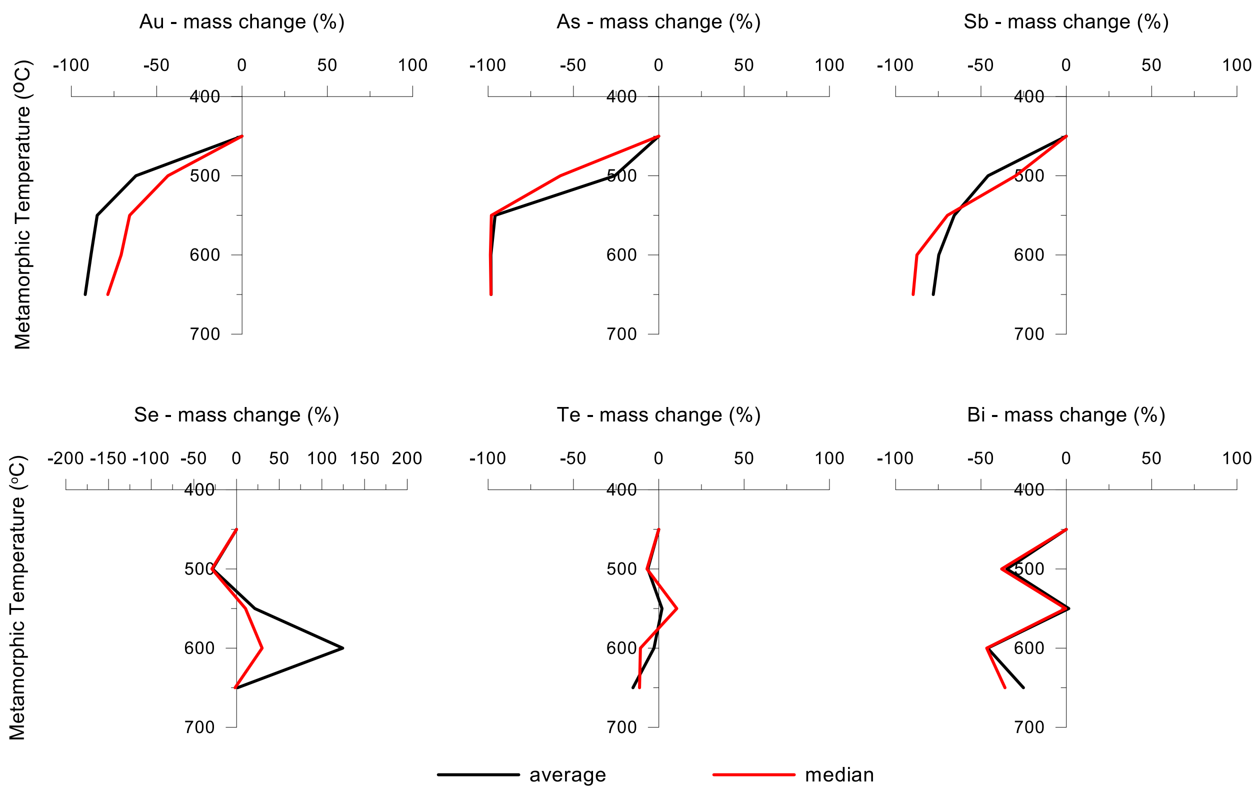

Figure 7.7. *Mass changes in % for Au, As, Sb, Se, Te and Bi for the rocks of the Pontiac Subprovince.*

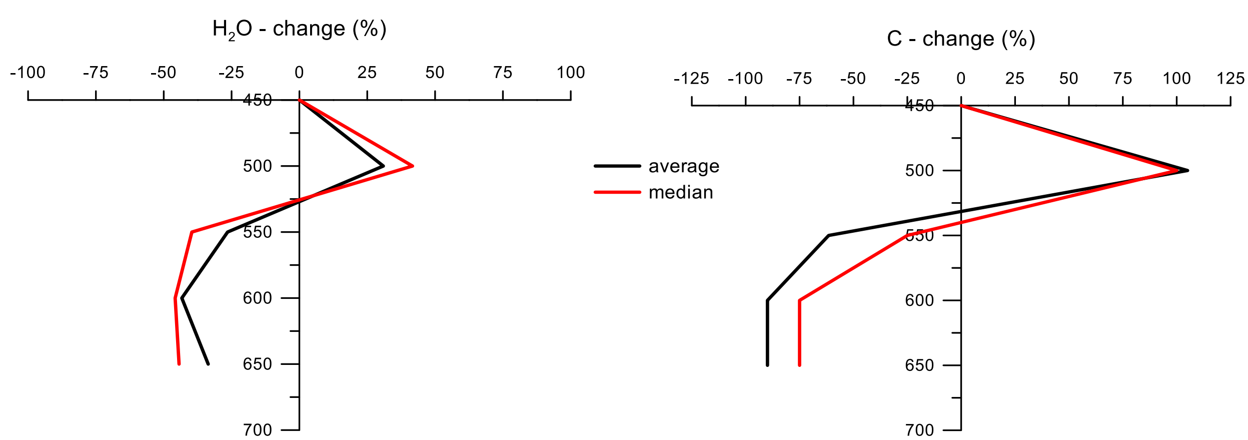

Figure 7.8. *Calculated changes in % for water and carbon for the rocks of the Pontiac Subprovince.*

Table 7.3. *Mass balance calculations for the rocks from the Pontiac Subprovince. Values are calculated assuming rock density of 2.7 gr·cm⁻³.*

		Au	As	Sb	H_2O	C
Biotite zone (Protolith) – ppm		0.0042	12.39	0.303	21305	990
Sillimanite Zone – ppm		0.0003	0.23	0.067	14700	110
Mass loss – ppm		0.0038	12.16	0.236	6605	890
Mass loss from :	**1 km³**	10.3 **t**	32839 **t**	638 **t**	20.2 **Mt**	2.4 **Mt**
	125 km³	1293 **t**	4.1 **Mt**	79779 **t**	2530 **Mt**	300 **Mt**
	30000 km³	310230 **t**	985.2 **Mt**	19.1 **Mt**	607000 **Mt**	72090 **Mt**

7.6.2. Implications for eastern and western Abitibi

The Abitibi Au deposits are situated at the southern part of the Abitibi Belt, proximal to the transcrustal Porcupine-Destor and Cadillac-Larder Lake fault zones which acted as fluid flow conduits during the collision of the Pontiac with the Abitibi Belt. The samples under study, come from the Pontiac subprovince which is only exposed in the eastern side of the Belt (Fig. 3.2) (Robert et al., 2005).

Within this extensive area in southern Abitibi, reported $\delta^{13}C$ values in hydrothermal vein carbonates vary significantly. Measurements of vein carbonates in metasomatized faults show that the $\delta^{13}C$ values appear to be lower in the eastern side than the ones from the western side of the Belt (Fig. 7.9) (Kerrich et al., 1987). For this study, rock sampling took place south of Rouyn-Noranda, exactly 50 km west of Cadillac, and south of Val d'Or, where Malartic deposit is situated (Fig. 4.1, 4.2.). As explained earlier, significant Au, As, Sb and C mobility occurred during metamorphism of the Pontiac rocks (Fig. 6.23). Based upon average values for C % per metamorphic zone, mass balance calculations revealed that a body of biotite zone Pontiac rock of 1 km^3 volume, would release ≈2.4Mt of carbon if metamorphosed to sillimanite zone, amphibolite facies conditions (Table 7.3). A higher proportion of organic C-rich rocks in the source area for the fluids would result in lower $\delta^{13}C$ values. Therefore, the Pontiac rocks, which are rich in organic C and exposed in the eastern side of south Abitibi, most probably account for the observed, lower $\delta^{13}C$ values. The absence of voluminous sedimentary rocks in the western side and the extensive presence of metavolcanics rocks account for the higher $\delta^{13}C$ values.

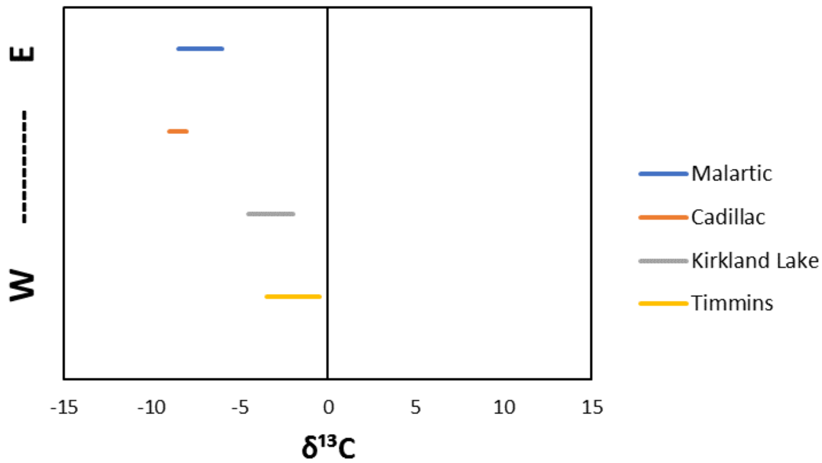

Figure 7.9. *Carbon isotopic compositions of hydrothermal carbonateσ from metasomatized fault zones at specified localities in the Abitibi Belt. Values after Kerrich et al. (1987). E-W distance not in scale.*

In addition, the Au deposits in the Timmins-Val d'Or Belt display differences in metal associations and some of them show variable enrichments in Te and Cu (Table 7.4) (Robert et al., 2005). This study shows that no significant mobilisation in either of these metals occurred during metamorphism of the Pontiac metasedimentary rocks (Fig. 6.23). Thus, these elements should have probably come from other sources, either metavolcanic rocks or having been transported from magmatic fluids.

The differences observed in isotopic signatures and metal associations in the deposits, indicate variable fertility between different parts of the Abitibi Belt, for different elements.

Table 7.4: *The orogenic Au deposits of the southern Abitibi Belt. Their exact locations are shown on Fig. 3.2.*

Gold deposit	Location in the Abitibi	Assemblage	Reference
Sigma-Lamaque	E	Au, Ag, As, W, ±Te, Mo, B	Robert et al., 2005
Camflo	E	Au, Ag, As, Sb, Te, ±W, Hg, Cu, Mo	Robert et al., 2005
Malartic	E	Au, Ag, As, Sb, Te, ±W, Hg, Cu, Mo	De Souza et al., 2017
Kerr Addison	C	Au, Ag, As, Sb, Te, ±W, Hg, Cu, Mo	Robert et al., 2005
Kirkland Lake	C	Au, As, W, ±Te, Mo, B	Robert et al., 2005
Pamour	W	Au, Ag, As, W, ±Te, Mo, B	Robert et al., 2005
Dome	W	Au, Ag, As, W, ±Te, Mo, B	Robert et al., 2005
Hollinger-McIntyre	W	Au, Ag, As, W, ±Te, Mo, B	Robert et al., 2005

7.6.3. A possible metasedimentary source for Au in the Abitibi

The Pontiac metasedimentary rocks, as reported by a number of researchers (Dimroth et al., 1982; Kerrich and Feng, 1992; Calvert and Ludden, 1999) are part of a relict accretionary prism which was regionally metamorphosed during the collision of the Pontiac subprovince with the southern part of the Abitibi Belt. The interpretation of the LITHOPROBE seismic survey suggests that the Pontiac sediments dip northwards underneath the southern Abitibi, with also an imbricated set of metasedimentary rocks and rocks of unknown affinity that have been suggested to be parts of the Pontiac subprovince (Kimura et al., 1993; Calvert and Ludden, 1999; Davis, 2002).

As discussed above a remarkable mobility of Au, As, Sb and C occurred during metamorphism of the rocks of the Pontiac subprovince with ≈10t, ≈32800t, ≈630t, 2.4Mt, and 20.2Mt of Au, As, Sb, C and H_2O respectively being mobilised from every km3 of Pontiac metasedimentary rock metamorphosed from biotite to sillimanite zone (Table 7.3). The presence of CO_2-rich, H_2O-poor fluid inclusions has been reported in some orogenic Au deposits and attributed to metamorphism of carbonaceous sediments (Gaboury, 2013). In addition, C-rich sediments with Au-As-rich diagenetic pyrites have already been proposed as potential sources for metals in orogenic Au deposits (Large et al., 2012). For the case of the Abitibi Belt, of all the elements analysed (61 in total) only Au, As, Sb and C, show systematic depletion with increasing metamorphic grade (Fig. 6.20, 6.21, 6.23). These metals are those that are most strongly enriched in the orogenic Au deposits of the area and it is noteworthy that the age of metamorphism for the Pontiac rocks (≈2.7 Ga) coincides with the age of orogenic Au deposits formation (≈2700-2630 Ma) (Robert et al., 2005) displaying syn- to post-peak timing. It is therefore possible that the Pontiac rocks comprise a potential metasedimentary source of metals and fluids to the southeastern Abitibi Greenstone Belt. The mobility of this suite of elements has been demonstrated in a number of other orogenic gold bearing metasedimentary terranes such as the Otago Schists of New Zealand (Pitcairn et al., 2006a; 2010; 2014) and the Dalradian of Scotland (Pitcairn et al., 2015). This study suggests that similar processes have mobilised metals during metamorphism of sedimentary rocks in the Archean. Thus, it is proposed that the Pontiac rocks, which lie at 20-30km depth and metamorphosed to amphibolite conditions, have possibly provided significant amount of Au, As, Sb, C and H_2O to the orogenic system.

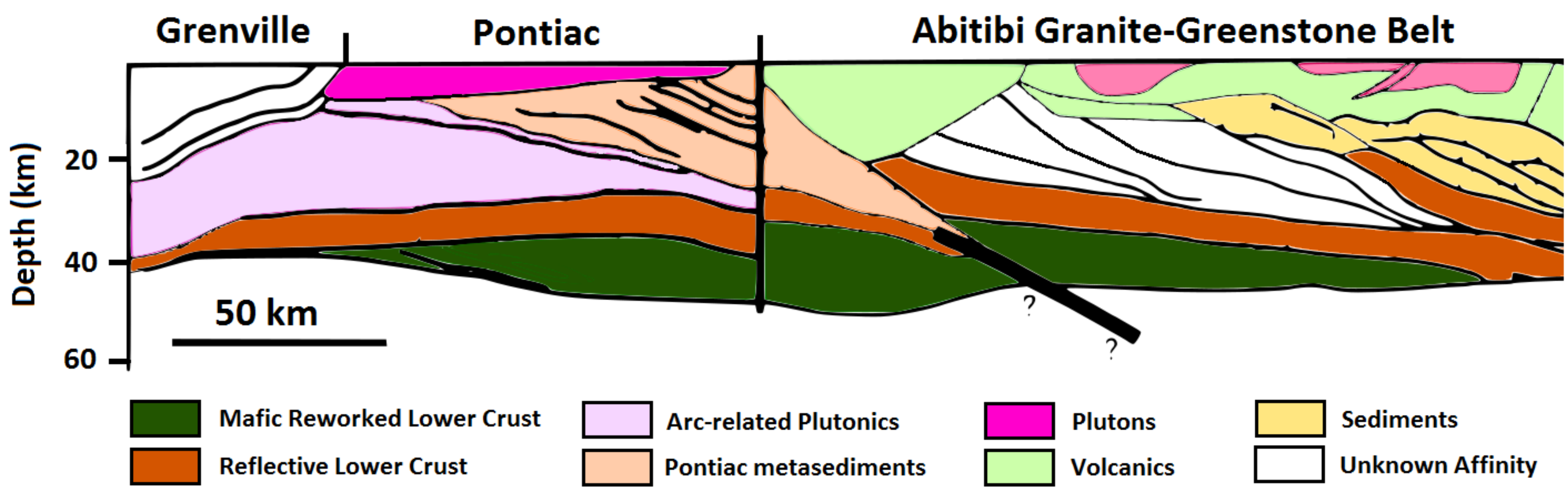

Figure 7.10. *Seismic cross-section interpretation for the southeastern Superior Province. Modified after Calvert and Ludden, 1999.*

8. Conclusions

This project aimed to test the metamorphic model for formation of orogenic gold deposits in the Archean-aged Abitibi Greenstone Belt, Canada, specifically investigated whether the metals and fluids could have been sourced from metasedimentary rocks in the region. After detailed study of metasedimentary rocks from the Pontiac subprovince and the southern Abitibi, and geochemical analyses including robust low-detection limit analyses for Au and related elements (As, Sb, Se, Te, Bi) and in situ LA-ICP-MS in sulphides, the following conclusions were drawn:

- Distinct and systematic depletions in Au, As, Sb, C and H_2O occurred during metamorphism of the metasedimentary rocks from the Pontiac subprovince. Average mass losses from the biotite zone greenschist to sillimanite zone amphibolite facies conditions, of 92%, 98%, 78%, 90% and 34% respectively were observed. No significant or systematic mobility was observed for Se, Te and Bi with increasing metamorphic grade (Fig. 6.21).
- The average trends with increasing metamorphic grade for Au, As and Sb correlate with those for C and LOI which is a proxy for H_2O, indicating their association during metamorphism. Sulphur concentrations which correlate strongly with Cu and Se, shows no systematic depletion during metamorphism (Fig. 6.23).
- The host mineral for gold is thought to be pyrite. Gold is only detectable in pyrite in lower-grade rocks (Table 6.5), therefore the Py-Po transition and associated reactions are responsible for Au-liberation in the fluid.
- The vast amount of metamorphic fluid was mainly produced during the transition from garnet zone greenschist to staurolite zone amphibolite facies conditions (Fig. 6.20). This timing and conditions coincide with the breakdown of chlorite which is considered as the controlling factor for fluid liberation during metamorphism. The hydrothermal fluid contained 89% H_2O and 11% C and transported Au, As and Sb away from the parent rocks.
- At least 10t Au, 32850t As, 630t Sb, 2Mt C and 20Mt of H_2O could be released from a cubic km (1 km^3) of biotite zone Pontiac rock if metamorphosed to sillimanite zone amphibolite facies conditions (Table 7.3).
- The relatively lower Au-values of the Cadillac and Porcupine samples in respect to those from the Pontiac, indicate variable Au-fertility between these sequences (Fig. 6.21). Different source rocks are suggested for the E and W Abitibi based on the occurrence and position of the Pontiac rocks. This is supported by previous C isotope investigations.
- Processes similar with those suggested in Phanerozoic orogenic terranes could have account for fluid production, metal mobility and therefore the formation of orogenic Au-deposits during the Archean.
- The Pontiac under-thrusts the southeastern Abitibi and mass balance calculations show large masses of metals and fluids being produced during metamorphism of these rocks. Therefore, the Pontiac metasedimentary rocks comprise a fertile source that could account for the bulk of metals currently enriched and mined in the orogenic Au-deposits of southeastern Abitibi Belt.

Acknowledgements

First of all, I would like to thank my supervisor Dr. Iain Pitcairn for the project he offered me with absolutely no hesitation. He is thanked for all the discussions we had, for his instructive opinions, comments and edits on my text. I really enjoyed this opportunity; doing fieldwork in Canada, being at the gold lab and studying orogenic-Au deposits. I am certain I gained a lot.

Then, both Clifford Patten and Arman Boskabadi are thanked for their help, handling the HF acid and preparing the samples for Au analyses. Clifford is also thanked for setting up the instrument for the As, Sb, Se, Te, Bi analyses during snowy days. Arman is thanked for getting me to know the SEM and for his constant presence. Thanks to Alexandre Peillod for his software tips and his opinions-knowledge upon the optical microscope. Dan Zetterberg is thanked for his assistance while working at the rock preparation lab. I would also like to thank Helena Bergman, Elisabeth Däcker, Arne Lif and Björn Eriksson because they were always kind and willing to help.

Johan Högmalm from the University of Gothenburg is thanked for setting me up for the LA-ICP-MS analyses and for doing the data reduction. Also, the PhD students Mikael Tillberg and Axel Sjöqvist for helping out with the instrument when Johan was away.

I would also like to thank all my friends from the university for the time we spent together the past two years. I had a great time.

And last, but not least, my parents, for their continuous support.

References

Ayer, J., Amelin, Y., Corfu, F., Kamo, S., Ketchum, J., Kwok, K., and Trowell, N., 2002, Evolution of the southern Abitibi greenstone belt based on U–Pb geochronology: autochthonous volcanic construction followed by plutonism, regional deformation and sedimentation: Precambrian Research, v. 115, no. 1–4, p. 63–95, doi: 10.1016/S0301-9268(02)00006-2.

Baxter, E.F., Ague, J.J., and Depaolo, D.J., 2002, Prograde temperature-time evolution in the Barrovian type-locality constrained by Sm/Nd garnet ages from Glen Clova, Scotland: Journal of the Geological Society, v. 159, no. 1, p. 71–82, doi: 10.1144/0016-76901013.

Beaudoin, G., and Chiaradia, M., 2016, Fluid mixing in orogenic gold deposits: Evidence from the H-O-Sr isotope composition of the Val-d'Or vein field (Abitibi, Canada): Chemical Geology, v. 437, p. 7–18, doi: 10.1016/j.chemgeo.2016.05.009.

Bédard, L.P., and Barnes, S.-J., 2002, A comparison of N-type semi-planar and coaxial INAA detectors for 33 geochemical reference samples: Journal of Radioanalytical and Nuclear Chemistry, v. 254, no. 3, p. 485–497, doi: 10.1023/A:1021685904319.

Benn, K., Miles, W., Ghassemi, M.R., and Gillett, J., 1994, Crustal structure and kinematic framework of the northwestern Pontiac Subprovince, Quebec: an integrated structural and geophysical study: Canadian Journal of Earth Sciences, v. 31, no. 2, p. 271–281, doi: 10.1139/e94-026.

Boynton, W. V, 1984, Cosmochemistry of the Rare Earth Elements: Meteorite Studies, *in* Rare Earth Element Geochemistry, Elsevier B.V., p. 63–114.

Bucher, K., and Grapes, R., 2011, Petrogenesis of Metamorphic Rocks: Springer Berlin Heidelberg, Berlin, Heidelberg.

Calvert, A.J., and Ludden, J.N., 1999, Archean continental assembly in the southeastern Superior Province of Canada: Tectonics, v. 18, no. 3, p. 412–429, doi: 10.1029/1999TC900006.

Camiré, G.E., Laflèche, M.R., and Ludden, J.N., 1993, Archaean metasedimentary rocks from the northwestern Pontiac Subprovince of the Canadian shield: chemical characterization, weathering and modelling of the source areas: Precambrian Research, v. 62, no. 3, p. 285–305, doi: 10.1016/0301-9268(93)90026-X.

Chown, E.H., Daigneault, R., Mueller, W., and Mortensen, J.K., 1992, Tectonic evolution of the Northern Volcanic Zone, Abitibi belt, Quebec: Canadian Journal of Earth Sciences, v. 29, no. 10, p. 2211–2225, doi: 10.1139/e92-175.

Constantin, M., 2009, Trace Element Data for Gold, Iridium and Silver in Seventy Geochemical Reference Materials: Geostandards and Geoanalytical Research, v. 33, no. 1, p. 115–132, doi: 10.1111/j.1751-908X.2008.00906.x.

Corfu, F., Krogh, T.E., Kwok, Y.Y., and Jensen, L.S., 1989, U–Pb zircon geochronology in the southwestern Abitibi greenstone belt, Superior Province: Canadian Journal of Earth Sciences, v. 26, no. 9, p. 1747–1763, doi: 10.1139/e89-148.

Corfu, F., and Noble, S.R., 1992, Genesis of the southern Abitibi greenstone belt, Superior Province, Canada: Evidence from zircon Hf isotope analyses using a single filament technique: Geochimica et

Cosmochimica Acta, v. 56, no. 5, p. 2081–2097, doi: 10.1016/0016-7037(92)90331-C.

Dare, S.A.S., Barnes, S.-J., Prichard, H.M., and Fisher, P.C., 2011, Chalcophile and platinum-group element (PGE) concentrations in the sulfide minerals from the McCreedy East deposit, Sudbury, Canada, and the origin of PGE in pyrite: Mineralium Deposita, v. 46, no. 4, p. 381–407, doi: 10.1007/s00126-011-0336-9.

Davis, D.W., 2002, U–Pb geochronology of Archean metasedimentary rocks in the Pontiac and Abitibi subprovinces, Quebec, constraints on timing, provenance and regional tectonics: Precambrian Research, v. 115, no. 1–4, p. 97–117, doi: 10.1016/S0301-9268(02)00007-4.

De Souza, S., Dubé, B., McNicoll, V., Dupuis, C., Mercier-Langevin, P., Creaser, R.A., Kjarsgaard, I., 2017, Geology and hydrothermal alteration of the world-class Canadian Malartic Gold Deposit: Genesis of an Archean stockwork-disseminated gold deposit in the Abitibi Greenstone Belt, Québec. Reviews in Economic Geology, 19

Dimroth, E., Imreh, L., Goulet, N., and Rocheleau, M., 1983a, Evolution of the south-central segment of the Archean Abitibi Belt, Quebec. Part II: Tectonic evolution and geomechanical model: Canadian Journal of Earth Sciences, v. 20, no. 9, p. 1355–1373, doi: 10.1139/e83-124.

Dimroth, E., Imreh, L., Goulet, N., and Rocheleau, M., 1983b, Evolution of the south-central segment of the Archean Abitibi Belt, Quebec. Part III: Plutonic and metamorphic evolution and geotectonic model: Canadian Journal of Earth Sciences, v. 20, no. 9, p. 1374–1388, doi: 10.1139/e83-125.

Dimroth, E., Imreh, L., Rocheleau, M., and Goulet, N., 1982, Evolution of the south-central part of the Archean Abitibi Belt, Quebec. Part I: Stratigraphy and paleogeographic model: Canadian Journal of Earth Sciences, v. 19, no. 9, p. 1729–1758, doi: 10.1139/e82-154.

Dubé, B., and Gosselin, P., 2007, Greenstone-hosted quartz-carbonate vein deposits: in Goodfellow, W.D., ed., Mineral Deposits of Canada: A Synthesis of Major Deposit-Types, District Metallogeny, the Evolution of Geological Provinces, and Exploration Methods: Geological Association of Canada, Mineral Deposits Division, , no. 5, p. 49–73.

Feng, R., and Kerrich, R., 1990, Geobarometry, differential block movements, and crustal, structure of the southwestern Abitibi greenstone belt, Canada: Geology, v. 18, no. 9, p. 870, doi: 10.1130/0091-7613(1990)018<0870:GDBMAC>2.3.CO;2.

Feng, R., and Kerrich, R., 1991, Single zircon age constraints on the tectonic juxtaposition of the Archean Abitibi greenstone belt and Pontiac subprovince, Quebec, Canada: Geochimica et Cosmochimica Acta, v. 55, no. 11, p. 3437–3441, doi: 10.1016/0016-7037(91)90502-V.

Feng, R., Kerrich, R., and Maas, R., 1993, Geochemical, oxygen, and neodymium isotope compositions of metasediments from the Abitibi greenstone belt and Pontiac Subprovince, Canada: Evidence for ancient crust and Archean terrane juxtaposition: Geochimica et Cosmochimica Acta, v. 57, no. 3, p. 641–658, doi: 10.1016/0016-7037(93)90375-7.

Feng, R., Kerrich, R., McBride, S., and Farrar, E., 1992, 40 Ar/ 39 Ar age constraints on the thermal history of the Archean Abitibi greenstone belt and the Pontiac Subprovince: implications for terrane collision, differential uplift, and overprinting of gold deposits: Canadian Journal of Earth Sciences, v. 29, no. 7, p. 1389–1411, doi: 10.1139/e92-112.

Gaboury, D., 2013, Does gold in orogenic deposits come from pyrite in deeply buried carbon-rich sediments?: Insight from volatiles in fluid inclusions: Geology, v. 41, no. 12, p. 1207–1210, doi: 10.1130/G34788.1.

Goldfarb, R.J., Baker, T., Dubé, B., Groves, D.I., Hart, C.J.R., and Gosselin, P., 2005, Distribution, Character, and Genesis of Gold Deposits in Metamorphic Terranes: Economic Geology 100th Anniversary Volume, v. 100, p. 407–450.

Goldfarb, R.J., and Groves, D.I., 2015, Orogenic gold: Common or evolving fluid and metal sources through time: Lithos, v. 233, p. 2–26, doi: 10.1016/j.lithos.2015.07.011.

Goldfarb, R.., Groves, D.., and Gardoll, S., 2001, Orogenic gold and geologic time: a global synthesis: Ore Geology Reviews, v. 18, no. 1–2, p. 1–75, doi: 10.1016/S0169-1368(01)00016-6.

Gromet, L.P., Haskin, L.A., Korotev, R.L., and Dymek, R.F., 1984, The "North American shale composite": Its compilation, major and trace element characteristics: Geochimica et Cosmochimica Acta, v. 48, no. 12, p. 2469–2482, doi: 10.1016/0016-7037(84)90298-9.

Groves, D.I., 1993, The crustal continuum model for late-Archaean lode-gold deposits of the Yilgarn Block, Western Australia: Mineralium Deposita, v. 28, no. 6, p. 366–374, doi: 10.1007/BF02431596.

Groves, D.I., Goldfarb, R.., Gebre-Mariam, M., Hagemann, S.., and Robert, F., 1998, Orogenic gold deposits: A proposed classification in the context of their crustal distribution and relationship to other gold deposit types: Ore Geology Reviews, v. 13, no. 1–5, p. 7–27, doi: 10.1016/S0169-1368(97)00012-7.

Guillong, M., Hametner, K., Reusser, E., Wilson, S. a, and Günther, D., 2005, Preliminary Characterisation of New Glass Reference Materials (GSA-1G, GSC-1G, GSD-1G and GSE-1G) by Laser Ablation-Inductively Coupled Plasma-Mass Spectrometry Using 193 nm, 213 nm and 266 nm Wavelengths: Geostandards and Geoanalytical Research, v. 29, no. 3, p. 315–331, doi: 10.1111/j.1751-908X.2005.tb00903.x.

Herron, M.M., 1988, Geochemical Classification of Terrigenous Sands and Shales from Core or Log Data: SEPM Journal of Sedimentary Research, v. Vol. 58, no. 5, p. 820–829, doi: 10.1306/212F8E77-2B24-11D7-8648000102C1865D.

Hronsky, J.M.A., Groves, D.I., Loucks, R.R., and Begg, G.C., 2012, A unified model for gold mineralisation in accretionary orogens and implications for regional-scale exploration targeting methods: Mineralium Deposita, v. 47, no. 4, p. 339–358, doi: 10.1007/s00126-012-0402-y.

Jackson, S.L., and Cruden, A.R., 1995, Formation of the Abitibi greenstone belt by arc-trench migration: Geology, v. 23, no. 5, p. 471, doi: 10.1130/0091-7613(1995)023<0471:FOTAGB>2.3.CO;2.

Jochum, K.P., Nohl, U., Herwig, K., Lammel, E., Stoll, B., and Hofmann, A.W., 2005, GeoReM: A New Geochemical Database for Reference Materials and Isotopic Standards: Geostandards and Geoanalytical Research, v. 29, no. 3, p. 333–338, doi: 10.1111/j.1751-908X.2005.tb00904.x.

Jochum, K.P., Weis, U., Stoll, B., Kuzmin, D., Yang, Q., Raczek, I., Jacob, D.E., Stracke, A., Birbaum, K., Frick, D.A., Günther, D., and Enzweiler, J., 2011, Determination of Reference Values for NIST SRM 610-617 Glasses Following ISO Guidelines: Geostandards and Geoanalytical Research, v. 35, no. 4, p. 397–429, doi: 10.1111/j.1751-908X.2011.00120.x.

Kerrich, R., and Cassidy, K.F., 1994, Temporal relationships of lode gold mineralization to accretion, magmatism, metamorphism and deformation — Archean to present: A review: Ore Geology Reviews, v. 9, no. 4, p. 263–310, doi: 10.1016/0169-1368(94)90001-9.

Kerrich, R., and Feng, R., 1992, Archean geodynamics and the Abitibi-Pontiac collision: implications for advection of fluids at transpressive collisional boundaries and the origin of giant quartz vein systems: Earth-Science Reviews, v. 32, no. 1–2, p. 33–60, doi: 10.1016/0012-8252(92)90011-H.

Kerrich, R., Fryer, B.J., King, R.W., Willmore, L.M., and van Hees, E., 1987, Crustal outgassing and LILE enrichment in major lithosphere structures, Archean Abitibi greenstone belt: evidence on the source reservoir from strontium and carbon isotope tracers: Contributions to Mineralogy and Petrology, v. 97, no. 2, p. 156–168, doi: 10.1007/BF00371236.

Kimura, G., Ludden, J.N., Desrochers, J.-P., and Hori, R., 1993, A model of ocean-crust accretion for the Superior province, Canada: Lithos, v. 30, no. 3–4, p. 337–355, doi: 10.1016/0024-4937(93)90044-D.

Lajoie, J., and Ludden, J., 1984, Petrology of the Archean Pontiac and Kewagama sediments and implications for the stratigraphy of the southern Abitibi belt: Canadian Journal of Earth Sciences, v. 21, no. 11, p. 1305–1314, doi: 10.1139/e84-135.

Large, R., Thomas, H., Craw, D., Henne, A., and Henderson, S., 2012, Diagenetic pyrite as a source for metals in orogenic gold deposits, Otago Schist, New Zealand: New Zealand Journal of Geology and Geophysics, v. 55, no. 2, p. 137–149, doi: 10.1080/00288306.2012.682282.

McCuaig, C.T., and Kerrich, R., 1998, P—T—t—deformation—fluid characteristics of lode gold deposits: evidence from alteration systematics: Ore Geology Reviews, v. 12, no. 6, p. 381–453, doi: 10.1016/S0169-1368(98)80002-4.

Mercier-Langevin, P., Lafrance, B., Becu, V., Dube, B., Kjarsgaard, I., and Guha, J., 2014, The Lemoine Auriferous Volcanogenic Massive Sulfide Deposit, Chibougamau Camp, Abitibi Greenstone Belt, Quebec, Canada: Geology and Genesis: Economic Geology, v. 109, no. 1, p. 231–269, doi: 10.2113/econgeo.109.1.231.

Mortensen, J.K., and Card, K.D., 1993, U–Pb age constraints for the magmatic and tectonic evolution of the Pontiac Subprovince, Quebec: Canadian Journal of Earth Sciences, v. 30, no. 9, p. 1970–1980, doi: 10.1139/e93-173.

Mueller, W.U., Friedman, R., Daigneault, R., Moore, L., and Mortensen, J., 2012, Timing and characteristics of the Archean subaqueous Blake River Megacaldera Complex, Abitibi greenstone belt, Canada: Precambrian Research, v. 214–215, p. 1–27, doi: 10.1016/j.precamres.2012.02.003.

Patten, C.G.C., Pitcairn, I.K., Teagle, D.A.H., and Harris, M., 2016, Sulphide mineral evolution and metal mobility during alteration of the oceanic crust: Insights from ODP Hole 1256D: Geochimica et Cosmochimica Acta, v. 193, p. 132–159, doi: 10.1016/j.gca.2016.08.009.

Pearson, V., and Daigneault, R., 2009, An Archean megacaldera complex: The Blake River Group, Abitibi greenstone belt: Precambrian Research, v. 168, no. 1–2, p. 66–82, doi: 10.1016/j.precamres.2008.03.009.

Phillips, G.N., and Powell, R., 2010, Formation of gold deposits: a metamorphic devolatilization model: Journal of Metamorphic Geology, v. 28, no. 6, p. 689–718, doi: 10.1111/j.1525-1314.2010.00887.x.

Pitcairn, I.K., Craw, D., and Teagle, D.A.H., 2014, The gold conveyor belt: Large-scale gold mobility in an active orogen: Ore Geology Reviews, v. 62, p. 129–142, doi: 10.1016/j.oregeorev.2014.03.006.

Pitcairn, I.K., Olivo, G.R., Teagle, D.A.H., and Craw, D., 2010, Sulfide evolution during prograde metamorphism of the Otago and Alpine schists, New Zealand: Canadian Mineralogist, v. 48, no. 5, p. 1267–1295, doi: 10.3749/canmin.48.5.1267.

Pitcairn, I.K., Skelton, A.D.L., and Wohlgemuth-Ueberwasser, C.C., 2015, Mobility of gold during metamorphism of the Dalradian in Scotland: Lithos, v. 233, p. 69–88, doi: 10.1016/j.lithos.2015.05.006.

Pitcairn, I.K., Teagle, D.A.H., Craw, D., Olivo, G.R., Kerrich, R., and Brewer, T.S., 2006a, Sources of Metals and Fluids in Orogenic Gold Deposits: Insights from the Otago and Alpine Schists, New Zealand: Economic Geology, v. 101, no. 8, p. 1525–1546, doi: 10.2113/gsecongeo.101.8.1525.

Pitcairn, I.K., Warwick, P.E., Milton, J.A., and Teagle, D.A.H., 2006b, Method for Ultra-Low-Level Analysis of Gold in Rocks: Analytical Chemistry, v. 78, no. 4, p. 1290–1295, doi: 10.1021/ac051861z.

Powell, W.G., Carmichael, D.M., and Hodgson, C.J., 1995, Conditions and timing of metamorphism in the southern Abitibi greenstone belt, Quebec: Canadian Journal of Earth Sciences, v. 32, no. 6, p. 787–805, doi: 10.1139/e95-067.

Robert, F., and Kelly, W.C., 1987, Ore-forming fluids in Archean gold-bearing quartz veins at the Sigma Mine, Abitibi greenstone belt, Quebec, Canada: Economic Geology, v. 82, no. 6, p. 1464–1482, doi: 10.2113/gsecongeo.82.6.1464.

Robert, F., Poulsen, K.H., Cassidy, K.F., and Hodgson, J.C., 2005, Gold Metallogeny of the Superior and Yilgarn Cratons: Economic Geology 100th Anniversary Volume, p. 1001–1033.

Seward, T.., 1973, Thio complexes of gold and the transport of gold in hydrothermal ore solutions: Geochimica et Cosmochimica Acta, v. 37, no. 3, p. 379–399, doi: 10.1016/0016-7037(73)90207-X.

Sillitoe, R.H., and Thompson, J.F.H., 1998, Intrusion-Related Vein Gold Deposits: Types, Tectono-Magmatic Settings and Difficulties of Distinction from Orogenic Gold Deposits: Resource Geology, v. 48, no. 4, p. 237–250, doi: 10.1111/j.1751-3928.1998.tb00021.x.

Stefánsson, A., and Seward, T.M., 2004, Gold(I) complexing in aqueous sulphide solutions to 500°C at 500 bar: Geochimica et Cosmochimica Acta, v. 68, no. 20, p. 4121–4143, doi: 10.1016/j.gca.2004.04.006.

Sylvester, P.J., Cabri, L.J., Tubrett, M.N., McMahon, G., Laflamme, J.H.G., and Peregoedova, A., 2005, Synthesis and evaluation of a fused pyrrhotite standard reference material for platinum group element and gold analysis by laser ablation-ICPMS: 10th International Platinum Symposium, , no. December 2015, p. 16–20.

Thompson, J.F.H., and Newberry, R.J., 2000, Gold deposits related to reduced granitic intrusions: Reviews in Economic Geology, v. 13, p. 377–400.

Tomkins, A.G., 2010, Windows of metamorphic sulfur liberation in the crust: Implications for gold deposit genesis: Geochimica et Cosmochimica Acta, v. 74, no. 11, p. 3246–3259, doi: 10.1016/j.gca.2010.03.003.

Wilson, S. a., Ridley, W.I., and Koenig, a. E., 2002, Development of sulfide calibration standards for the laser ablation inductively-coupled plasma mass spectrometry technique: J. Anal. At. Spectrom., v. 17, no. 4, p. 406–409, doi: 10.1039/B108787H.

Wyman, D.A., Kerrich, R., and Polat, A., 2002, Assembly of Archean cratonic mantle lithosphere and crust: plume–arc interaction in the Abitibi–Wawa subduction–accretion complex: Precambrian Research, v. 115, no. 1–4, p. 37–62, doi: 10.1016/S0301-9268(02)00005-0.